FEASIBILITY STUDY OF NOVEL BIOACTIVE GLASS PREPARED FROM BAGASSE AND CASSAVA RHIZOME FOR BONE TISSUE ENGINEERING APPLICATIONS

POONNAPHOB SOPAPAN

A THESIS SUBMITTED IN PARTIAL FULFILLMENT OF THE REQUIREMENTS FOR THE DEGREE OF DOCTOR OF PHILOSOPHY

MAJOR IN PHYSICS

FACULTY OF SCIENCE

UBON RATCHATHANI UNIVERSITY

ACDEMIC YEAR 2020

ACKNOWLEDGEMENT

This work won't have been possible without the support of my doctoral advisors, Assoc. Prof. Raewat Laopaiboon and Assoc. Prof. Jintana Laopaiboon. It has been an honor to be them graduate student and learn the basics of glass science and its properties from them. With the great efforts to explain things clearly and simply, they helped to guide and support me from the initial to final stage which enabled me to develop an understanding of the subject. Throughout my thesis-working period, they provided encouragement, good advice, good teaching and a lot of good ideas. Special thanks are directed to the committee members, Dr. Nuan La-ong Srakaew for her comments and suggestions, Assoc. Prof. Dr. Supakorn Pukird, Dr. Orathai Thumthan and Dr. Somkid Pencharee for their kindly advices and helpful suggestions.

Additionally, I would like to thank all faculty members in Department of Physics, Faculty of Science, Ubon Ratchathani University for their teaching and technical supports for this work. I gratefully express my appreciation to Mr. Thon Thongklom and Faculty of Engineering, Ubon Ratchathani University for allowing to use Vickers microhardness tester and facility. I gratefully appreciate to Dr. Oruethai Jaiboon for suggestion about the analysis of some parts of the results in this dissertation. I would like to thank Department of Physics, Ubon Ratchathani University for the use of ultrasonic flaw detector and Department of Chemistry for allowing to prepare the simulated body fluid (SBF) solution. Thanks also go to the Science Achievement Scholarship of Thailand (SAST) for financial support during this study.

Finally, I take this opportunity to sincerely thank all my family members for their love, encouraging and understanding. It would be completely impossible without them. Specifically, my parent's advice has encouraged and inspired me to stay focused and head towards the right direction. Last but not least, I am thankful to all my friends, I also express my appreciation to everyone that I could not mention their names all here for their helps, kindness and friendship.

Poonnaphob Sopapan

Researcher

บทคัดย่อ

เรื่อง	:	การศึกษาความเป็นไปได้ของแก้วชีวภาพแบบใหม่ที่เตรียมจากชานอ้อยและเหง้ามันสำปะหลังสำหรับการประยุกต์ใช้ในงานทางด้านวิศวกรรมเนื้อเยื่อกระดูก
ผู้วิจัย	:	ปุณณภพ โสภาพันธ์
ชื่อปริญญา	:	ปรัชญาดุษฎีบัณฑิต
สาขาวิชา	:	ฟิสิกส์
อาจารย์ที่ปรึกษา	:	รองศาสตราจารย์เรวัฒน์ เหล่าไพบูลย์
อาจารย์ที่ปรึกษาร่วม	:	รองศาสตราจารย์จินตนา เหล่าไพบูลย์
คำสำคัญ	:	แก้วชีวภาพ, เทคนิคคลื่นเสียงอัลตร้าโซนิกแบบควบคุมแรงกด, สมบัติเชิงกล, พฤติกรรมการออกฤทธิ์ทางชีวภาพ, วิศวกรรมเนื้อเยื่อกระดูก

แก้วชีวภาพที่เตรียมจากชานอ้อยและเหง้ามันสำปะหลังแสดงคุณสมบัติที่น่าสนใจนอกเหนือจากต้นทุนต่ำและเป็นมิตรกับสิ่งแวดล้อม แก้วสองชุดที่อยู่บนพื้นฐานของระบบ B_2O_3–P_2O_5–Na_2O–CaO–BG และ B_2O_3–P_2O_5–Na_2O–CaO–CR โดยที่ BG คือชานอ้อย และ CR คือเหง้ามันสำปะหลัง ถูกสร้างขึ้นโดยใช้เทคนิคการหลอมละลายแล้วทำให้เย็นตัวอย่างรวดเร็ว การศึกษาความเป็นไปได้ในการใช้ชานอ้อยและเหง้ามันสำปะหลังเพื่อสร้างแก้วชีวภาพแบบใหม่ได้รับการประเมินผ่านสมบัติทางกายภาพ สมบัติเชิงกล โครงสร้าง ลักษณะทางสัณฐานวิทยา และความทนทานต่อสารละลาย ความหนาแน่นของตัวอย่างแก้วที่ได้จากการวัดตามหลักการของอาร์คิมีดีสและคำนวณตามกฎการรวมกันขององค์ประกอบได้รับการศึกและเปรียบเทียบ การวัดความเร็วคลื่นเสียงอัลตราโซนิกของตัวอยางแก้วที่มีสัดส่วนของชานอ้อยและเหง้ามันสำปะหลังแตกต่างกัน ทำได้โดยใช้เทคนิคอัลตราโซนิกแบบควบคุมแรงกดด้วยหัววัดแบบตรงและแบบมุม ที่ความถี่ 4 เมกะเฮิร์ต โมดูลัสยืดหยุ่น อัตราส่วนของปัวส์ซอง และความแข็งระดับไมโคร คำนวณได้จากข้อมูลความเร็วคลื่นเสียงและความหนาแน่นของตัวอย่างแก้ว นอกจากนี้ความแข็งระดับไมโครของตัวอย่างแก้วยังวัดได้โดยใช้เครื่องทดสอบความแข็งแบบวิคเกอร์โดยใช้โหลดที่มีค่าเท่ากับ 0.98 นิวตัน แก้วชีวภาพแบบใหม่ที่ใช้สำหรับงานทางด้านวิศวกรรมเนื้อเยื่อกระดูกได้รับการทดสอบความว่องไวทางชีวภาพแบบหลอดทดลองทั้งก่อนและหลังการแช่ในสารละลายแบบจำลองของเหลวในร่างกาย (SBF) ที่อุณหภูมิ 37 องศาเซลเซียส เป็นเวลา 1, 7 และ 14 วัน การเปลี่ยนแปลงทางโครงสร้างและลักษณะทางสัณฐานวิทยา รวมถึงความสามารถในการยึดเกาะของกระดูกถูกประเมินโดยการวัด XRD FTIR และ SEM ในงานวิจัยนี้ พฤติกรรมการสลายตัวของตัวอย่างแก้วและค่า pH ของสารละลาย SBF ยังได้รับการพิจารณาด้วย ผลการศึกษาพบว่าการเพิ่มขึ้นของปริมาณชานอ้อยและเหง้ามันสำปะหลังในแก้วนำไปสู่การเพิ่มขึ้นของความหนาแน่น ความเร็วคลื่นเสียงอัลตร้าโซนิก โมดูลัสยืดหยุ่น และความแข็งระดับไมโคร ค่าความแข็งระดับไมโครที่ได้จากทั้งสองเทคนิคถูกนำมาเปรียบเทียบกันและพบว่าทั้งสองค่ามีความสัมพันธ์ที่สอดคล้องกัน ผลการทดลองการสูญเสียน้ำหนักและค่า pH ของสารละลาย เพิ่มขึ้นตามระยะเวลาการแช่ การเพิ่มปริมาณชานอ้อยและเหง้ามันสำปะหลังลงในแก้วช่วยให้อัตราการละลายของแก้วลดลง

ข้อมูล XRD ก่อนแช่ตัวอย่างแก้วในสารละลาย SBF ยืนยันลักษณะความเป็นอสัญฐาณของแก้ว ในขณะเดียวกันสเปกตรัม FTIR ก็สนับสนุนหน่วยโครงสร้างภายในของแก้วที่สอดคล้องกับกลุ่มบอเรตเป็นส่วนใหญ่ นอกจากนี้ลักษณะทางสัณฐานวิทยาบนพื้นผิวแก้วก่อนแช่ แสดงลักษณะพื้นผิวที่เรียบพร้อมกับร่องรอยที่เกิดจากการขัด หลังการแช่ตัวอย่างแก้วในสารละลาย SBF รูปแบบของ XRD เผยให้เห็นถึงพีคบางตำแหน่งที่สอดคล้องกับลักษณะเฉพาะของสารประกอบแคลเซียมฟอสเฟสที่อยู่ในรูปของบรูไชท์และไฮดรอกซีอะพาไทต์ ในทำนองเดียวกันสเปกตรัม FTIR ที่ประมาณ 550–610 cm^{-1} และ 980–1060 cm^{-1} ระบุว่าเป็นพันธะของ P–O ที่เกี่ยวข้องกับการเกิดชั้นของแคลเซียมฟอสเฟส นอกจากนี้ภาพถ่าย SEM ยังแสดงให้เห็นการเกาะกลุ่มกันของอนุภาคกลมขนาดเล็กจำนวนมากบนพื้นผิวแก้วซึ่งบ่งชี้ถึงการก่อตัวของแคลเซียมฟอสเฟส ผลการทดลองที่ได้จากวิเคราะห์ด้วยเทคนิค XRD FTIR และ SEM ยืนยันการก่อตัวของไฮดรอกซีอะพาไทต์ หรือความสามารถในการยึดเกาะของกระดูกบนพื้นผิวแก้วหลังจากแช่ในสารละลาย SBF

ABSTRACT

TITLE : FEASIBILITY STUDY OF NOVEL BIOACTIVE GLASS PREPARED FROM BAGASSE AND CASSAVA RHIZOME FOR BONE TISSUE ENGINEERING APPLICATIONS
AUTHOR : POONNAPHOB SOPAPAN
DEGREE : DOCTOR OF PHILOSOPHY
MAJOR : PHYSICS
ADVISOR : ASSOC. PROF. RAEWAT LAOPAIBOON
CO- ADVISOR : ASSOC. PROF. JINTANA LAOPAIBOON
KEYWORDS : BIOACTIVE GLASS, PRESSURE-CONTROLLED ULTRASONIC TECHNIQUE, MECHANICAL PROPERTY, BIOACTIVE BEHAVIOR, BONE TISSUE ENGINEERING

Bioactive glass prepared from bagasse and cassava rhizome exhibits interesting properties in addition to low cost and being environmentally friendly. Two glass series based on B_2O_3–P_2O_5–Na_2O–CaO–BG and B_2O_3–P_2O_5–Na_2O–CaO–CR, where BG is bagasse and CR is cassava rhizome, were fabricated by a melt quenching technique. A feasibility study was undertaken using bagasse and cassava rhizome as novel bioactive glass and results were evaluated physically, mechanically, structurally, morphologically and in terms of degradation properties. The densities of the prepared glasses were measured and calculated based on, respectively, Archimedes' principle and additive rule, and results were studied and compared. The ultrasonic velocities of the glass samples with different mix proportions of bagasse and cassava rhizome were measured based on a pressure-controlled ultrasonic technique at the frequency of 4 MHz through normal and angle probes. The elastic moduli, Poisson's ratio and microhardness were calculated from an acoustic velocity and a density data of the glass samples. Vickers hardness tester was also applied to determine the microhardness of the glass using the applied load of 0.98 N. A set of the novel glasses for bone tissue engineering was tested *in vitro* bioactivity before and after immersion in the simulated body fluid (SBF) solution during exposure at 37 ℃ for 1, 7 and 14 days. The structural and morphological changes including bone bonding ability were assessed by performing XRD, FTIR and SEM measurements. The

degradation behavior of the glass samples and pH change of SBF solution were also considered in this work. The results found that the addition of bagasse and cassava rhizome leads to an increase of the densities, ultrasonic wave velocities, elastic moduli and microhardness values in all prepared glasses. The values of microhardness obtained from both techniques were compared and a good correlation was observed. The results of the weight loss and pH value of the solution increased with longer time periods. The addition of bagasse and cassava rhizome into the glasses leads to a decrease of the dissolution rate. Before soaking in the SBF solution, XRD data was observed to confirm the amorphous nature of the glasses while FTIR spectra supported the internal structural units of the prepared glass, corresponding to main borate groups. Additionally, the surface morphology before immersion showed a flat surface with deep grooves. After immersion, the XRD patterns illustrated some peaks corresponding to calcium phosphate phases in the form of brushite and hydroxyapatite. Likewise, the FTIR spectra about 550–610 cm^{-1} and 980–1060 cm^{-1} indicated the P–O bonds related to the calcium phosphate layer formation. Moreover, the SEM images showed the agglomeration of many small rounded particles on the glass surface, indicating the formation of calcium phosphate layers. These XRD, FTIR and SEM results confirmed the formation of hydroxyapatite or bone bonding ability on glass surface after immersion in the SBF solution.

CONTENTS

CONTENTS (CONTINUED)

LIST OF TABLES

LIST OF FIGURES

LIST OF FIGURES (CONTINUED)

LIST OF FIGURES (CONTINUED)

LIST OF FIGURES (CONTINUED)

CHAPTER 1
INTRODUCTION

1.1 Motivation and background

Biomaterials have been extensively applied as bone augmentation in treating patients with accidental bone loss, degeneration of bone and other severe bone-related diseases like bone cancer, osteoporosis and so on [1-2]. Generally, an ideal biomaterial for bone regeneration should be biodegradable, biocompatible and/or innocuous with human biological tissue including exhibits suitable mechanical and elastic properties close to those of the tissue to be replaced. Also, it must act as a skeleton framework and stimulate to new bone creation in the surrounding area [3-4]. Over the years, the field of glasses caused a revolution in health maintenance and paved the way for modern biomaterial-driven regenerative medicine. The concept of "bioactive material" with the invention of 45S5 Bioglass®, appeared in 1969s, was introduced by Larry Hench and the subsequent category of materials that stemmed from this research has been used to formulate various glass-based biomaterials today [5-8]. The mechanism of bonding in such pioneer silicate bioactive glass systems involves partial dissolution of modifiers which leads to the formation of a silica-gel layer and subsequent formation of a calcium phosphate surface layer [9-10]. The soluble silicon has played a significant role in tissue repair and osteogenesis. Moreover, there are many studies indicate that functional ions and other dissolution products from bioactive glasses, when released in the human physiological system in a controlled manner, can be used to activate genes that stimulate the body to repair itself. *In vitro* studies reported that, during the dissolution of 45S5, the ion release seems to induce angiogenesis and stimulate osteoblasts proliferation and new bone growth [11-12]. Some bioactive glasses are also able to bond to both bone and soft/hard connective tissue. This discovery has led to the field of the generation bioresorbable materials with potential tissue-engineering applications. Bioactive glass has performed acceptably and is widely used today in order to repair or reconstruct bone disorders [13-14]. It is regarded as one of the most widely investigated and commercially successful biomaterials applied in medicine and dentistry [15].

Applications include dental implants, percutaneous devices and use in periodontal treatment, orthopedics, spinal surgery, scaffold design, drug delivery, gene transfection and cancer treatment [16-17].

Bioactive glasses containing calcium and boron have gained high interest as biomaterials for bone tissue engineering owing to good bioactivity and biocompatibility including low melting point, high thermal stability, and mechanical durability [18-20]. After soaking in simulated body fluid (SBF) solution, they are characterized by their higher reactivities when compared to silicate-based glasses, which result in faster hydroxyapatite formation [21-22]. Borate glasses show antibacterial effects against several microorganisms. These glasses have also been found to close the wounded area faster than other bioactive glasses. This also allowed for increased collagen deposition into the ulcerated area [23]. The main problem of borate-based bioactive glasses, however, is that their solubilities are too fast, which makes decreasing of stabilization of the glass network and toxic effect on human fibroblast cells. The varying solubility of bioactive borate glasses affects their biological performance because products obtained from ion exchange reaction are known to stimulate angiogenesis and osteogenesis both *in vitro* and *in vivo* [19,24]. The easiest ways to reduce the rate of boron dissolution, in general, is adjustment the composition and preparation technique of the bioactive glass. For instance, the addition of some trace elements (e.g. Si, Ca, Ti, Zn, Mg, Al) in borate glass has been expressed to slow down the chemical degradation of the borate glass and lead to a lesser toxic effect on human biological cells than the undoped glass [12]. Additionally, some additive agents can also enhance other properties of bioactive glasses. In borate glasses, it is an established fact that boron is a laminar network consisting of three and/or four coordination numbers. Hence, the glassy B_2O_3 can have a triangle and/or tetrahedron forming three and four oxygen coordinated neighbors as structural units, and the high strengths of covalent B–O bonds enables borates to form stable glasses [25-26]. Introduction of some trace elements into glass network rearranges the glass internal structure by converting $[BO_3]$ to $[BO_4]$ structural units and leads to the formation of various borate groups. These additives also act as a modifier oxide in the glass matrix and a nucleating agent for crystallization of the glass [27-28]. These glass systems have been under intense research to understand biocompatibility and bioactivity through *in vitro* and *in vivo* techniques.

Besides biocompatible and bioactive behavior, the mechanical and structural properties of bioactive glasses are considered to be very important in evaluating the effectiveness of glass used for bone replacement. However, the mechanical testing of glass materials is quite difficult because it is a fragile material and difficult to mold. The method of assessing its elasticity and strength is therefore quite limited. Among the diverse methods required high precision, ultrasonic non-destructive technique is found to be the versatile tool for understanding the association of the structural characteristics and mechanical properties of amorphous materials [29]. The ultrasonic examination helps to understand the interatomic and ionic forces including the potentials in lattice structure [30-31]. The acoustic velocity as well as the density of glasses can be considered as parameters of elastic constants related directly to changes in the glass structure. Combined with the use of FTIR, the confirmation of the structural units of glass components has been received continuous attention. Moreover, this measurement can also describe the microhardness of materials, which is correlated directly with its strength, wear resistance and other mechanical properties [32-33]. As a result, microhardness investigation by various techniques is widely considered for material evaluation. Since the values of elastic moduli and microhardness depended on an applied load, the design to control pressure on the ultrasonic measurement is required. Therefore, the consideration of the most appropriate materials for specific application requires a knowledge of their mechanical and structural properties.

Recently, the world society has campaigned to reduce the use of pure chemicals and promoted to apply more recycling or natural products. Biomass developed from agricultural production wastes and energy crops is discovered abundantly in nature, especially tropical countries like Thailand [34-35]. Bagasse and cassava rhizome are the biomass sources derived from valuable by-products in sugar extraction and waste of cassava fructification, respectively. These wastes are often burned as fuel to generate electricity. However, incineration of bagasse and cassava rhizome as an energy source causes serious disposal problems, especially air pollution (PM2.5 and PM10) [36-38]. There are several studies of using bagasse and cassava rhizome ashes in many alternative applications such as production of ceramic, bio-composite, biomaterial, cement and concrete, etc [39-41]. Conversion of these ashes into the raw materials for preparing bioactive glass is one of alternative ways that may provide enormous benefits,

because it is compatible with human biological tissue. Several studies have tried to modify properties of bioactive glass by adding some of pure elements into the glass network. An interesting new direction is the substitution of these pure materials by biomass materials. Bagasse and cassava rhizome ashes not only contain SiO_2 and CaO that can be the main composition, but also contain some elements stimulating new bone formation also including angiogenesis inducement, anti-inflammatory effect, bone cell adhesion and stability such as Al, Mg, Sr, Ti, Zn and so on (see in Table 3.1). Therefore, the replacement of pure materials by these agricultural wastes for fabrication of bioactive glass can be a novel way in recycling these wastes. Borate-based glasses added with bagasse and cassava rhizome, moreover, may be candidates for bone tissue engineering applications where controlled-release glasses with lower degradation rates are required.

1.2 Objectives

1.2.1 To fabricate and characterize a novel bioactive glass prepared from treated bagasse and cassava rhizome via melt quenching method

1.2.2 To study the effects of bagasse and cassava rhizome on physical, mechanical, structural, and bioactive behaviors of soda-lime borate glass system

1.2.3 To compare the structure and morphology of the bioactive glass before and after immersion in SBF solution

1.2.4 To study the effects of bagasse and cassava rhizome on dissolution rate of the soda-lime borate bioactive glass as well as pH of the solution

1.3 Scopes of research

The search for novel materials which can be substituted bone has received continuously attention for many years. There is a significant amount of work that has been conducted in the tissue engineering field to fabricate materials capable of bone regeneration. It is apparent that the number of parameters that affect both bioactivity and degradation is very large and can be very specific for each material. Glasses and glass-ceramics for bone regeneration could be used in different parts of the human body where load-bearing may or may not be essential. This makes every material unique in many terms, not only of properties, but also composition and processing characteristics.

Taking all these into account, it is understandable why research in the field is so demanding but also so challenging.

Although there are numerous publications on the potential use of combinations of glasses or bioactivity fillers for bone regeneration, little information exists on the assessment of glass prepared from agricultural wastes or fly ash natural materials. Therefore, the scope of this research was to fabricate a novel biomaterial based on soda-lime borate glasses added with bagasse and cassava rhizome, and then investigate them in terms of *in vitro* bioactivity, degradability, structural, physical, and mechanical properties. A comparison between these compositions containing a glass material before and after SBF solution would provide an understanding of the degradation rates and the different reactions between glasses and dopants leading to bone regeneration. The elastic moduli and microhardness parameters have been evaluated through pulse-echo ultrasonic technique. The pressure-controlled technique for measuring ultrasonic wave velocities was designed to control a suitable applied load. Vickers hardness tester was also applied to determine microhardness of the glass using an applied load of 0.98 N. Moreover, the bioactive glass is studied through structure and morphology before and after immersion in SBF solution. It also includes monitoring the pH values of the solution in each period of time.

1.4 Expected outcomes

1.4.1 Ability to maximize utilization of agricultural wastes, bagasse and cassava rhizome, by fabricating novel bioactive glasses

1.4.2 Knowledge and technique for testing on mechanical properties with pulse-echo ultrasonic and Vickers microhardness techniques

1.4.3 Knowledge and technique for *in vitro* bioactivity test to study the structural, morphological properties before and after soaking in SBF solution to evaluate the hydroxyapatite formation on glass surface

1.4.4 Knowledge of degradability behavior of bioactive glass added with bagasse and cassava rhizome

1.5 Research sites

1.5.1 Department of Physics, Faculty of Science, Ubon Ratchathani University, Thailand

1.5.2 Glass Technology Excellent Center (GTEC), Faculty of Science, Ubon Ratchathani University, Thailand

1.5.3 Department of Chemistry, Faculty of Science, Ubon Ratchathani University, Thailand

1.5.4 Department of Industrial Engineering, Faculty of Engineering, Ubon Ratchathani University, Thailand

1.5.5 Scientific Equipment Center, Ubon Ratchathani University, Thailand

CHAPTER 2
THEORETICAL BACKGROUND AND LITERATURE REVIEW

All of the theoretical background and literature review will be clearly presented in this chapter. This chapter begins with an overview of bone tissue engineering and bone physiology. It then covers the characteristics of how to treat damaged bones and bone replacement materials. Principles of bone tissue engineering are introduced to understand a basic of tissue transplantation in the human. To understand more, the information about bones in the human has been put forward. Biomaterials used as bone graft substitutes, especially bioactive glass that studied in this work, are reviewed. After that, the properties and several tools for evaluating the feasibility of using the bioactive glass as a bone graft material *in vitro* are briefly demonstrated. It ends with the related works to more understand this research have been reconsidered and summarized.

2.1 Concept of bone tissue engineering

Damage of tissues and organs in humans due to congenital deformities, trauma, and diseases remains major healthcare challenges worldwide [42-43]. The demand of reparation or regeneration on engineered bone tissue has been continually growing every year in direct relation to the increasing of the human population. Defect of tissues can be replaced or repaired by transplantation. Tissue transplantation including bone and tooth in human has been performed continuously, which however is seriously limited by the number of available donors and the effective biocompatible materials inclusive high process cost [43]. Tissue engineering (TE) is an interdisciplinary field technology that combines materials engineering, biomedical engineering and cell biology into developing functional substitutes to restore the structures and functions of damaged or degenerated tissues. Tissue engineering is one of the promising alternative approaches to treat the loss or malfunction of a tissue or organ without the limitations of current therapies [43-44]. Tissue engineering strategies a three-dimensional structure, termed “biomaterial scaffold”, fabricated from a suitable artificial or natural material. An ideal scaffold for bone tissue engineering applications should not only provide a passive

structural support for bone cells, but it also should favorably affect bone formation by stimulating osteoblastic cell proliferation and differentiation [45]. Figure 2.1 illustrates the concept of tissue engineering and its procedures. Engineered biomaterial is able to serve as temporary scaffolds and promote the reorganization of the cells to form a functional tissue or organ.

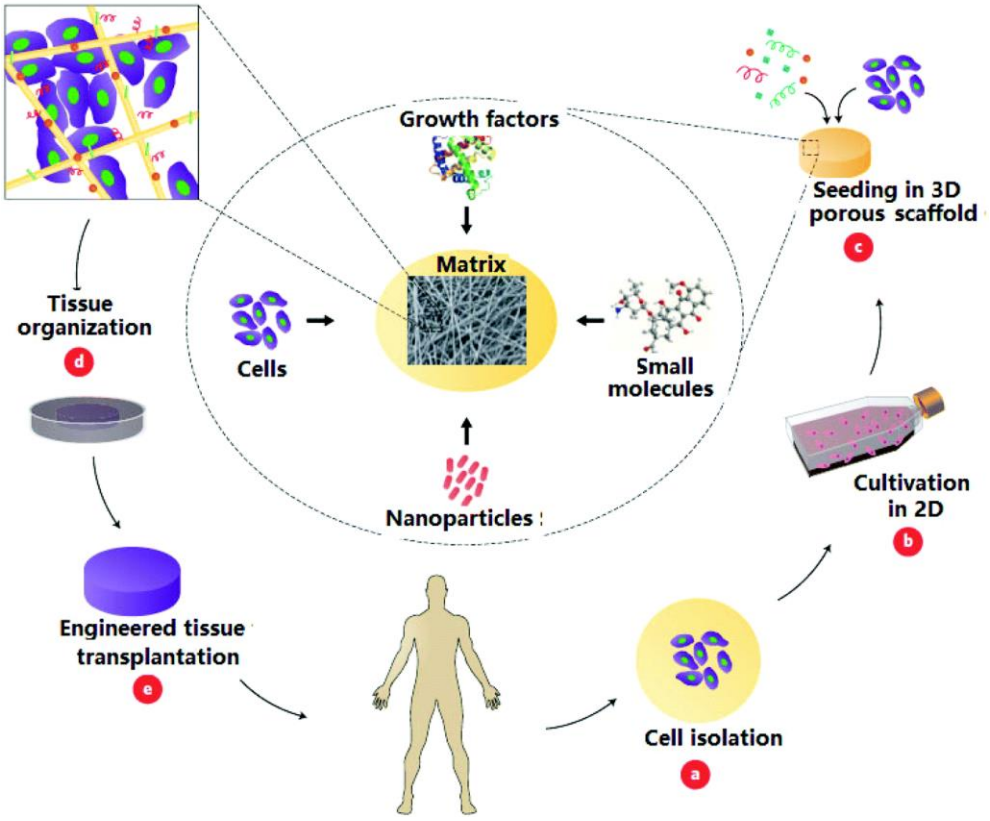

Figure 2.1 A schematic overview of the steps involved in tissue engineering concept and its procedures [43]

Tissue engineering applies cells, materials, and biochemicals to develop biological substitutes that restore, maintain, or improve function of damaged tissues or organs. Successful tissue regeneration necessitates the design of an advanced smart biomaterial, as a temporary extracellular matrix (ECM) scaffold, that is capable of inducing host cells to assume highly specialized functions [46]. Specific cells isolated from the patient are seeded in or onto scaffold materials after being efficient expanded under *in vitro* 2D cultivation. The scaffolds can be loaded with drugs, growth factors with the main aim

of stimulating the cells. The scaffold–cell constructs are further cultivated to form a functional tissue or organ. After the successful formation of a functional tissue or organ, the construct is transplanted into the defect sites of the patient [43-44].

2.2 Bone tissue and physiology

Bone tissue (osseous tissue) differs greatly from other tissues in the human body. Bone is hard and many of its functions depend on that characteristic hardness. Later discussions in this chapter will show that bone is also dynamic in that its shape adjusts to accommodate stresses. This section will examine the gross anatomy of bone first and then move on to its histology.

2.2.1 Bone tissue engineering

Although human bones have a certain self-healing ability, they are powerless for large bone defects. To overcome the problems, bone tissue engineering is proposed on the basis of tissue engineering. Bone tissue engineering aims to induce new tissue repairing and regeneration by the synergy of cells, signals and scaffolds [47]. A scaffold composed of biomaterials is a carrier of cells and signals. Figure 2.2 presents the major strategies of bone tissue engineering.

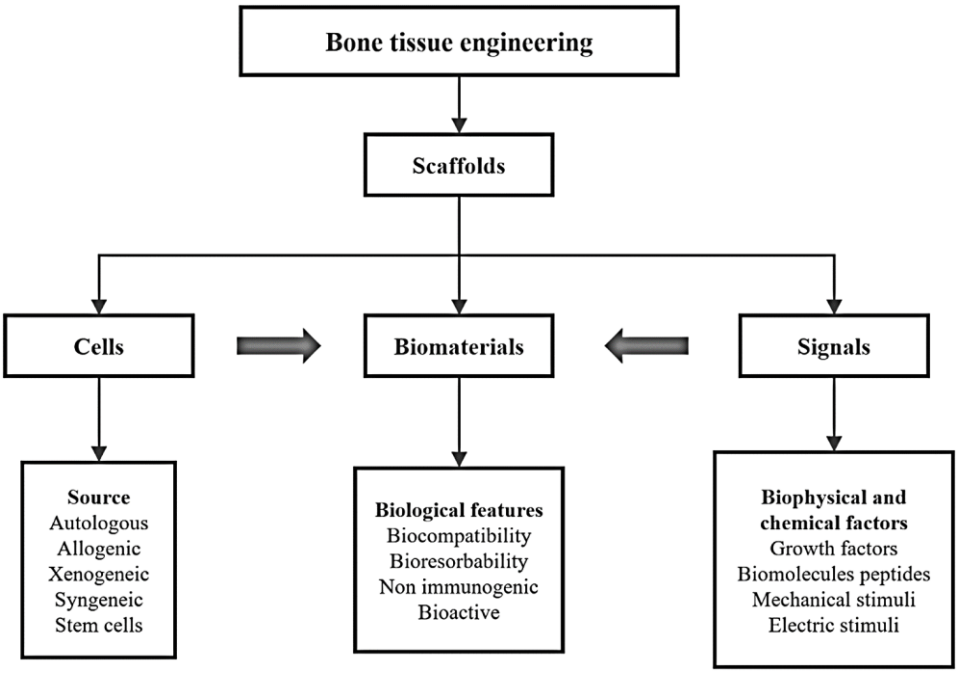

Figure 2.2 Diagram showing strategies for bone tissue engineering [47]

Bone is the second most common transplanted tissues after blood, as bone failure can widely result from trauma, tumor, bone related diseases or aging [48-49]. A lot of worldwide patients have been received bone defect repairs with an enormous cost, and they are likely to increase in the near future. Bone grafting is a wide variety of surgical procedure replacing damaged bone in order to repair bone fractures or stimulate the formation of new bone [49-50]. All methods of bone grafting involve adding some materials to the specific site where bone is needed as a means of stimulating a new or more effective bone healing response. The bone graft acts as a temporary calcium deposit on which a patient's own bone eventually grows and replaces in the bone-fusing process called "creeping substitution" [51]. There are key principles involved in successful bone grafts; (1) guiding the reparative growth of the natural bone (osteoconduction), (2) encouraging undifferentiated cells to become active osteoblasts (osteoinduction), and (3) living bone cells in the graft material contribute to bone remodeling (osteogenesis) [52-53]. Allograft (cadaveric bone obtained from a donor) and autograft (bone harvested from the patient’s own body) are considered the standard for the common bone grafting technique, especially when the defect site requires large volumes of bone [48,53]. The problem is that there is only limited bone can be harvested, and there is risk of donor site morbidity. In addition, a large proportion of patients suffer significant pain at the donor site. Currently there is a shortage in allograft bone graft material. Therefore, there is a strong demand to find alternative solutions for treating bone defects.

A robust way for bone repair and regeneration has been successfully done in bone tissue engineering field with synthetic materials (often made of hydroxyapatite or other naturally occurring and biocompatible substances) with similar mechanical properties to bone. Most bone grafts are expected to be reabsorbed and replaced as the natural bone heals over a few months’ time. As the substitution of bone by biomaterials has shown great potential, there has been an increasing demand for biomaterials, which are also called bone graft materials. The biomaterials are designed to mimic the extracellular matrix (ECM) of desired bone and act as temporary matrices for cell attachment, proliferation, migration, differentiation and ECM deposition, with consequent bone in-growth until the new bone tissue is totally restored/regenerated.

2.2.2 Classification and function of bone [52,54]

Bone, which is alive and dynamic, is the most well-differentiated organ that originates from mesenchymal tissue. In terms of function, bone is primarily a structural, load-bearing organ. It provides protection to vital organs and bears loads that the body experiences, both from external forces and those that occur from muscle contraction. Bone provides the anchor point for that muscle contraction through its specialized tendon insertion sites. Bone's ligament insertion sites, which have the same structure as its tendon insertion sites, are essential to the function of joints. The articular cartilage that covers the ends of long bones, and which constitutes the bearing surfaces of joints, allows locomotion by the lower extremities and the positioning of the hands in space by the upper extremities. Bone also acts as a metabolic organ in its role as the storage depot of calcium and phosphate. It is the largest reservoir of calcium in the body, and the constant remodeling of bone mobilizes its calcium as one component of the process that tightly mediates calcium homeostasis. Bone remodeling also serves a structural purpose. The remodeling process positions the available mineralized bone tissue in an optimum distribution to bear the loads experienced by the skeleton.

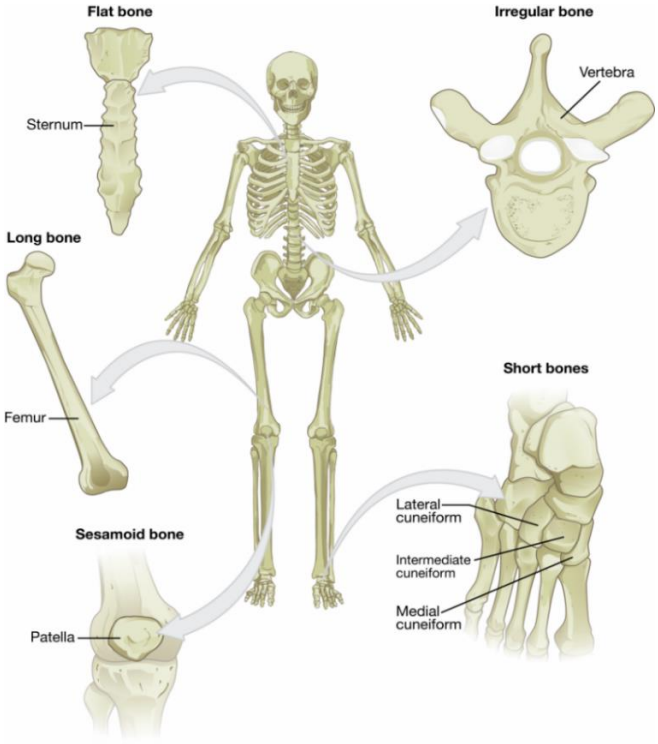

Figure 2.3 The classification of bones according to their shapes [54]

There are two basic types of bone tissue; cortical and cancellous bones. The cortical bone (also known as compact) is dense and homogeneous and forms the walls of bone. The cancellous bone (also known as trabecular or spongy) is composed of slender intertwined pieces of bone enclosing a space filled with non-bone tissue. It is found in the interior of normal bone. The bone in its entirety can also be classified according to shape comprising long bone, short bone, flat bone, irregular bone, and sesamoid bone, as shown in Figure 2.3.

Bone tissue is a model of biological efficiency with multiple functions as shown in Figure 2.4. The skeleton as a structural material must be strong enough to support the body weight and light enough for efficient movement. Bones in the load-bearing skeleton, as a material depends on the function, must be able to show stiffness under high loads (strength) and to absorb energy without fracturing (toughness) [55]. According to the announcement of Currey, strength is usually measured in well-controlled situations, whereas toughness accords better with what goes on in the rough-and-tumble of real life [56]. Other functions depending on bone structure include protection of internal organs, especially the brain. In addition to these structural functions, the bone tissue acts as a reservoir for minerals and protein important to the function of the body, especially calcium and phosphorus. These minerals, incorporated into bone tissue, can be released back into the bloodstream to maintain levels needed to support physiological processes. Bone is an important buffer for acid loads. Bone cells secrete endocrine hormones which regulate mineral metabolism and influence energy metabolism. Bone cells form niches that protect the hematopoietic stem cells.

Some functions of the skeletal system are more readily observable than others. While the body is moving, the bones facilitate the movement by serving as points of attachment for muscles and protect the soft organs of body. Just as the steel beams of a building provide a scaffold to support its weight, the bones and cartilages of skeletal system compose the scaffold that supports the rest of the body. Without the skeletal system, the body would be a limp mass of organs, muscle, and skin. Bones also protect internal organs from injury by covering or surrounding them. For example, the ribs protect the lungs and heart and the bones of the cranium (skull) protect the brain.

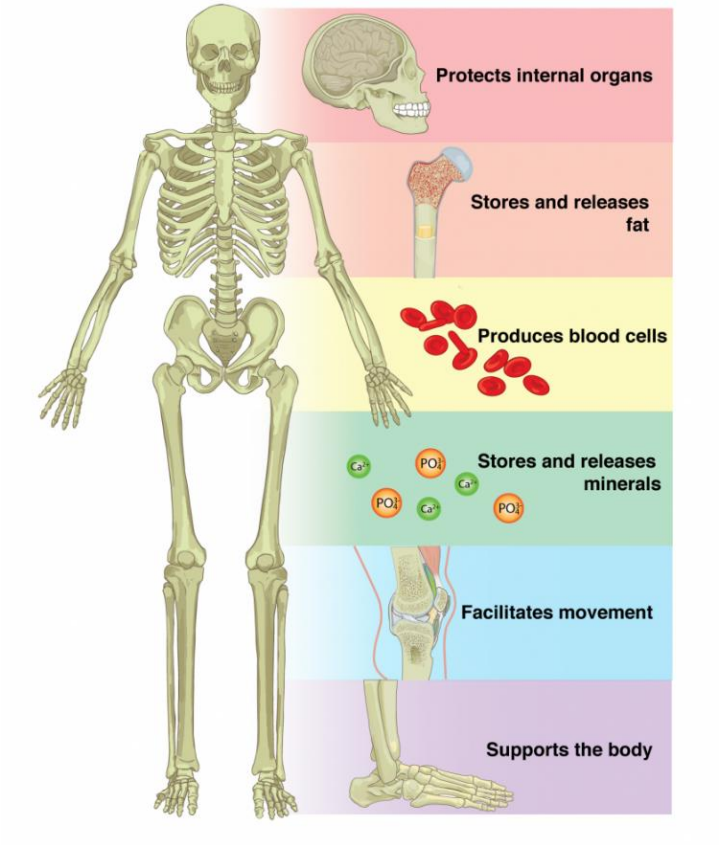

Figure 2.4 The functions of the skeletal system [54]

2.2.3 Bone structure and composition

Bone is a complex heterogeneous material with versatile structural and mechanical properties organized from the nanoscale to the macro-scale in hierarchical levels. It has a multifunctional structure that performs an important role in endocrine function, mineral homeostasis, mechanical support and protection [57].

As has been already aforementioned, the bone tissue is generally a mineralized tissue of two types; cortical bone and cancellous bone. The structure of these two types are shown in Figure 2.5; structure of a long bone with a magnified cross section of the interior. Although cortical and cancellous bones are made of the same matrix materials and cells, they are different in how they are organized, and their distributions and concentrations vary based on the bone's overall function. Cortical bone is dense so that it can withstand compressive forces, while cancellous bone has open spaces and is supportive, but also lightweight and can be readily remodeled to accommodate changing body needs [54].

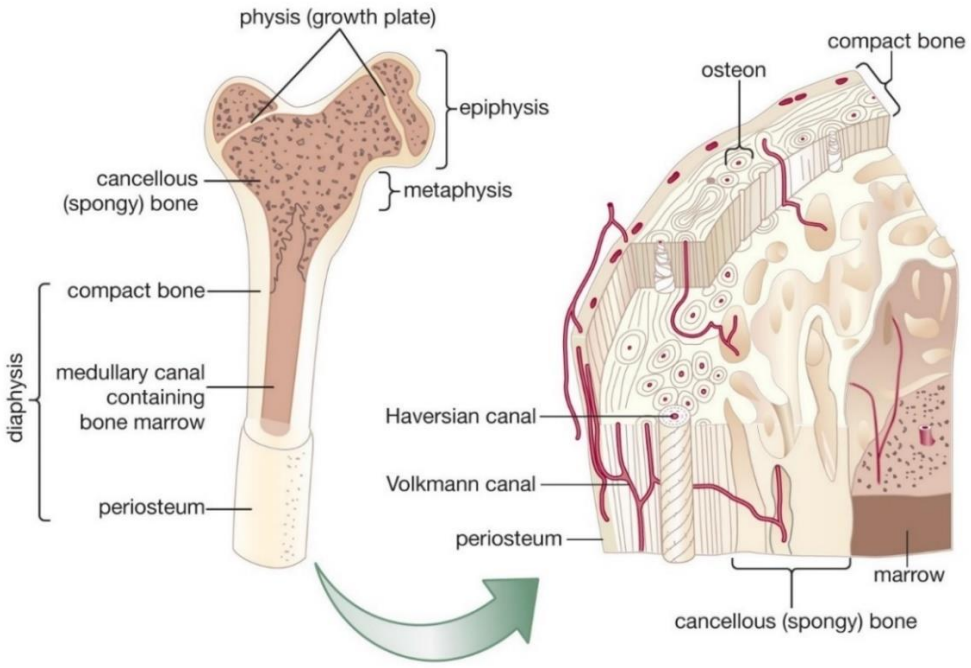

Figure 2.5 Structure of cortical and cancellous bone in a human long bone with a magnified cross section of the interior [58]

Cortical bone synonymous with compact bone implies forms the cortex or outermost shell of most bones. It is much harder, stiffer and stronger than cancellous bone. When compared to cancellous bone, the cortical bone is much more dense (~5 to 10% porosity) and accounts for 80% of the total bone mass [43,59]. The thickness of cortical bone in the pelvis ranges from 0.5 mm to 3 mm whereas in the femur the thickness ranges from 0.5 mm to over 1 cm in the shaft.

Cancellous bone, which is also referred to as trabecular or spongy bone, is porous bone found in the ends of long bones, proximal to joints. The cancellous bone has an open, honeycomb structure with a typical porosity of 50 to 95% and makes up the remaining 20% of total bone mass but has nearly 10 times the surface area of cortical bone. Cancellous bone is highly vascular and is composed of struts called trabeculae, each approximately 200 μm in thickness, as shown in Figure 2.6. At times the trabeculae appear to be organized into orthogonal arrays; often they are more randomly arranged. In contrast to cortical bone, cancellous bone is much more flexible, softer and less dense [60].

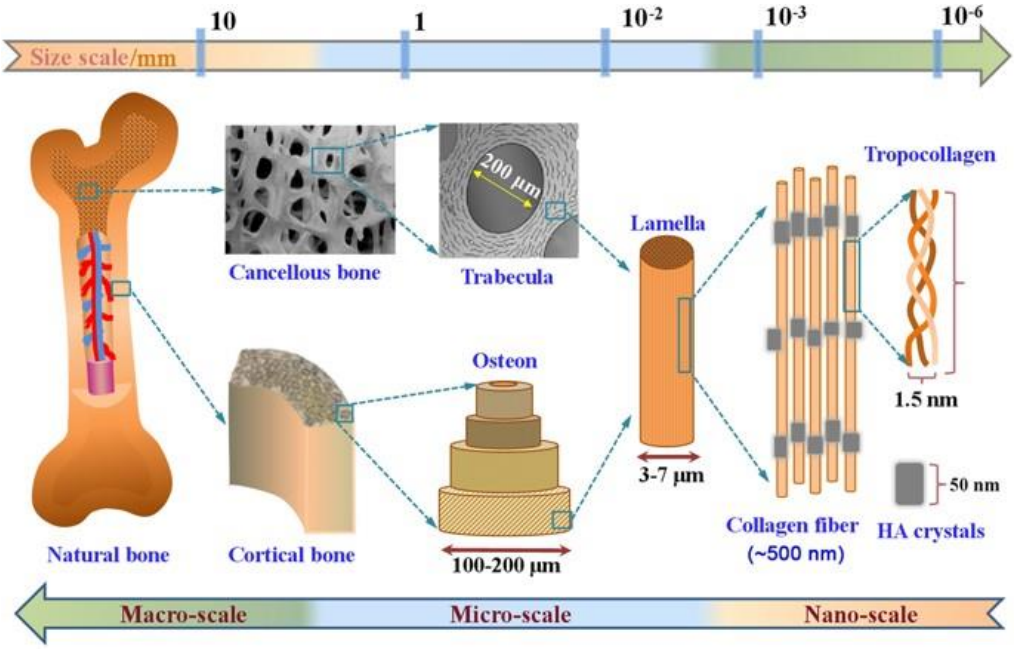

Figure 2.6 The chemical compositions and levels of hierarchical structural organization of natural bone [60]

Bone is a type of rigid and dense connective tissue, which constitutes part of the skeletal system. The architecture of bone is able to be described in terms of multi-scale structure as shown in Figure 2.6. These levels include macroscopic scale (cortical bone and cancellous bone); micrometer scale: a fibril array, its corresponding array patterns and osteons (100-200 μm); and nanometer scale: mineralized collagen fibrils (~500 nm) and embedded hydroxyapatite crystals (1.5–50 nm) [57].

In terms of composition, the cortical bone is comprised of inorganic mineral, organic protein (collagen, proteoglycans and non-collagenous protein), and water. Figure 2.7 shows schematic of bone composition between cortical and cancellous, including the brief composition of cortical bone. The mineral content in bone termed hydroxyapatite ($Ca_{10}(PO_4)_6(OH)_2$) is approximately 70% by weight and provides bone with rigidity and compressive strength [61]. The collagen imparts bone flexibility and tensile strength, while also imparting loci for the nucleation of bone mineral crystals. The specific role of the proteoglycans and non-collagenous protein is not entirely clear, and may function to control the location or rate of mineralization in bone. About 8% of the bone by weight consists of the water presented as bonded to other molecules.

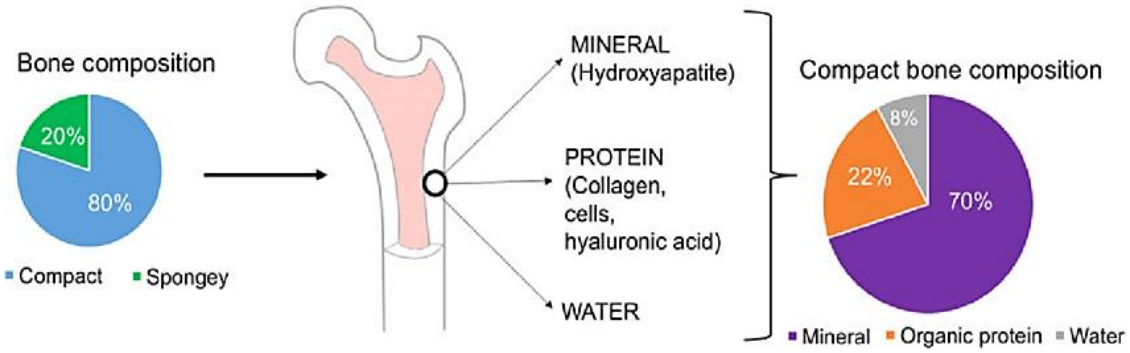

Figure 2.7 Schematic showing chemical composition of bone between compact (cortical) and spongy (cancellous) [61]

2.2.4 Different types of bone cells [54-55,58,62-63]

Bone is a connective tissue and like all connective tissues contains relatively few cells and large amounts of extracellular matrix. By mass, bone tissue matrix consists of 30% of collagen fibers and 70% of calcium phosphate salt. The collagen provides a scaffolding surface for inorganic salt crystals to adhere. These salt crystals form when calcium phosphate and calcium carbonate combine to create hydroxyapatite. Hydroxyapatite also incorporates other inorganic salts like magnesium hydroxide, fluoride, and sulfate as it crystallizes, or calcifies, on the collagen fibers. The hydroxyapatite crystals give bones their hardness and strength, while the collagen fibers give them a framework for calcification and gives the bone flexibility so that it can bend without being brittle.

Although bone cells compose less than 2% of the bone mass, they are crucial to the function of bones. There are four characteristic types of bone cells: osteoblasts, osteocytes, osteogenic cells, and osteoclasts. Osteogenic cells are undifferentiated and develop into osteoblasts. Osteoblasts deposit bone matrix. When osteoblasts get trapped within the calcified matrix, they become osteocytes. Osteoclasts develop from a different cell lineage and act to resorb bone. Figure 2.8 illustrates four classes of cells found within bone tissue.

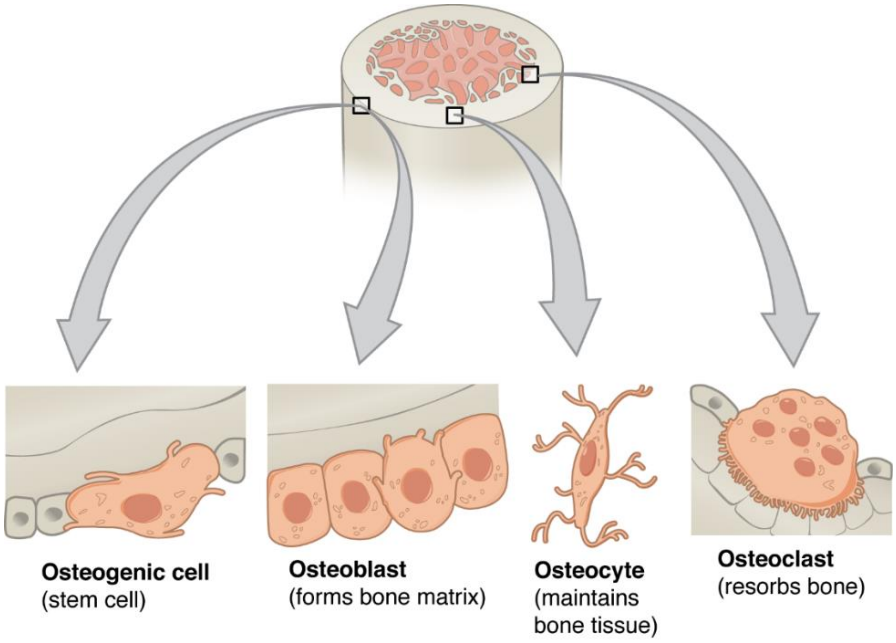

Figure 2.8 The category of bone cells within bone tissue [54,63]

The osteoblast is found in the growing portions of bone, including the endosteum and the cellular layer of the periosteum. The main function of osteoclasts is the resorption of bone matrix and mineralization and the forming new bone. It is easily recognized by its multinucleation as a result of several pre-osteoclasts' joining. Osteoblasts, which do not divide, synthesize and secrete the collagen matrix and other proteins. These cells act by adhering to the bone at sealing zone across where enzymes surrounding the osteoblast are secreted, the osteoblast become trapped within it. After resorption, osteoclasts undergo the death of cells when osteoblasts take over to produce the bone matrix. The mature osteoblasts are responsible for producing bone organic matrix and new bone formation. At the end of bone remodeling, the osteoblasts either become bone-lining cells or are absorbed into the bone as osteocytes which are the primary cell of mature bone and the most abundant cells in the bone (>90%) when the osteoblasts are no longer needed for matrix synthesis. Each osteocyte is located in a small cavity in the bone tissue. Osteocytes are responsible for holding the bone together whereas the lining cells protect the bone from harmful chemicals. In addition, the osteocyte maintains the mineral concentration of the matrix via the secretion of enzymes.

The structure and functions of bone cells contributed to a better understanding of bone biology. It has been suggested that there is a complex communication between bone cells and other organs, indicating the dynamic nature of bone tissue. The dynamic nature of bone means that new tissue is constantly formed, and old, injured, or unnecessary bone is dissolved for repair or for calcium release. The cells responsible for bone resorption, or breakdown, are the osteoclasts. These multinucleated cells originate from monocytes and macrophages, two types of white blood cells, not from osteogenic cells. Osteoclasts are continually breaking down old bone while osteoblasts are continually forming new bone. The ongoing balance between osteoblasts and osteoclasts is responsible for the constant but subtle reshaping of bone. The function and location of all the bone cells are presented in Table 2.1.

Table 2.1 Review of bone cells, their functions and locations [54]

Cell type	Function	Location
Osteogenic cells	Develop into osteoblasts	Endosteum, cellular layer of the periosteum
Osteoblasts	Bone formation	Endosteum, cellular layer of the periosteum, growing portions of bone
Osteocytes	Maintain mineral concentration of matrix	Entrapped in matrix
Osteoclasts	Bone resorption	Endosteum, cellular layer of the periosteum, at sites of old, injured, or unneeded bone

2.2.5 Bone fracture and repair [49,54,63-64]

A fracture is a cracked or broken bone. Bone generally has the ability to completely regenerate but requires a very small fracture space. A closed reduction is the treated procedure when a broken bone is manipulated and set into its natural position without surgery. Open reduction requires surgery to expose the fracture and reset the bone. While some fractures can be minor, others are quite severe and result in grave complications.

Fractures are classified by their complexity, location, and other features (see in Figure 2.9). Some fractures may be described using more than one term because it may have the features of more than one type (e.g., an open transverse fracture). The common types of fractures have been clarified as outlined in Table 2.2.

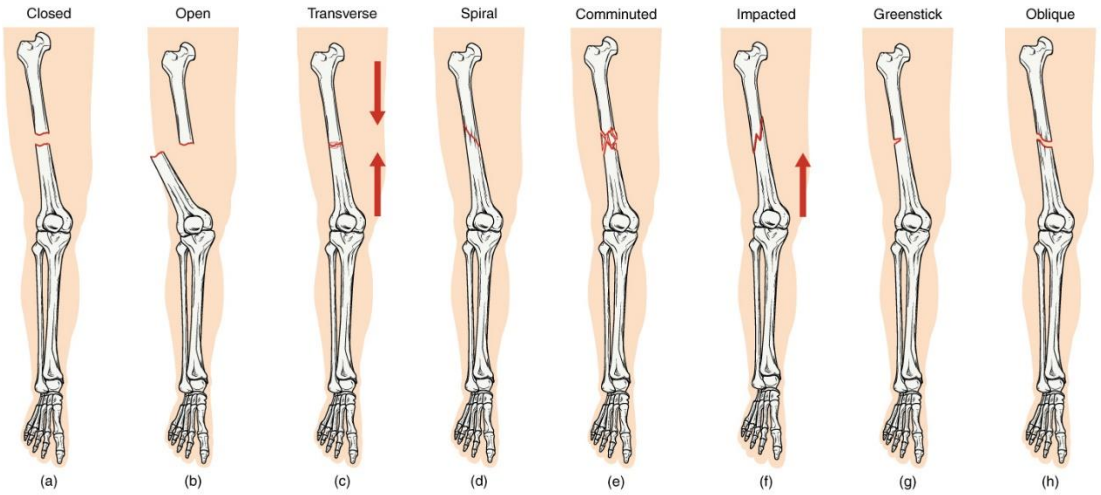

Figure 2.9 Fracture Types: (a) closed fracture, (b) open fracture, (c) transverse fracture, (d) spiral fracture, (e) comminuted fracture, (f) impacted fracture, (g) greenstick fracture, and (h) oblique fracture [54]

A broken fracture in bone is characterized by the loss of anatomic continuity and mechanical stability of bone. It can be caused by actively (sports, accidents, falls) or passively (low bone density, osteoporosis). The main types of bone fractures are simple, comminuted, and stress fractured. In simple fracture, bone is subjected to bending or torsion, resulting in a transverse, oblique or splined fracture, which separates the bone into two fragments. In comminuted fracture, bone is broken into several pieces, and in some cases shatters, as a consequence of a high velocity impact, such as a car accident and a high fall. In those cases, bone healing is challenging, not even able to restore in its original form. Stress fracture caused by low magnitude forces repetitively applied over long time can lead to compounding microdamage. Unlike simple and comminuted fractures, which heal via spontaneous repair processes, the stress fracture naturally repairs through normal bone remodeling. However, prolonged loading and irreparable microdamage may cause eventual failure of the bone joining.

Table 2.2 Description of the fracture types in bone [54]

Type of fracture	Description
Closed (or simple)	A fracture in which the skin remains intact
Open (or compound)	A fracture in which at least one end of the broken bone tears through the skin; carries a high risk of infection
Transverse	Occurs straight across the long axis of the bone
Spiral	Bone segments are pulled apart as a result of a twisting motion
Comminuted	Several breaks result in many small pieces between two large segments
Impacted	One fragment is driven into the other, usually as a result of compression
Greenstick	A partial fracture in which only one side of the bone is broken
Oblique	Occurs at an angle that is not 90 degrees

Depending on the type, severity of the fracture and distance between bone fragments, bones may heal directly by building new bone onto the fracture site (direct bone healing) or may heal in a process like endochondral bone formation (indirect bone healing). Direct bone healing is essentially bone remodeling in which osteoblasts and osteoclasts unite broken structures. With indirect bone healing, the process is more complicated and similar to endochondral bone formation in which broken bones form cartilaginous patches before growing new bone. In this process, blood released from any vessel torn by the fracture when a bone broke. These vessels could be in the periosteum, osteons, and/or medullary cavity. The blood begins to clot, and about six to eight hours after the fracture, the clotting blood has formed a fracture hematoma (Figure 2.10a). The disruption of blood flow to the bone results in the death of bone cells around the fracture.

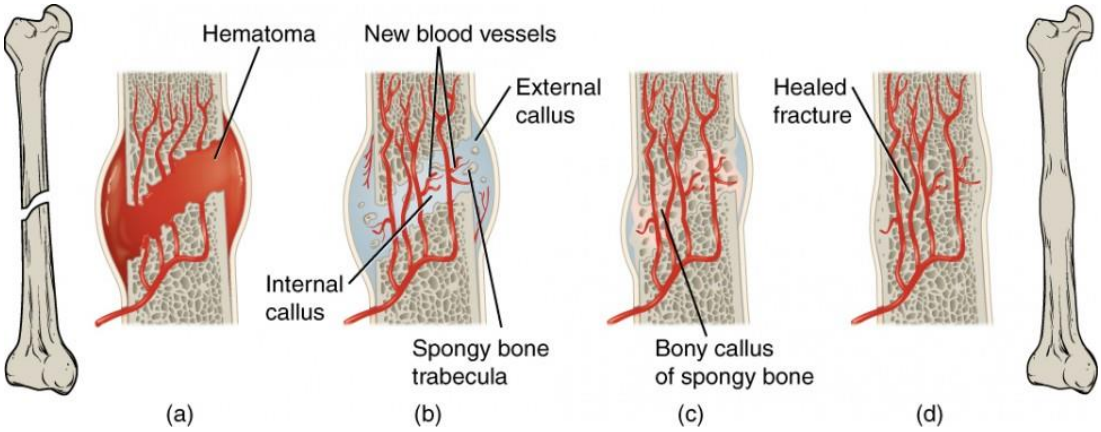

Figure 2.10 Stages in fracture repair: (a) a hematoma arisen from broken blood vessels, (b) formation of new blood vessels and calluses, (c) erosion of the cartilage and replacement by trabecular bone, and (d) conversion of immature bone to mature bone [54,64]

Within about 48 hours after the fracture, stem cells from the endosteum of the bone separate into chondrocytes which then secrete a fibrocartilaginous matrix between the two ends of the broken bone. This matrix connects the opposite ends of the fracture into an internal callus over several days to weeks. The periosteal chondrocytes form and working with osteoblasts create an external callus of cartilage and bone, respectively, around the outside of the break (Figure 2.10b). Simultaneously, these temporary soft calluses stabilize the fracture.

The osteoclasts absorb again the dead bone while osteogenic cells become active, divide, and differentiate into more osteoblasts. The cartilage in the calluses is replaced by trabecular bone via endochondral ossification (destruction of cartilage and replacement by bone), as shown in Figure 2.10c. This new bony callus is also called the hard callus.

Over several more weeks or months, compact bone replaces spongy bone at the outer margins of the fracture and the bone is remodeled in response to strain (Figure 2.10d). Once healing and remodeling are complete a slight swelling may remain on the outer surface of the bone, but quite often, no external evidence of the fracture remains. This is why bone is said to be a regenerative tissue that can completely replace itself without scars.

2.3 Biomaterials

Biomaterial or biocompatible material is commonly defined as nonviable materials that has been engineered to interact with biological systems for a medical purpose-either a therapeutic or a diagnostic one [65,66]. As a science, biomaterials are about fifty years old. The study of biomaterials has experienced steady and strong growth over its history, with many companies investing large amounts of money into the development of new products. Biomaterials encompass elements of medicine, biology, chemistry, physics, tissue engineering and material science [67].

Biomaterial is defined as a synthetic material that is in contact with the human tissue and that does not cause a toxic response within the human body as a consequence of its presence [68-69]. The use of non-biological materials as surgical implants is not new and especially the substitution of bone parts in the human body have been reported for centuries. However, only in the course of the 20th century have biomaterials acquired an important role in medicine, due to the introduction of sterilization techniques. Previously, surgical interventions were generally unsuccessful as a result of infections.

2.3.1 History of biomaterials

In the long history of human development, tissues and organs have evolved with respect to function after millions of years, but humans have been using artificial substitutes to repair damaged tissues only for decades. The limitations of bone replacement materials have resulted in the utilization of synthetic alternative materials for bone repair, replacement and enhancement. “Biomaterials” appeared in the early 1960s [70]. There are different types of biomaterials, i.e., biopolymers, bioceramics, biodegradable metals, etc. These materials have to be biocompatible and non-toxic.

The history of using biomaterials for scaffolds based on four different generations is briefly introduced. The first generation of biomaterials appeared in the 1960s. It aimed to achieve the performance of the biomaterial to match the replaced tissue with the least toxic reaction to the host. Generally, they are biologically inert, and interact minimally with the surrounding tissues. The first generation of biomaterials mainly includes: metals, synthetic polymers and ceramics. The most important feature of the second-generation biomaterials is their bioactive nature, and some biomaterials could be biodegradable *in vivo* studies [47]. They consist of synthetic and natural

polymers, calcium carbonates, calcium sulfates, calcium phosphates, and bioactive glasses. The third generation, the biomaterials are designed to induce specific beneficial biological responses by the addition of instructive substances based on the second-generation biomaterials with excellent properties and/or new biomaterials with outstanding performance. Some of the instructive substances include, but are not limited to, biological factors or external stimuli [15,47]. Fourth-generation biomaterials that can monitor extracellular and intracellular electrical processes are important for understanding both intra- and intercellular signaling and how cells communicate across large networks. Cellular electrical recording can reveal the fundamental behavior of cells and a cell network's response to external environmental stimuli [71].

2.3.2 Ideal characteristics of biomaterials

Any biomaterials must have some significant properties in order to be used in contact with human tissues. Apart from the specifications for its particular application, it must have a good resistance to corrosion and to wear, has to be non-carcinogenic, and finally the products of corrosion must be less toxic as possible [66,72]. The innovation of a biomaterial depends on its application so that different requirements may lead sometimes to very different and maybe opposite properties. In tissue engineering for example scaffolds need to be biodegradable so that the new tissue produced by cells can replace gradually the polymer or the bioactive glass of the scaffold. On the other hand, for instance in the case of an osteosynthesis plate, a stable material is required, which is wear resistant and does not degrade too quickly. Generally, the biomaterials for requirement can divide as follow [73]:

(1) Biocompatibility: The material must not induce a negative response in the host’s body, but rather favor good tissue-implant integration, especially at the interface between the implant and the tissue. However, there is almost always an initial inflammatory reaction when the material is implanted. If the inflammation remains for a long time it can cause tissue necrosis, and this has to be avoided.

(2) Serializability: The material must be sterilizable. The common methods include ethylene oxide sterilization, gamma rays and autoclaving. One technique is preferred rather than another according to the type of material that is being treated. For example, it is not possible to use autoclaving with most of polymers because they can depolymerize. In this case is therefore more desirable to use a gamma-rays sterilization.

(3) Formability: This is related to the possibility to shape the material for a particular function in an easy and economical way. It depends on the ability of the material to be shaped to suit a particular requirement. Furthermore, the material must be able to be shaped economically using engineering fabrication processes. For example, the wide use of coronary artery stents, is also due to the efficiency of the fabrication process that, through a heat treatment and cold working of the material, enables to have a product with high durability.

According to their behavior once implanted into the body, biological materials can differentiate into three different categories:

(1) Biocompatible materials: When the concentration of the substances they release is non-toxic, so they almost do not cause any inflammation reaction and they are not rejected by the surrounding tissues.

(2) Bioactive materials: The bioactive materials are generally associated with a positive reaction of the tissue. The reaction at the interface between the implant and the tissue is very important, so, for instance, the formation of new bone at the implant-tissue interface is a parameter that can characterize a bioactive material.

(3) Resorbable materials: The resorbable materials are hydrolytically and enzymatically degradable. They are able to completely disappear after implantation, avoiding the necessity of a second surgery, e.g., biodegradable sutures made with poly (lactic acid) or poly (glycolic acid).

2.4 Bioactive glass materials

Bioactive glass is able to be defined by its name itself, which include “Bioactive”, refers to one that elicits a specific biological response at the interface of the material which results in the formation of a bond between the tissues and the material, and “Glass”, often defined as solid that possesses a non-crystalline solid (amorphous) structure at the atomic scale and that exhibits a glass transition when heated towards the liquid state [74]. It is generally composed of network forming, modifying and intermediate oxides. Briefly, bioactive glass has been designed to elicit a particular biological reaction at the interface of the material, which stimulates cell proliferation, gene response and the formation of a bond between living tissues and the material.

Bioactive glass is important to the field of biomaterials as one of the first completely synthetic materials that seamlessly bonds to bone. The bioactive glasses are a subset of inorganic biomaterials with clear bone bonding and osteoinductive properties due to its similar mineral content [75]. Bioactive glass is normally used to produce a hydroxyapatite layer on a surface, which bonds firmly with living bone strengthening the tissue [23]. When bioactive glasses were exposed to physiological fluids, tenacious bonds will be formed with bone via the formation of bone-like hydroxyapatite (HA) layers bonds and the biological interaction of collagen with the material surface. These surface reactions lead to the release of critical concentrations of soluble ions, e.g., Si, Ca, P, B, and Na. These ions induce favorable responses both intracellular and extracellular, that result in rapid bone formation [75-76]. However, these materials can only be used in a low stress bearing area, due to their weakness and low fracture resistance.

Bioactive glasses show unique systems because they can elicit a suitable biological response. They are able to form bonds with soft and hard tissues by means of reactions' series. The formed interface between the glass and the tissue is therefore strong and compliant [76]. This makes these materials the superior choice in tissue engineering scaffolds. Furthermore, bioactive glasses have high tissue integration and regeneration quality. A range of bioactive glasses with attractive properties, like biocompatibility and bioactivity, and synthesized by newer methods have been developed. Both degradation and bioreactivity can also be influenced by varying their chemical composition and structure [77]. The surface characteristics and the mechanical properties of bioactive glasses are also favorable for application in bone replacement materials. Various investigations have been undertaken to obtain bioactive glasses in different forms, such as bulk, powder, composites, and porous scaffolds. Bioactive glasses are used as implants to repair or replace parts of the body; long bones, vertebrae, joints, and teeth [78]. Moreover, they are effective in treatment of osteomyelitis and are associated with the release of angiogenic factors.

2.4.1 Structure and classification of bioactive glass

The first bioactive glass, 45S5 Biogalss®, was first developed by Hench et al. [6] in 1969, and represent a group of reactive materials that are able to bond to mineralized bone tissue in physiological environment [77]. Over fifty years, the field of

bioactive glasses is widely used in the biomedical area and has experienced an impressive expansion worldwide, with numerous different compositions of bioactive glasses being investigated and finding a wide range of applications [5,14,77]. Besides common silica-based glasses, there are many categories of bioactive glasses. These major categories can be divided into silicate-based glasses, phosphate-based glasses, and borate-based glasses. These bioactive glasses are comprehensively reviewed elsewhere [11-13, 16-21]. The chemical composition of some bioactive glasses is shown in Table 2.3.

Table 2.3 Compositions of various bioactive glasses used clinically for medical and dental applications [1,12,79-80]

Compositions (wt%)	**45S5**	**13-93**	**6P53B**	**58S**	**70S30C**	**13-93B1**	**13-93B3**	**P50C35N15**
SiO_2	45.0	53.0	52.7	58.2	71.4	34.4	-	-
P_2O_5	6.0	4.0	6.0	9.2	-	3.8	3.7	71.0
B_2O_3	-	-	-	-	-	19.9	56.6	-
Na_2O	24.5	6.0	10.3	-	-	5.8	5.5	9.3
K_2O	-	12.0	2.8	-	-	11.7	11.1	-
MgO	-	5.0	10.2	-	-	4.9	4.6	-
CaO	24.5	20.0	18.0	32.6	28.6	19.5	18.5	19.7

In common glass production, monovalent oxides such as Na_2O are added to act as fluxing agents, decreasing considerably the melting temperatures of the glasses, and thus reducing the production costs. However, binary compositions of alkali silicate glasses have low chemical durability. For this reason, the oxides of divalent cations, such as CaO, are added to stabilize the glass. Common window glass is usually based on the soda–lime–silica (Na_2O–CaO–SiO_2) system. In the case of most bioactive glasses, the base components are usually SiO_2, Na_2O, CaO, and P_2O_5.

Among the numerous possibilities of cataloguing glasses, they can be classified according to their compositions. Usually, this takes into consideration the network former oxide that are present in the composition. Therefore, glasses can contain just one network former oxide, such as silicate, phosphate, and borate glasses, or more complex compositions with mixed glass network former oxides such as borosilicate, phosphosilicate, or borophosphate glasses.

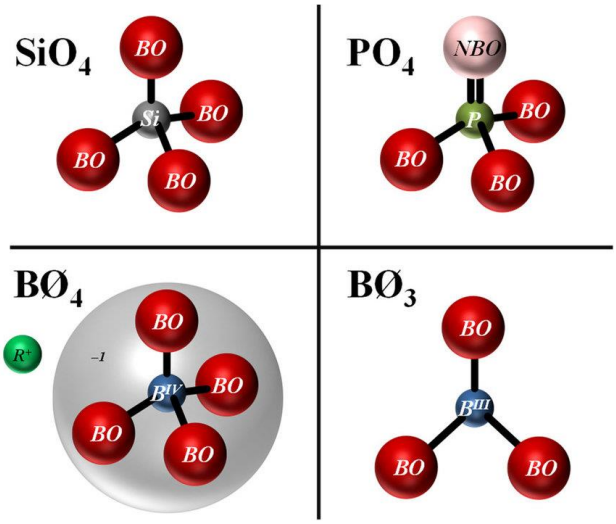

Figure 2.11 Schematic representation of structural units that build up an oxide glass network (R stands for a generic network modifier cation; Ø corresponding to BO atoms) [14]

By introducing some components such as alkali and alkaline earth oxides into the vitreous oxide networks, the extra oxygens do not form bridges, but rather form free ends, these have a different structural functionality. Depending upon the type of structural function, the oxide glasses are divided into three components [14]:

(1) Network formers are the components that build the glass network by forming oxygen tetrahedra and oxygen triangles, which are also called network units or structural units. The network formers are the essential components of the glass, being able to form 3D structures. These units are connected to each other by corner sharing creating oxygen bridges, which are called bridging oxygens (BO), as described by random network theory. The common examples are SiO_2, B_2O_3, and P_2O_5. Their schematic representations are presented in Figure 2.11.

(2) Network modifiers are the components that break down the glass network by creating terminal oxygens, which are also called non-bridging oxygens (NBO). The common examples are alkali and alkaline earth oxides.

(3) Intermediate oxides are the components that assume either the role of network formers or network modifiers, depending on glass composition. Some of the most common examples are MgO and Al_2O_3 (which is often not welcome in bioactive glasses, because contents greater than 1.5 wt.% Al_2O_3 in the glass tend to turn it bioinert, inhibiting bone bonding.

2.4.1.1 Silicate bioactive glasses [1,14,43,81]

Silicon dioxide (SiO_2), a common component of sand, is the most common network former due to the high valence of silicon (Si^{4+}). The basic building unit of silicate glasses is the SiO_4 tetrahedron (see in Figure 2.11), which can be connected to up to a maximum of four other tetrahedra through covalent bonds via its corners. Adding network modifiers to glass composition results in the disruption of the continuity of the glassy network due to the cleavage of some of the tetrahedra Si–O–Si bonds, leading to the formation of NBO groups and resulting in a decrease in the number of BO and network connectivity.

Silicate-based glasses are the most widely applied bioactive glass which is based on the 3D glass-forming SiO_2 network in which silicon (Si) is four-fold coordinated to oxygen (O). These glasses offer remarkable advantages as the inorganic components of composite scaffolds due to their high bioactivity index, and their ability to bond to both soft and hard connective tissues. They are osteogenetic and osteoconductive materials while there is another type of bioactive materials such as HA that exhibit only osteoconductivity. With their unique biological properties such as excellent bioactivity, biocompatibility, as well as osteogenic and potential angiogenic effects, there has been extensive and continuous research work on silicate glasses for biomedical applications including bone tissue engineering. The superior bioactivity of 45S5 is due to its relatively low SiO_2 content, high Na_2O and CaO content, and high CaO/P_2O_5 ratio. Another popular bioactive glass designated “13-93”, is based on the 45S5 composition, but it has a relatively higher SiO_2 content and additional network modifiers, i.e., K_2O and MgO. 13-93 glass has a suitable viscous flow behavior and it exhibits lower tendency to crystallize than 45S5. These features mean that 13-93 glass

has better processing characteristics than 45S5. However, 13-93 glass degrades more slowly than 45S5 which may be a disadvantage for some applications. Both types of silicate bioactive glasses are known to support cell proliferation and differentiation *in vitro* (culture experiments) and to enhance bone formation *in vivo* (animal experiments). In addition to 45S5 and 13-93 glasses, several other silicate-based bioactive glasses such as 58S and 70S30C have also been widely researched.

Silicate bioactive glass acts as a miracle material, because these compositional oxides provide unique characteristic features. Its surface becomes highly reactive when exposed to physiological environments due to the presence of high amounts of Na_2O, CaO, and P_2O_5. Recently, additional elements such as magnesium, strontium, fluorine, iron, and silver have been intentionally incorporated in the silicate network composition to enhance the material properties. In addition, silicate-based glasses have been shown to increase the secretion of vascular endothelial growth factor *in vitro* and to enhance vascularization *in vivo*, suggesting that scaffolds containing controlled concentrations of bioactive glass might stimulate neovascularization, which is beneficial to large tissue engineered constructs.

2.4.1.2 Phosphate bioactive glasses [1,12,14,43,82]

Phosphate glasses consist of an inorganic phosphate network of PO_4^{3-} tetrahedral units, with each one connected to a maximum of three other phosphate tetrahedral units through covalent P–O–P bonds. The structure of P retains its fourfold coordination throughout the full composition range from pure P_2O_5 to orthophosphates fully saturated with alkali oxides. Structurally, the effect of the incorporation of network modifier oxides into phosphate glasses is similar to the effect in silicate glasses, i.e., the P–O–P bonds are broken, and NBO atoms are formed. When these glasses contain more modifiers than phosphate, they are often called invert glasses, and the glass properties are dominated by ionic bonds between NBOs and modifier cations, rather than the covalent P–O–P bonds

Phosphate-based glasses have gained high interest as bone filling material for bone tissue engineering because of their high solubility, which can be tailored by varying the composition, and their chemical similarity to the inorganic phase of human bone. Moreover, early studies on phosphate glasses have shown that they are non-toxic with regard to macrophage cells promoting adequate support for osteoblastic

cell responses. The structure of phosphorus oxide is based on a tetrahedron unit. Phosphorus is a pentavalent ion and so the formation of P−O tetrahedron with four bridging oxygens would produce an impracticable unit with a net positive charge of +1. A charge balanced tetrahedron is able to be created, however, if one of the oxygens builds a double bond with the ion, while the other three oxygens form bridging oxygen with adjacent tetrahedral. Details of the structure of vitreous phosphate are dependent upon the source of P_2O_5 used to produce the melt.

Phosphate bioactive glasses have been proposed to develop materials which are able to completely dissolve into safe non-toxic dissolution products after they have performed their functions. These glasses are based on P_2O_5 as glass-forming network, and CaO and Na_2O as modifiers. The dissolution rate of phosphate glasses can be tailored by modifying their compositions for example by adding appropriate oxides such as TiO_2, CuO and Fe_2O_3 into the glass composition. Phosphate bioactive glasses have been used as controlled release vehicles of antibacterial ions, e.g., silver, copper, zinc and gallium. Ionic dissolution products of highly soluble phosphate glasses have been shown to affect osteoblastic cell behavior in a dissolution rate depending manner. The glass compositions with lower CaO content, and thus lower dissolution rate, upregulated the proliferation of osteoblast cells and expression of genes, whereas glasses with higher CaO content caused inhibitions of osteoblastic cell growth and bone antigen expression. These bioactive glasses containing at least 46 mol% CaO do not produce any toxic effect on cells, but support attachment and proliferation of cells. In addition, they are promising as smart materials for soft tissue engineering applications because they can be spun into fibers and be used in flexible structures. Although phosphate glasses are also very interesting, they do not present bioactivity in the sense of the ability to form a calcium-phosphate (CaP) layer that bonds with bone.

2.4.1.3 Borate bioactive glasses [1,43,83]

Borate bioactive glasses are very reactive inorganic materials exhibiting relatively low chemical durability and consequently they convert more rapidly and completely to an HA-like material when compared to silicate bioactive glasses. The borate-based bioactive glass has controllable degradation rates in order to match the rate at which actual bone is formed. Bone formation has been shown to

enhance when using this type of material. The conversion mechanism of borate bioactive glasses to apatite is similar to that of silicate bioactive glasses. The bioactivity and degradation rate of borate glasses can be varied from hours to months by changing the glass composition. In addition, the sintering behavior of borate glasses is more controlled than that of silicate glasses because they undergo viscous flow sintering more readily. As a trace element, boron is required for bone health. Borate bioactive glasses have been found to support cell proliferation and differentiation *in vitro* and tissue infiltration *in vivo*. Under static *in vitro* cell culture conditions, some borate bioactive glasses will exhibit toxicity to cells if borate ions release too much. However, the toxicity was diminished under dynamic *in vivo* culture conditions.

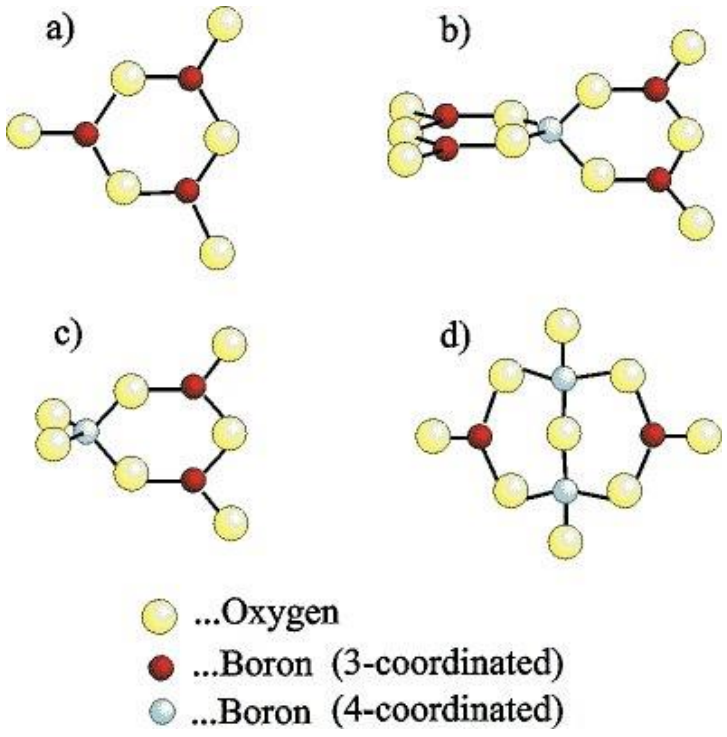

Figure 2.12 Structural groups represented in alkali borate glasses; (a) boroxol, (b) pentaborate, (c) triborate and (d) diborate groups [83]

The structure of vitreous boric oxide is able to be built of trigonal planar BO_3 and/or tetrahedral BO_4 units, as shown in Figure 2.12. Boron atoms in pure B_2O_3 glass are triangularly coordinated (boroxol group). The introduction of network modifying oxides to the glass would bring about some borons changing to tetrahedral coordination and more network connectivity. The difference in dimensionality, borate glass being planar versus the silicon-oxygen tetrahedra, can be used to explain the radical difference in the glass transition temperatures (T_g) of silica glass versus borate glass (T_g of B_2O_3 is ~260°C, while that of SiO_2 is ~1100°C). Further descriptions of glass structures always address the number and arrangement of bridging and non-bridging bonds which link each of the building blocks to their neighbors, i.e., the connectivity of the network. Most models for vitreous networks only consider connectivity as evidenced in the concentration and distribution of non-bridging oxygen (NBO). Network connectivity should not be considered solely in terms of NBO concentrations. Alkali borate glass, as an instance, is believed to convert boron ions from 3-fold (N_3) to 4-fold (N_4) coordination without the formation of NBOs with the addition of small concentrations of alkali oxides to the glasses.

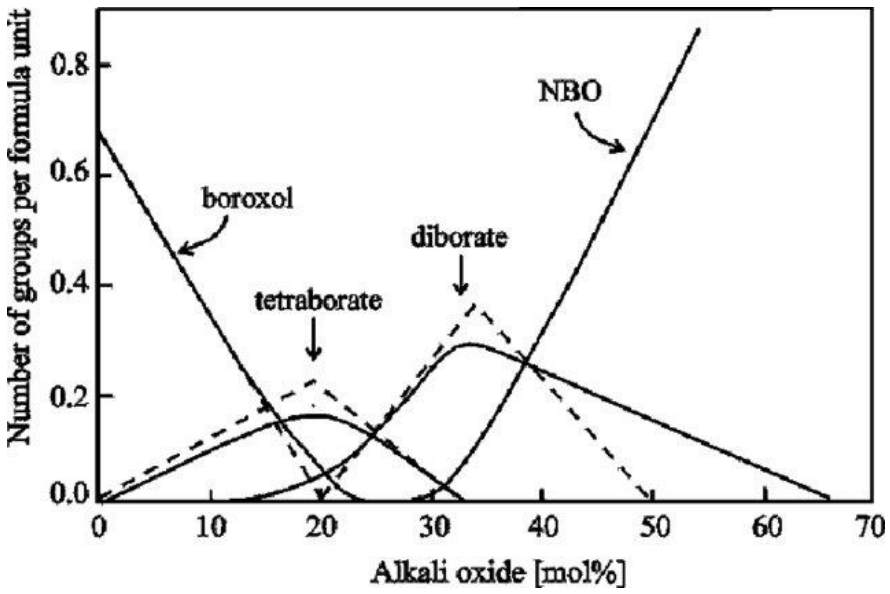

Figure 2.13 Effect of alkali oxide on the relative concentrations of intermediate range units in borate glasses (---- simple theory, — experimental results) [83]

The borate glass structure can convert from BO_3 to BO_4 units with no NBO formation by the addition of alkali oxide. This addition of alkali oxides (R_2O) to borate glass would increase T_g while the opposite would occur in silicate glass. The addition of R_2O to SiO_2 would increase the formation of NBOs thus lowering the T_g. Further addition of R_2O to B_2O_3 shows a continuous increase in T_g to a maximum and then a reversal in the property and compositional trend, known as the borate anomaly. This anomaly is associated with the coordination number of the composition and the transformation of planar boroxyl (3-fold coordination) groups to tetrahedral (4-fold coordination) and then to the diborate groups as the R_2O groups increase, as illustrated in Figure 2.13.

2.4.1.4 Ion-doped bioactive glasses

In addition to the typical compositions mentioned above, different amounts of other oxides can also be incorporated into bioactive glasses of silicate, phosphate or borate composition to adjust specific properties; for example, TiO_2, ZnO and AgO impart antibacterial properties to bioactive glasses, CuO can impart angiogenic effects [83-84]. Furthermore, some trace elements have also been incorporated into glass compositions, especially to provide the material with useful properties relevant for tissue regeneration. Although trace elements have beneficial effects, the risk of toxicity at high levels must be avoided, and for each considered ion further research is required.

It is believed that more similar system such as the host body will increase the bioactivity of the implant. The release of these ions after exposure to a physiological environment tends to improve the bioactive activities of the implant related to both osteogenesis and angiogenesis [74]. Thus, recent trend is to incorporate different ions into the composition of bioactive glasses to enhance their physical characteristics and therapeutic benefit. This incorporation of different ions in the composition of glass is called doping and it is very crucial for production of functional materials. In many cases, it was found that the functionality of the material is directly dependent on the doping elements. In some other cases, doping may improve surface structure of the implant or the physical attributes of it. Influences and functions of introduction of some specific ions on the characteristics of bioactive glass are summarized and collected as shown in Table 2.4.

Table 2.4 Effect and function of some ions on bioactive glass properties [11-12,14,74]

Ion	Effects and functions
Ca	• Supporting the osteoblast proliferation, differentiation and extracellular matrix (ECM) mineralization • Increasing expression of growth factors
Sr	• Showing the beneficial effects on bone cells and bone formation *in vivo* • Promising the agent for treating osteoporosis • Enhancing the metabolic activity in osteoblasts • Altering the bioactivity and rate of HA formation
Mg	• Stimulating the new bone formation • Increasing the bone cell adhesion and stability
Al	• Decreasing the degradation rate and consequently lower bioactivity • Stabilizing the glass structure
Zn	• Showing the anti-inflammatory effect and stimulates bone formation *in vitro* by activation protein synthesis in osteoblasts • Regulating transcription of osteoblastic differentiation genes
Ti	• Decreasing the degradation rate • Showing the strong antibacterial efficacy
Zr	• Increasing the fracture toughness • Non-toxic substance release • Decreasing the bioactivity
Cu	• Significant amounts of cellular Cu are found in human endothelial cells when undergoing angiogenesis • Promoting the synergetic stimulating effects on angiogenesis • Stimulating the proliferation of human endothelial cells • Inducing the differentiation of mesenchymal cells towards the osteogenic lineage
Ag	• Comprising antibacterial activity to bioactive glass • Influencing on the toxicity of bioactive glass • Declining the dissolution of the bioactive glass
F	• Decreasing the glass transition and glass crystallization • Enhancing the biocompatibility • Promoting the formation of fluorapatite (FAP)

2.4.2 Glass synthesis methods

Depending upon the required physical, chemical, structural, and biological properties, numerous routes can be employed for glass synthesis. Route selection also depends upon the production amount and compositional constituents required. All these techniques have their own implications regarding practicability and deployment. Some popular glass synthesis techniques of glass are explained in the following sections.

2.4.2.1 Melt quenching technique [73,74,85,86,87]

The melt quench technique, the classical way to obtain a glass by quickly cool downing of the molten material enough so that crystallization does not have time to occur, is the earliest known technique for preparation of glasses. More than 99% of the practical glasses are synthesized via this technique. The melt-quench technique is based on the fusion of crystalline raw materials (oxides, acids, or carbonates) into a viscous liquid, followed by the casting of melt through rapid quenching. During the initial heating process, these raw materials undergo a series of chemical and physical changes to produce the melt. Conversion of this melt to a homogeneous liquid may require further processing, including the removal of any un-melted batch remnants, impurities, and bubbles. The melt quenching method has certain advantages over the other techniques: (1) easiest of the known synthesis techniques; (2) high flexibility in the geometrical shape of glass; (3) easement in obtaining large materials in comparison with a single crystal; (4) high flexible regarding composition; (5) easy to improve its properties by changing compositions. The above-mentioned advantages have led to the increased popularity of the melt-quenching technique, and it has been extensively used to synthesize oxide/oxyhalide glasses.

The process of solidification without crystallization is called vitrification. As the temperature decreases, there is a reduction in the specific volume until the freezing point (T_f) which is equivalent to the melting point (T_m) for the inverse process of heating. There are two possible ways to continue the process at T_m. Primarily, a discontinuous change of volume appears, and crystallization occurs in the ABC curve. Another process, crystallization is avoided and liquid passes to a super cooled state as the path of the AD curve. The formation process of the crystalline and non-crystalline phase states is presented in Figure 2.14.

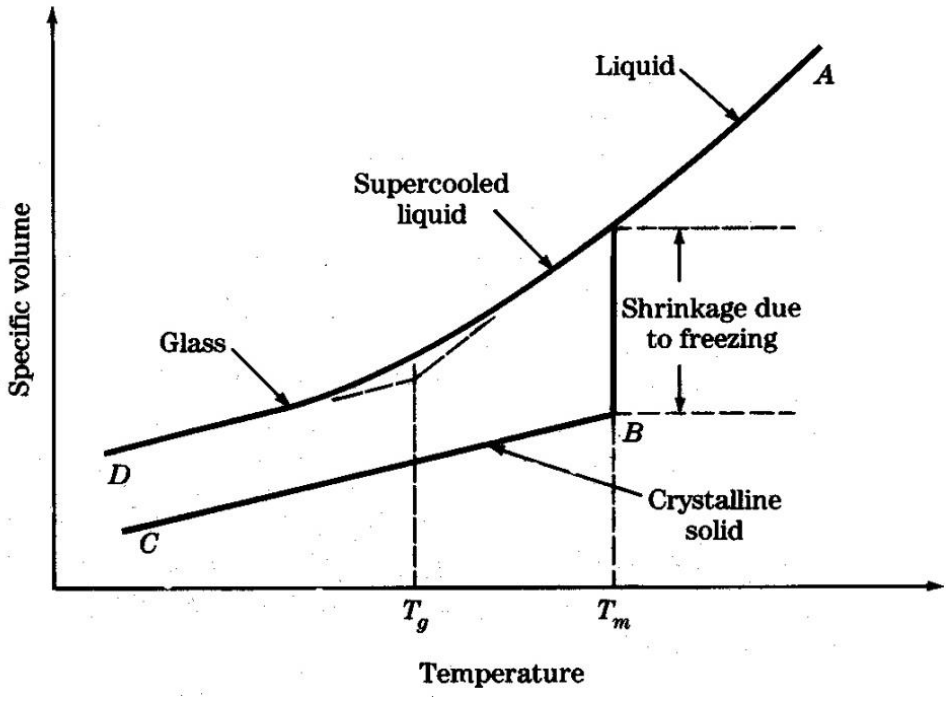

Figure 2.14 A schematic representation of the vitrification process with respect to the variation in the specific volume [87]

In the first case, after the crystallization has terminated, the slope of the curve becomes smaller as the solid contracts again. On the contrary, if the liquid transforms into a glass, below T_m there is no evidence of change in the coefficient of contraction of the super cooled liquid compared with the original liquid. Then after the glass transition temperature (T_g), the slope of the curve becomes similar to that of the crystalline solid. This temperature marks the transition of the supercooled liquid to a glassy state. The glass transition temperature, unlike T_m that is fixed, is a function of the cooling rate so that, for a constant pressure, as the cooling rate increases, the T_g slightly shifts to higher values of temperature. For this reason, it is better to speak of a transition interval rather than a transition temperature, where the limits of the interval are identified by the highest and slowest cooling rate used to determine T_g [88].

Most of those bioactive glasses were produced by melting raw materials at an elevated temperature because it is a simple, low-cost technique and does not take much time to complete. It typically involves raw materials selection, weighing, mixing of components in appropriate proportion and removal of impurities to get a

homogeneous melt. The reactivity of a glass in aqueous solutions is strongly dependent on the composition of the glass and thus the choice of composition is very important. Because the limited range of glass composition shows bioactivity, the glass composition should be chosen in a way so that it can be melted and formed into required shapes with available methods. The raw materials can be divided into five different categories according to their role: network former, network modifier, intermediate oxide, colorant, fluxing and fining agents. Glass formers are the most important components of glass as they form the matrix of the glass structure. Silica (SiO_2), phosphoric acid (P_2O_5) and boric acid (B_2O_3) are the most common type of glass former normally present in oxide glass. In between these silica is widely used; however, the melting temperature of silica is too high (1600–1725°C) and so different types of flux such as Na_2O and PbO can be used to decrease the melting temperature of the mixture. The addition of flux sometime degrades the properties of glass, which can be overcame by introducing different property modifier or intermediates such as boron, sodium, magnesium, titanium and calcium. Colorants are used to control the color in the final product. Finally, fining agents such as arsenic, antimony oxides, potassium and sodium nitrates are added to raw materials to remove bubbles from the melt. During melting of the raw materials inside the furnace, they react with each other and carbon dioxide and water vapor emission takes place, which causes the formation of bubbles. To raise the bubbles up to the upper surface of the melt, low viscosity is maintained. Batch particle size and their mixing in proper proportion are other factors that provide homogeneity in glass structure.

2.4.2.2 Sol-gel synthesis [74,85,89]

Sol-gel glasses are made by a chemical-based process at much lower temperatures than the traditional processing methods. The method has been recently accepted by a number of research groups to make a new generation of bioactive glass and offers assurance for tailoring the composition to match the specific requirements. Recently, scientists have preferred the sol-gel method in order to increase the specific surface area, and thus, the surface reactivity and degradability of the material. It also provides better control over homogeneity and purity. An overview of the sol-gel technologies and their products is shown in Figure 2.15.

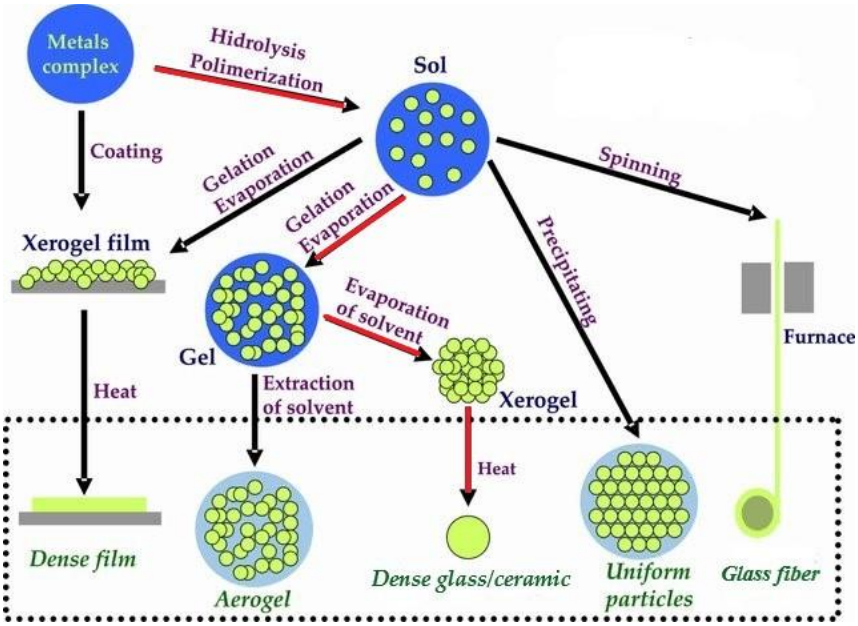

Figure 2.15 An overview of the sol-gel process [89]

In glass synthesis, there are generally three methods for making sol-gels: gelation of colloidal particles, controlled hydrolysis and condensation of metal alkoxide precursors followed by drying at ambient pressure. All the three methods create a three-dimensional, interconnected network. Gels can be categorized into three types, such as alcogels, xerogels and aerogels. Alcogels are generally alcohol based, whereas xerogels are formed from thermal removal of pore liquid. Gels with low density (80 kg/m^3) and large pore volumes (up to 98%) are called aerogels, which are the result of removal of pore liquid from the rigid network without collapsing it. Coagulation of the colloids, while they are standing in a mold or on a substrate (used as coating film), results in the conversion of sol into gel. The obtained gel is dried and sintered into a pore-free dense glass or glass film. The sintering is usually done at a temperature which is slightly above the glass transition temperature. The disadvantage of sol-gel synthesis is that the shrinkage of the wet gel produces fractures in the prepared glass. Other problems are the preferential precipitation of a particular oxide during sol formation for multicomponent glasses made from alkoxide precursors, and the heterogeneous precipitation of metal salts on the surface during the drying of a gel which was made using aqueous solutions of metal salts as the source of alkali, alkaline-earth oxides, etc. Although the sol-gel process has some disadvantages, this process has been extensively

applied for synthesis of bioactive glasses. This is because it works at relatively lower temperatures. The creation of the latest category of mesoporous bioactive glass (MBG) was possible only because of its sol-gel synthesis roots.

The starting materials are normally inorganic metals or metal organic compounds such as metals complexes that are subjected to a series of hydrolysis and polymerization reactions to form a sol. By processing the sol, several ceramic and/or glass materials can be obtained. Thin films are prepared on a piece of substrate by dip-coating or spin coating. To obtain the aerogel, which is a highly porous and extremely low-density material, the liquid is removed under a supercritical condition. Ultra-fine and uniform ceramic powders are formed by precipitation, spray pyrolysis, or emulsion techniques. A simple description of the sol-gel synthesis route is that a sol is prepared by dissolving metal ion complexes in a suitable organic solvent, and then by hydrolyzing, the sol forms as a colloidal metal oxide/hydroxide precipitate. After heating, the sol is transformed into a gel in which the metal oxide or hydroxide particles form a polymeric network enclosing the solvent. Then, the gel is heated at higher temperatures and the organic compounds are evaporated or decomposed, allowing the inorganic solid to crystallize, as shown in Figure 2.16.

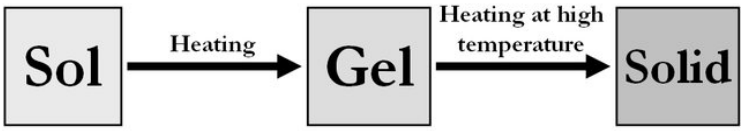

Figure 2.16 The basic steps of the sol-gel method [89]

2.4.2.3 Chemical vapor deposition [90]

Chemical vapor deposition (CVD) technique is based on the thermally activated, homogeneous oxidation or hydrolysis of an initial metal halide vapor (or mixture of metal halides) to form particulate glass material, followed by viscous sintering of the soot into solid, inclusion-free, glass 10 Applications of Nanocomposite Materials in Dentistry bodies. The oxidation or hydrolysis reaction is usually activated by either oxygen plasma or oxy-hydrogen flame. In the hydrolysis of halides by oxygen plasma, an oxide, along with the halogen gas (generally chlorine), is released as byproduct, but in hydrolysis using oxy-hydrogen flame, the byproduct

formed with oxide is HCl. The difference in both hydrolysis techniques is the level of OH contained in the glass, which is 1000 times more while using oxy-hydrogen flame for hydrolysis. The disadvantage of the CVD method is that it imposes restrictions on the preparation of glasses containing alkali, alkaline earth, and rare earth metals. The CVD process is extensively used to synthesize glasses and glassy alloys.

2.4.2.4 Microwave synthesis [85]

Microwave assisted synthesis of bioactive glass has been gaining attention in recent years. Microwave synthesis is a rapid and low-cost powder synthesis method in which can help to reaction in a short time and can modify the reaction environment to produce nano phase powders. For synthesis, the precursors were dissolved in de–ionized water and transferred to the ultrasonic bath. The irradiation time was varied to obtain the optimum synthesis condition. Microwave operation was performed in a second batch of powders after the ultrasonic irradiation. The obtained amorphous powder was washed in de–ionized water and filtered. After drying for 24 hours in oven at 80 ℃ the powders were calcined at 700 ℃ for the development of bioactive glass.

2.5 Mechanism of bioactive glass

Bioactive glass describes a group of surface reactive glass-ceramic biomaterials that are biocompatible and bioreactive. These products are applied in the repairing of bone in the human body which are broken or diseased [91]. The market is growing very rapidly, with new clinical applications being developed. Bioactive glass works via surface reactions inserted into the body, which promote the healing of tissues in the body, and eventually dissolve completely leaving only tissue [92]. Bioactive glasses exhibit unique properties for bone tissue engineering showing osteoinductive behavior, ability to bond to soft tissue as well as to hard tissue and to form HA layer when exposed to biological fluid [93]. This layer is responsible for the strong bonding between bioactive glasses and human bone. For instance, the ionic dissolution products from 45S5 Bioglass® (e.g. Si, Ca, P) and from other silicate-based glasses stimulate expression of several genes of osteoblastic cells [94]. Furthermore, bioactive glasses were shown to stimulate angiogenesis *in vitro* and *in vivo*, whilst possible antibacterial and inflammatory effects of bioactive glasses have also been investigated [5].

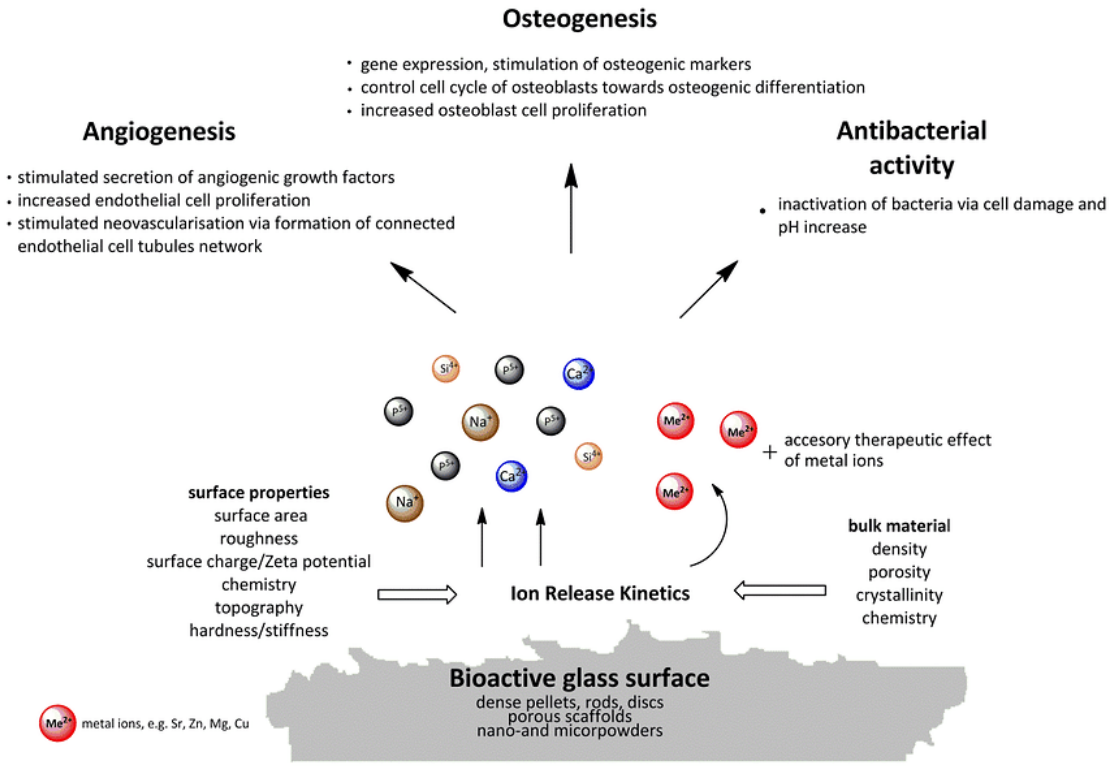

Figure 2.17 A schematic overview of biological responses to ionic dissolution products of bioactive glasses [12]

In the fact that ionic dissolution products from inorganic materials are keys to understand and assume the behavior of bioactive glasses *in vitro* and *in vivo*, in the context of tissue engineering applications. Since many trace elements such as Sr, Cu, Zn, Mg or Co present in the human body are known for their anabolic effects in bone metabolism, in order to mimic the natural system new approaches for enhancing bioactivity, beneficial and appropriate ions are being introduced. As indicated above, the subsequent release of these ions after exposure to a physiological environment is believed to favorably affect the behavior of human cells and to enhance the bioactivity of the scaffolds related to both osteogenesis and angiogenesis. The biological responses to ionic dissolution products of bioactive glasses is given in Figure 2.17.

When a bioactive glass is immersed in an aqueous solution, like the body fluid, it is possible to occur the processes: leaching and formation of silanols; dissolution of the glass network; and precipitation. For example, when 45S5 Bioglass® implanted, the reaction with the surrounding physiological fluid caused the formation of a hydroxyl

carbonated apatite (HCA) layer at the material surface. The HCA layer has a similar composition to hydroxyapatite, the mineral phase of bone, a quality which allows for strong interaction and integration with bone. This process, the reaction related to the bioactive glass response to the environment within the body and the process of integration with bone, occurs over the scale of several weeks or months (Figure 2.18).

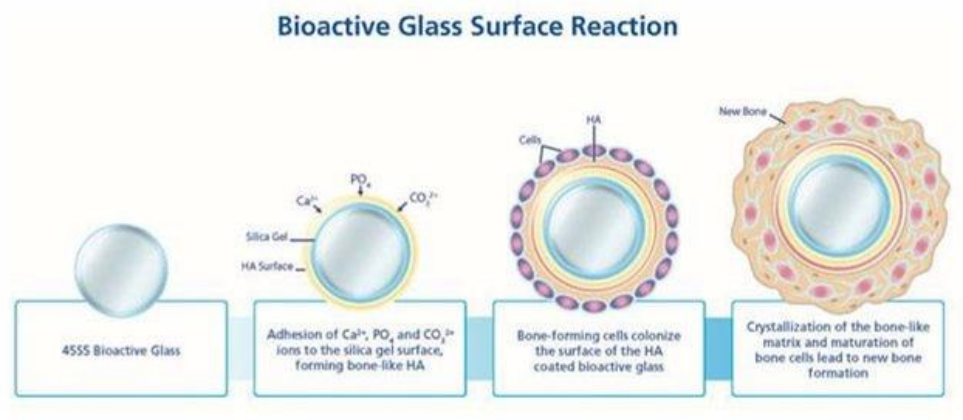

Figure 2.18 Surface reaction of bioactive glass (45S5) [85]

The steps of mechanism of the reaction related to bioactive glass response to the environment within the body and the process of integration with bone on 45S5 bioactive glass are separated as follows [85]:

(1) The glass network releases alkali or alkaline earth ions (i.e. Na^+ and Ca^{2+}) exchanging cations with hydrogen ions (H^+ or H_3O^+) proceeding from surrounding bodily fluid solution. These modifying ions leads to high values of the interfacial pH, usually more than 7.4. The reaction below shows this process, which causes hydrolysis of silica groups. As this occurs, the pH of the solution increases.

$$Si-O-Na^+ + H^+ + OH^- \quad \rightarrow \quad Si-OH^+ + Na^+(aq) + OH^-$$

(2) Due to an increase in the hydroxyl (OH^-) concentration at the surface, a dissolution of the glass network occurs, seen by the breaking of Si–O–Si bonds. Soluble silica is transformed to the form of silic-acid ($Si(OH)_4$) and silanol (Si–OH) creation occurs at the material surface. The reaction occurring in this stage is shown below:

$$Si-O-Si + H_2O \quad \rightarrow \quad Si-OH + OH-Si$$

(3) The silanol groups at the material surface condense and re-polymerize to form a silica-gel layer at the surface of glass. As a result of the first steps, the surface contains very little alkali content. The condensation reaction is shown below:

$$Si-OH + Si-OH \rightarrow Si-O-Si$$

(4) Amorphous calcium and phosphate ions (Ca^{2+} and PO_4^{3-}) gather at the silica-rich layer (created in step 3) from both the surrounding bodily fluid and the bulk of the glass. This creates a layer composed primarily of calcium-phosphate rich layer (CaP) on the silica layer surface.

(5) The CaP film created in step 4 incorporates carbonate anions (OH^- and CO_3^{2-}) from the solution, causing the crystallization which is called an hydroxycarbonate apatite (HCA). The mechanism of nucleation and growth of HCA appears to be the same *in vivo* and *in vitro* and is accelerated by the presence of hydrated silica.

(6) Growth factors adsorption to the surface of glass due to its structural and chemical similarities to hydroxyapatite.

(7) Stem cells and osteoprogenitor cells at the HCA surface differentiate to become osteogenic cells typically present in bone tissue, particularly osteoblasts.

(8) The attached and differentiated osteoblasts generate and deposit extracellular matrix (ECM) components, primarily type I collagen, the main protein component of bone.

(9) The collagen ECM becomes mineralized as normally occurs in native bone. Nanoscale hydroxyapatite crystals form a layered structure with the deposited collagen at the surface of the implant.

(10) Following these reactions, bone growth continues as the newly recruited cells continue to function and facilitate tissue growth and repair. The bioactive glass implant continues to degrade and be converted to new extracellular matrix (ECM) material.

2.6 Archimedes' principle for density measurement

The density measurement of glass sample at room temperature is applied using the Archimedes' principle. It is a law of physics fundamental to fluid mechanics. Archimedes' principle states that the upward buoyant force (F_B) that is exerted on a body immersed in a fluid, whether partially or completely submerged, is equal to the weight of the fluid that the body displaces [95]. The weight of the displaced fluid is directly proportional to the volume of the displaced fluid (if the surrounding fluid is of uniform density). Figure 2.19 presents the density measurement based on Archimedes' principle.

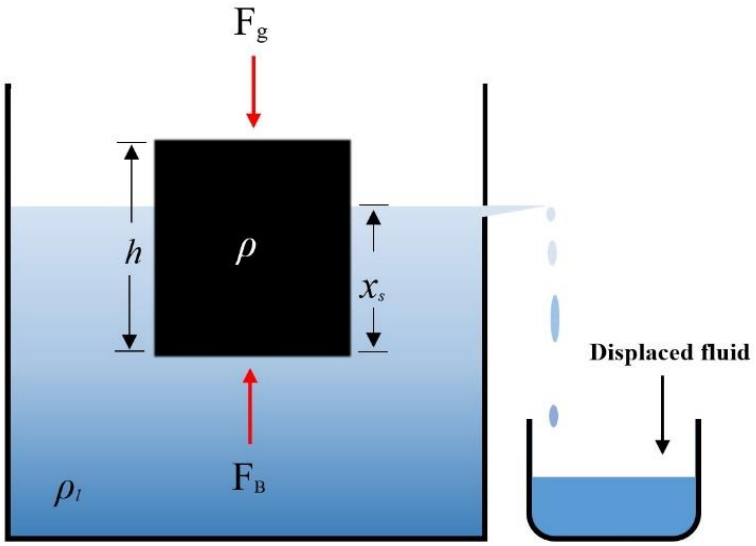

Figure 2.19 Density measurement based on Archimedes' principle

Any object, totally or partially immersed in a fluid or liquid, is buoyed up by a force equal to the weight of the fluid displaced by the object. Archimedes' principle allows the buoyancy of an object partially or fully immersed in a fluid to be calculated. The downward force on the object is simply its weight. The upward, or buoyant, force on the object is that stated by Archimedes' principle, above [96]. Thus, the net force on the object is the difference between the magnitudes of the buoyant force and its weight. If this net force is positive, the object rises; if negative, the object sinks; and if zero, the object is neutrally buoyant that is, it remains in place without either rising or sinking.

Consider a cuboid immersed in a fluid as shown in Figure 2.19, with one of its sides orthogonal to the direction of gravity. The fluid will exert a normal force on each face, but only the normal forces on top and bottom will contribute to buoyancy. The pressure difference between the bottom and the top face is directly proportional to the height (difference in depth of submersion). Multiplying the pressure difference by the area of a face gives a net force on the cuboid – the buoyancy, equaling in size the weight of the fluid displaced by the cuboid. By summing up sufficiently many arbitrarily small cuboids this reasoning may be extended to irregular shapes, and so, whatever the shape of the submerged body, the buoyant force is equal to the weight of the displaced fluid.

2.7 Mechanical behavior

The mechanical behaviors of a material affect how it behaves as it is loaded. The elastic modulus of the material affects how much it deflects under an external force (load), and the strength of the material determines the stresses that it can withstand before it fails. The ductility of a material also plays a significant role in determining when a material will break as it is loaded beyond its elastic limit [97]. Because every mechanical system is subjected to loads during operation, it is important to understand how the materials that make up those mechanical systems behave.

Normally, stress is the force causing the deformation divided by the area to which the force is applied, and strain is the ratio of the change in some parameter caused by the deformation to the original value of the parameter. The relationship between stress and strain in a material is determined by subjecting a material specimen to a tension or compression test. In this test, a steadily increasing axial force is applied to a test specimen, and the deflection is measured as the load is increased. These values can be plotted as a load-deflection curve, as shown in Figure 2.20. The deflection in the test specimen is dependent on both the material's elastic modulus as well as the geometry of the specimen (area and length). Since we are interested material behavior without regard to geometry, it is useful to generalize the data to remove the effect of geometry. This is done by converting the load values to stress values and converting the deflection values to strain values [98]:

$$Stress : \sigma = \frac{P}{A_0} \tag{2.1}$$

$$Strain : \varepsilon = \frac{L - L_0}{L_0} = \frac{\Delta L}{L_0} \tag{2.2}$$

In the equation for stress, P is the load and A_0 is the original cross-sectional area of the test specimen. In the equation for strain, L is the current length of the specimen and L_0 is the original length.

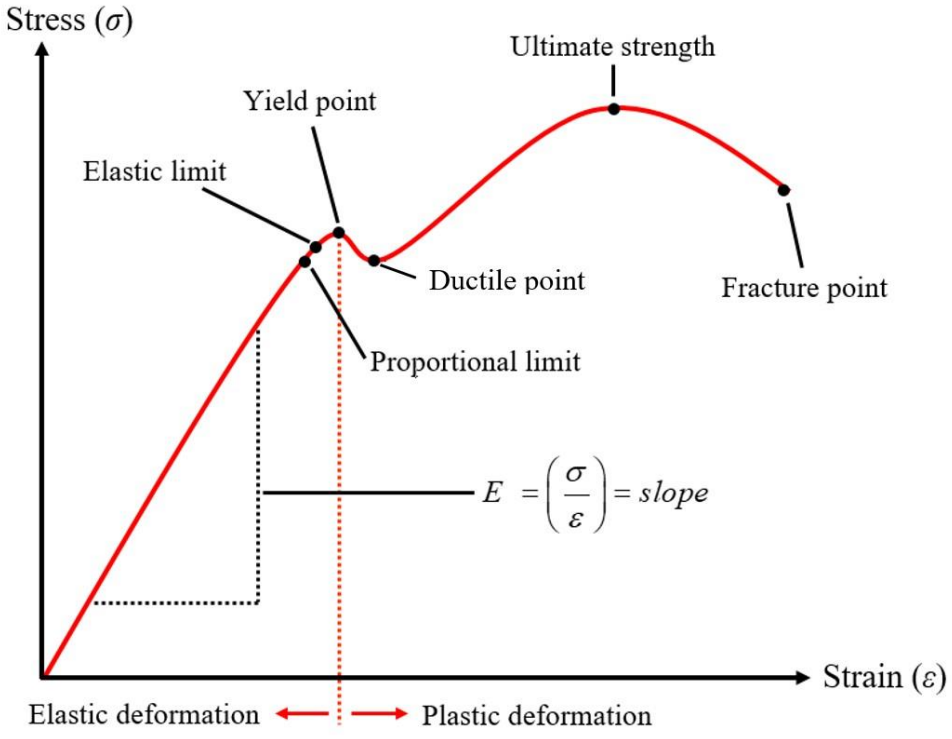

Figure 2.20 Diagram of the stress–strain curve of material (Reproduced with some modifications from J.M. Gere) [99]

Stress-strain curve illustrates the complete picture of mechanical behavior of material. It is a graph which represents stress value against strain value of the given material, when the material is subjected to increasing pull. There are several points of interest in the diagram above [98-99]:

(1) Proportional limit: It is the point up to which Hooke's law is applicable, representing the maximum value of stress at which the stress-strain curve is linear. For example, stress is directly proportional to strain.

(2) Elastic limit: There is always the limiting value of load up to which strain totally disappear on removal of load material possess elastic nature and properties till elastic limit. Up to this point material obtains its original configuration on removing load.

(3) Yield point: The stress beyond which material becomes plastic. Load at which permanent deformation of material starts.

(4) Ductile point: Beyond this point neck forms where the local cross-sectional area becomes significantly smaller than original material acquires plastic nature.

(5) Ultimate strength: The point at up to which material can withstand maximum load and ultimate strength with maximum elongation. large deformation possible before failure.

(6) Fracture point: The stress which makes the material failure or break.

There are several parameters for evaluating mechanical properties such as elastic modulus, Poisson's ratio, microhardness. These parameters indicate the resistance to elastic and/or plastic deformation in materials. Elastic moduli yield a macroscopic view of material stiffness, and reflect both the interatomic bonding energies and the connectivity [100-101]. Glassy materials have markedly different elastic properties depending much on the glass composition and microstructural features because very different materials with all kinds of interatomic bonding can be formed in glasses. The elastic moduli are thus important parameters for the general understanding of the structural and mechanical behaviors in glass materials [100, 102]. The characteristic of the elastic moduli (L, G, K, E) to the direction of forces exerted on the material are shown in Figure 2.21. The parameters used to evaluate mechanical properties can be shown as following:

2.7.1 Longitudinal modulus

In amorphous material, the longitudinal modulus (L) is interrelated with the independent elastic constants for an isotropic solid [101]. It is parameter indicated resistance to force along the length of the material [103] (see in Figure 2.21a).

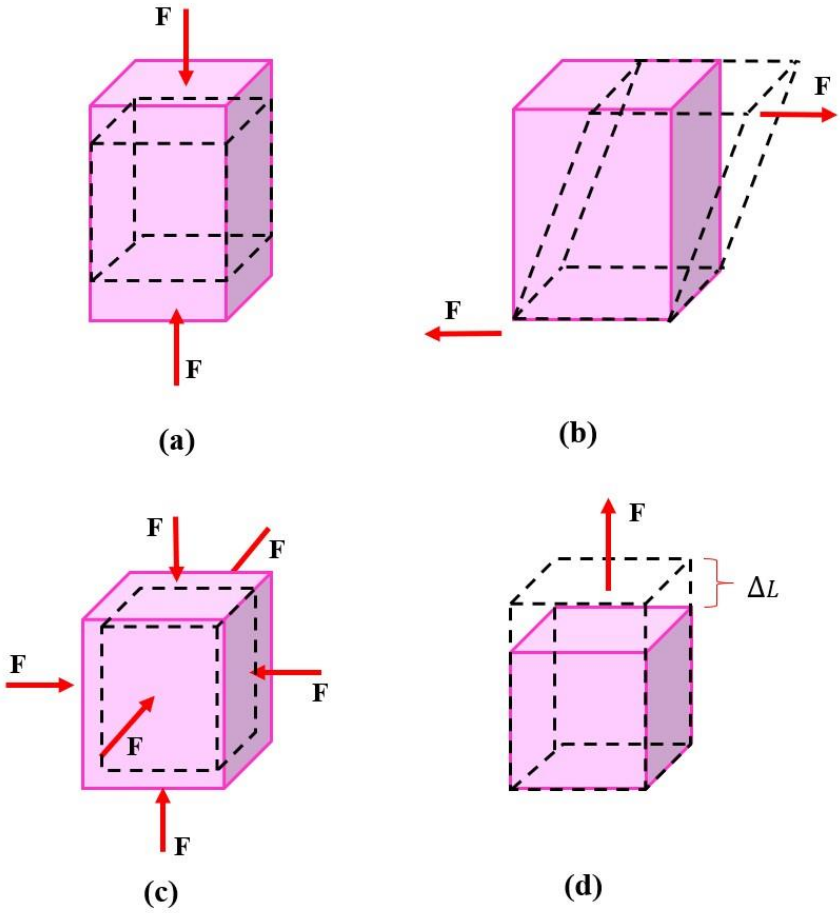

Figure 2.21 Direction of the force exerted on the material for representing the behavior of elastic moduli; (a) Longitudinal modulus, (b) Shear modulus, (c) Bulk modulus, and (d) Young's modulus

2.7.2 Shear modulus

The shear modulus (G) or modulus of rigidity describes an object's tendency to shear (the deformation of shape at constant volume) when acted upon by opposing forces; it is defined as shear stress over shear strain [103], as shown in Figure 2.21b. The shear modulus is also part of the derivation of viscosity.

2.7.3 Bulk modulus

The bulk modulus (K) describes volumetric elasticity, or the tendency of an object to deform in all directions when uniformly loaded in all directions, as shown in Figure 2.21c. It is defined as volumetric stress over volumetric strain, and is the inverse of compressibility [103].

2.7.4 Young's modulus

Young's modulus (E), also known as modulus of elasticity, is a quantity that measures an object or substance's resistance to being deformed elastically (i.e., non-permanently) when a stress is applied to it [103-104]. The modulus of elasticity is a value that indicates the strength of a material or resistance to stress with a force acting in one direction as shown in Fig.2.21d. The elastic modulus of an object is defined as the slope of its stress–strain curve in the elastic deformation region (see in Figure 2.20). A stiffer material will have a higher elastic modulus.

2.7.5 Poisson's ratio

Poisson's ratio (σ) is defined as the ratio of lateral contraction to the longitudinal extension when stress is applied uniaxially [103], as shown in Figure 2.22. When a material is elongated under mechanical stress, its cross-sectional area is reduced. Poisson's ratio also measures the deformation in the material in a direction perpendicular to the direction of the applied force. As well known, Poisson's ratio value has sensitive on the variation in glass network which include both changes in its cross-link density [105]. Glassy materials exhibit a wide range of values of Poisson's ratio from 0.1 to 0.4 [106].

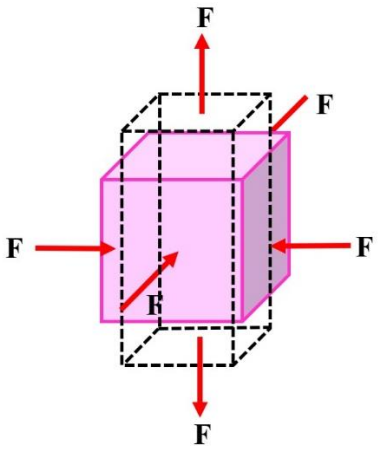

Figure 2.22 Direction of force on the material for representing the Poisson's ratio

2.7.6 Microhardness

Microhardness is a measure of surface properties and can be related to elastic modulus, toughness and surface tension. It is the property of the material which enables it the ability to resist being permanently or plastic deformation, usually by penetration or indentation [32]. However, the term microhardness may also refer to stiffness or temper, or to resistance to bending, cutting, polishing, or grinding [107]. The greater the hardness of the material, the greater the resistance it has to deformation. The multiplicity of definitions, and corresponding multiplicity of hardness measuring instruments, together with the lack of a fundamental definition, indicates that hardness may not be a fundamental property of a material, but rather a composite one including yield strength, work hardening, true tensile strength, modulus of elasticity, and others. A microhardness property value is the result of a defined measurement procedure (its property of rigidity of materials). For ceramics and most polymer (like glass), microhardness is defined as the considered plastic deformation of the surface [108]. Microhardness measurements are widely used for the quality control of materials because they are quick and considered to be non-destructive tests when the marks or indentations produced by the test are in low stress areas.

2.8 Ultrasonic technique

The most standard test used to determine the mechanical properties of biomaterials is the compressive and tensile strength measurement. Even if the compressive strength is thought to be the most related property to the forces acting during mastication, failure often occurs due to tensile or shear stresses. As well known that a glass material exhibits a typical thermoplastic and brittle behavior that seems to have a significant influence, especially on fracture toughness [97]. The thermoplastic nature of the glass is supported also by its dynamic mechanical behavior resulting in a sharp loss peak. With high precision and non-destructive method, the ultrasonic technique is therefore accepted as a versatile tool for understanding the association of the structural characteristics and mechanical properties in amorphous materials [29].

2.8.1 **Basic principle** [109-110]

In general, ultrasonic testing is based on the capture and quantification of either the reflected waves (pulse-echo) or the transmitted waves (through-transmission). A typical pulse-echo ultrasonic inspection system consists of several functional units, such as the pulser/receiver, transducer, and a display device, as shown in Figure 2.23. A receiver is an electronic device that can produce high voltage electrical pulses. Driven by the pulser, the transducer generates high frequency ultrasonic energy. The sound energy is introduced and propagates through the materials in the form of waves. When there is a discontinuity (such as a crack) in the wave path, part of the energy will be reflected back from the flaw surface. The reflected wave signal is transformed into an electrical signal by the transducer and is displayed on a screen. Knowing the velocity of the waves, travel time can be directly related to the distance that the signal traveled. From the signal, information about the reflector location, size, orientation and other features can sometimes be gained.

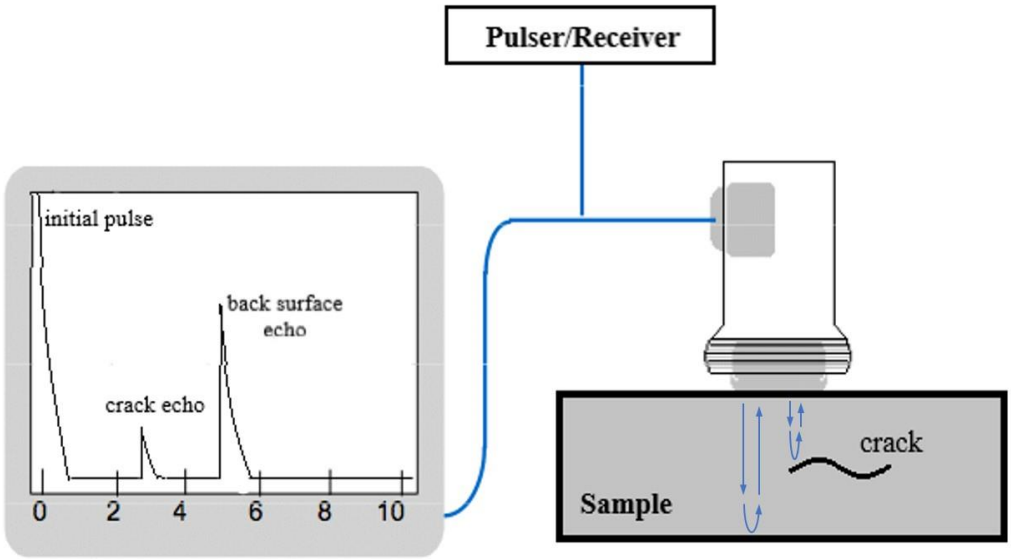

Figure 2.23 Diagram of typical ultrasonic pulse echo system [111]

2.8.2 Wave propagation in ultrasonic testing [110-112]

Ultrasonic testing is based on the vibration in materials which is generally referred to as acoustics. All material substances are comprised of atoms, which may be forced into vibrational motion about their equilibrium positions. Many different patterns of vibrational motion exist at the atomic level; however, most are irrelevant to acoustics and ultrasonic testing. Acoustics is focused on particles that contain many atoms that move in harmony to produce a mechanical wave. When a material is not stressed in tension or compression beyond its elastic limit, its individual particles perform elastic oscillations. When the particles of a medium are displaced from their equilibrium positions, internal restoration forces arise. These elastic restoring forces between particles, combined with inertia of the particles, lead to the oscillatory motions of the medium.

In solids, sound waves can propagate in four principal modes that are based on the way the particles oscillate. Sound can propagate as longitudinal waves, shear waves, surface waves, and in thin materials as plate waves. Longitudinal and shear waves are the two modes of propagation most widely used in ultrasonic testing. The particle movement responsible for the propagation of longitudinal and shear waves is illustrated in Figure 2.24.

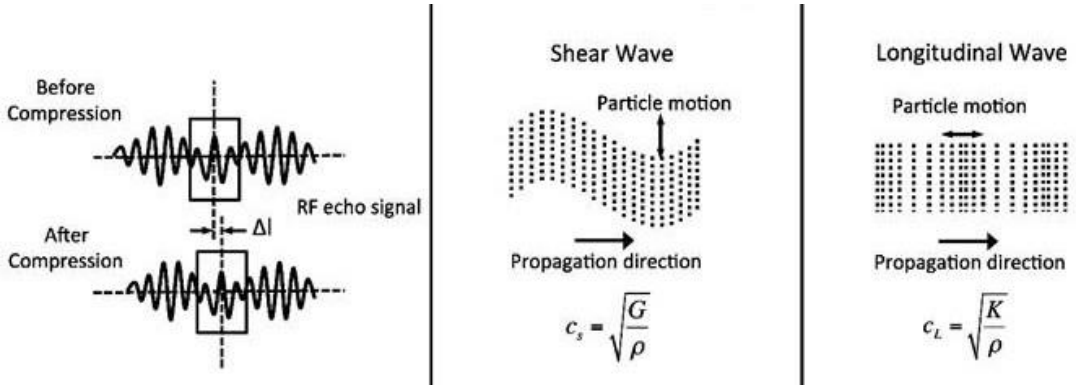

Figure 2.24 Propagation of longitudinal and shear waves [113]

2.8.2.1 Longitudinal wave [110,113]

The oscillations occur in the longitudinal direction or the direction of wave propagation. Since compression and expansion forces are active in these waves, they are also called pressure or compression waves. They are also sometimes called density waves because material density fluctuates as the wave moves. Compression waves can be generated in gases, liquids, as well as solids because the energy travels through the atomic structure by a series of compressions and expansion movements.

2.8.2.2 Shear wave [110,113]

In a shear wave (also called transverse wave), particles oscillate at a right angle or transverse to the direction of propagation. Shear wave requires an acoustically solid material for effective propagation, and hence, is not effectively propagated in materials such as liquids or gasses. Notice that the shear wave is relatively weak when compared to longitudinal wave. In fact, a shear wave is usually generated in materials using some of the energy from longitudinal wave, and consequently a shear wave travels slower than longitudinal wave. Also, the reflected shear wave is reflected at a smaller angle than the reflected longitudinal wave when a longitudinal wave is reflected inside the material. This is also due to the fact that the shear wave has a slower velocity and shorter wavelength than longitudinal wave of the same frequency within a given material.

2.8.3 Measurement of elastic constants

Acoustic waves of high frequencies (about 10^{11} Hz) can be considered as artificial phonons. Ultrasonic is a very powerful tool in this regard and are suitable for the investigation of phonons and their interactions with other degrees of freedom in crystals; in particular, with order parameter variations or phase transitions. Generally, acoustic waves of very short duration are excited and detected using piezoelectric transducers bonded to the end faces of the crystal sample under study [114]. Ultrasonic wave velocity measurements for waves of both longitudinal and shear polarizations along the symmetry directions allow one to evaluate all the diagonal elements of the elastic constant matrix. In order to determine the off-diagonal elastic constants, one has to measure velocities of propagation of ultrasonic waves along anyone arbitrary direction in the symmetry planes (x-y, y-z and x-z.) [115].

The determination of elastic properties of glass is mostly essential as it involves the mechanical strength for the glass. The various advantages of ultrasonic technique over mechanical and other methods include the determination of the material properties without harming, comparative analysis loading and also, it provides the information about internal arrangements of the constituent oxides. This is possibly due to the interaction of ultrasonic waves with macro, micro and submicroscopic particles during wave propagation into the glasses. Figure 2.25 shows the ultrasonic measurement for longitudinal wave velocity and transverse wave velocity by using normal beam probe and angle beam probe respectively.

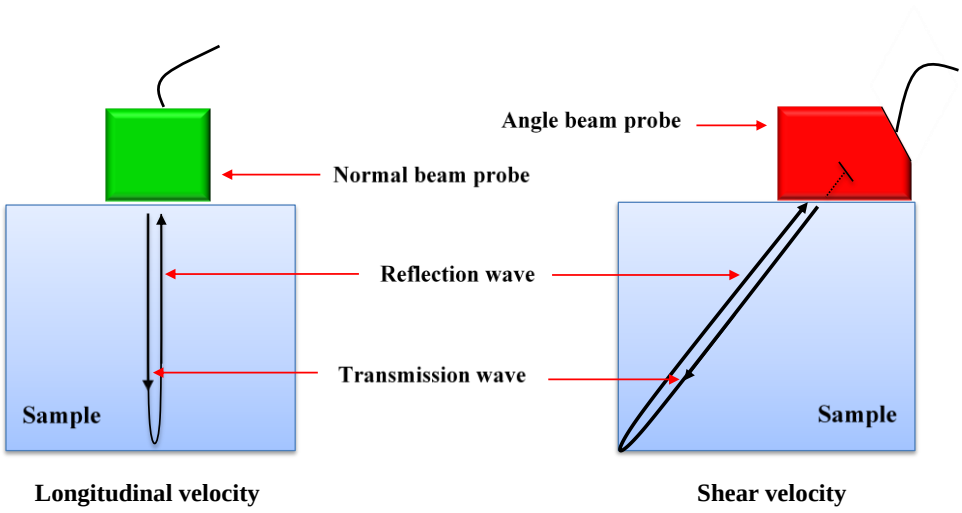

Figure 2.25 Ultrasonic measurement of longitudinal and shear velocities

For the measurement of ultrasonic velocity in the materials samples, the ultrasonic wave is generated from a ceramic transducer with a resonant frequency and acts as transmitter-receiver at the same time. The ultrasonic wave velocity is able to be calculated as give in the following relation [31,116].

$$v = \frac{2x}{\Delta t} \tag{2.3}$$

where x is the sample thickness (mm) and Δt is time interval (s).

2.9 Vickers microhardness determination

Measurement of the microhardness of the material is a quick and simple method of finding mechanical property data for the bulk material from a small sample. It is especially suited for determining the hardness of thin film coatings or the surface hardness of case-hardened parts. Additionally, its measurement is also appropriate in cases of multi-phase, non-homogeneous or prone to cracking [117]. Microhardness is the hardness of a material as determined by forcing an indenter into the surface of the material under loads. In microhardness testing, the indentation is usually so small that it is to be measured with a microscope. It is also capable of determining hardness of different micro constituents within a material structure.

Vickers hardness (HV) is a measure of the hardness of a material, calculated from the size of an impression produced under load by a pyramid shaped diamond indenter [107]. The Vickers test is a modification of the Brinell test, which is a small diamond pyramid is pressed into the sample under loads that are much less than those used in the Brinell test. The Vickers testing, shown in Figure 2.26, applies a square-base diamond pyramid indenter which is prone to measure the microhardness in brittle materials better than the Brinell test method.

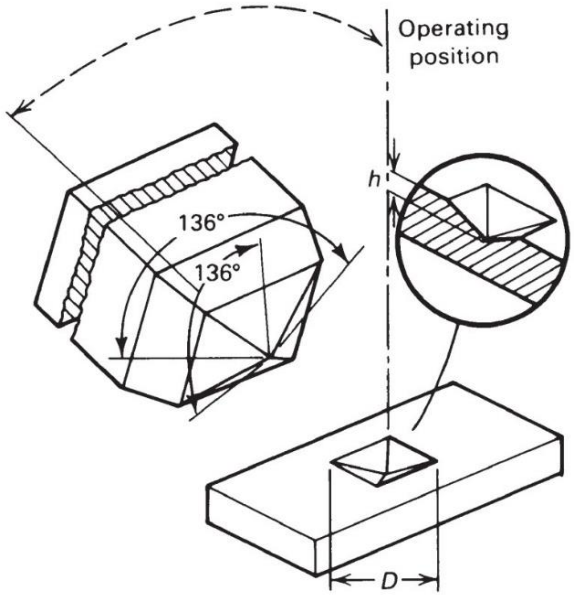

Figure 2.26 Schematic of the indenter used for the Vickers test [118]

The Vickers test is reliable for measuring the hardness of metals, and also used on ceramic and glass materials. The Vickers machine uses a penetrator that is square in shape, but tipped on one corner so it has the appearance of a playing card "diamond". The Vickers indenter is a 136 degrees square-based diamond cone, the diamond material of the indenter has an advantage over other indenters because it does not deform over time and use [117-118]. The Vickers impression is more easily "read" for area size than the circular impression of the Brinell method. Like the Brinell test, the Vickers number is determined by dividing the load by the surface area of the indentation (H=P/A) [117]. To perform the Vickers test, the specimen is placed on an anvil that has a screw threaded base. The anvil is turned raising it by the screw threads until it is close to the point of the indenter. With start lever activated, the load is slowly applied to the indenter. The load is released and the anvil with the specimen is lowered. The operation of applying and removing the load is controlled automatically.

2.10 Scanning electron microscope

Scanning electron microscopy (SEM) is a method that creates for high-resolution imaging of surfaces by scanning it with a high energy stream of electrons. The SEM uses electrons for imaging, much as a light microscope uses visible light. The advantages of SEM over light microscopy include much higher magnification (>100,000X) and greater depth of field up to 100 times that of light microscopy.

2.10.1 Basic principle [119]

Figure 2.27 illustrates the scheme of typical SEM. This equipment is operated in vacuum system. The SEM generates a beam of incident electrons in an electron column above the sample chamber. The electrons are produced by a thermal emission source, such as a heated tungsten filament, or by a field emission cathode. The energy of the incident electrons can be as low as 100 eV or as high as 30 keV depending on the evaluation objectives. The electrons are focused into a small beam by a series of electromagnetic lenses in the SEM column. Scanning coils near the end of the column direct and position the focused beam onto the sample surface. The electron beam is scanned in a raster pattern over the surface for imaging. The beam can also be focused at a single point or scanned along a line for x-ray analysis.

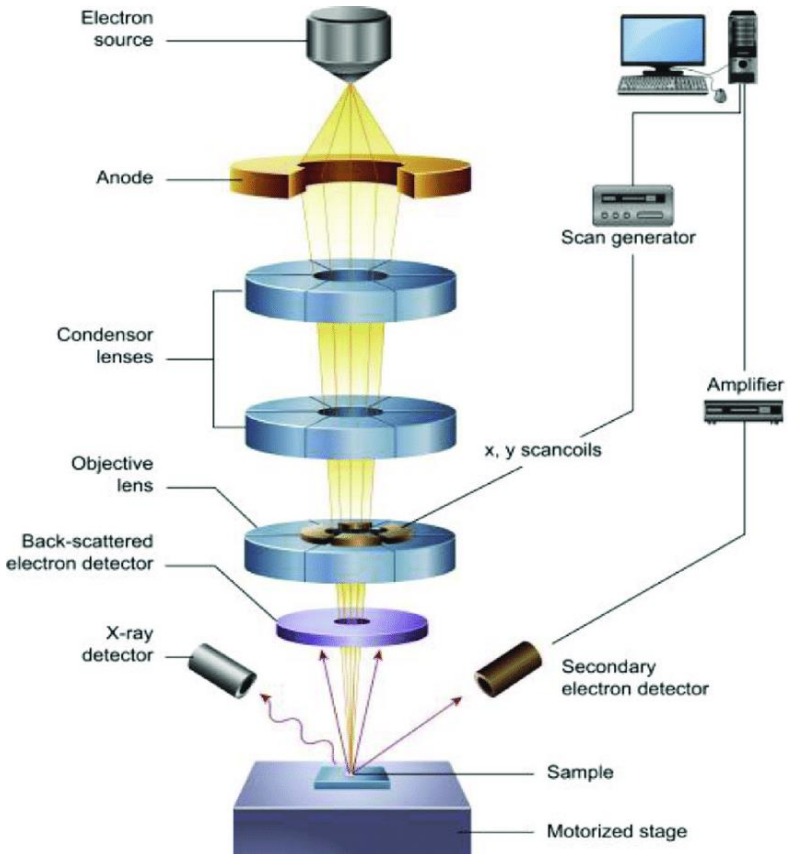

Figure 2.27 Schematic drawing of the typical SEM column [120]

To create an SEM image, the incident electron beam is scanned in a raster pattern across the sample's surface. The emitted electrons are detected for each position in the scanned area by an electron detector. By synchronizing the position in the image scan to that of the scan of the incident electron beam, the display represents the morphology of the sample surface area. The incident electrons cause electrons to be emitted from the sample due to elastic and inelastic scattering events within the sample's surface and near-surface material. High-energy electrons that are ejected by an elastic collision of an incident electron, typically with a sample atom's nucleus, are referred to as backscattered electrons. The energy of backscattered electrons will be comparable to that of the incident electrons. Emitted lower-energy electrons resulting from inelastic scattering are called secondary electrons. Secondary electrons can be formed by collisions with the nucleus where substantial energy loss occurs or by the ejection of loosely bound electrons from the sample atoms.

2.10.2 Analytical information

Electron microscopes are versatile instruments that can provide a wide range of information depending on the user's needs. As the name implies, electron microscopes employ an electron beam for imaging. Different signals result between interaction between electrons and matter, each of which carry useful information about the sample. It's the choice of the microscope's operator which signals to capture. The Signals emitted from different parts of the electron beam interaction with a specimen is presented in Figure 2.28. Some signals are used for analysis in different applications, for example, secondary electron is used to analyze the surface; characteristic X-ray is used to analyze elemental elements; Auger electron is used to analyze elements on nanometer level and failure analysis; backscattered electron is used to analyze atomic arrangement or phase type. The analytical SEM that applied from some of these signals can differentiate as follow [119, 121]:

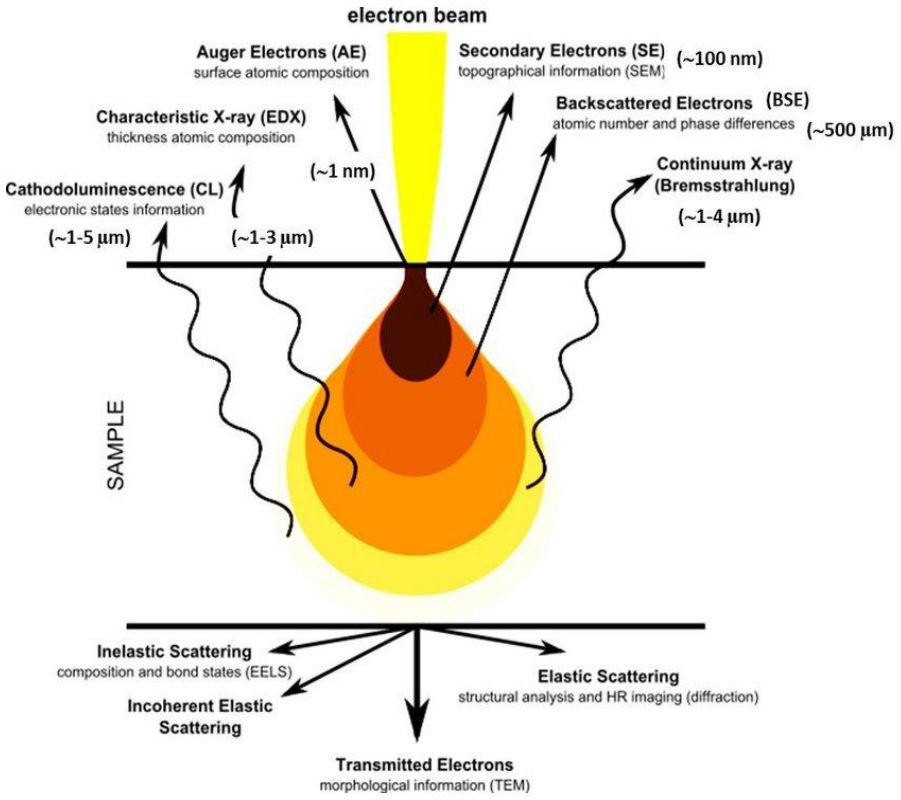

Figure 2.28 Signals produced by interaction between electrons and matter [121]

2.10.2.1 Secondary electron imaging

This mode provides high-resolution imaging of fine surface morphology. Inelastic electron scattering caused by the interaction between the sample's electrons and the incident electrons results in the emission of low-energy electrons from near the sample's surface. The topography of surface features influences the number of electrons that reach the secondary electron detector from any point on the scanned surface. This local variation in electron intensity creates the image contrast that reveals the surface morphology.

2.10.2.2 Backscatter Electron Imaging

This mode provides image contrast as a function of elemental composition, as well as, surface topography. Backscattered electrons are produced by the elastic interactions between the sample and the incident electron beam. These high-energy electrons can escape from much deeper than secondary electrons, so surface topography is not as accurately resolved as for secondary electron imaging. The production efficiency for backscattered electrons is proportional to the sample material's mean atomic number, which results in image contrast as a function of composition, i.e., higher atomic number material appears brighter than low atomic number material in a backscattered electron image.

2.10.2.3 Field Emission SEM (FESEM)

SEMs that use a thermal emission source (i.e., tungsten filament) to generate the electron beam are generally adequate for most samples and provide satisfactory resolution at magnifications up to about 100,000X. However, for high resolution and high magnification imaging a cold field emission (FE) gun provides the best resolution available for SEM. The cold FE gun extracts electrons from the FE cathode by applying a strong electrical field close to a very sharp tip. This method of electron extraction results in a higher electron yield and a smaller beam size, which thus provides a brighter signal with better resolution. The useful magnification for FESEM imaging ranges up to 500,000X. A second advantage of FESEM is that high resolution imaging can be performed with very low accelerating voltages. At low voltage, very fine features are more readily observed, and many non-conductive materials can be examined without applying a conductive coating. Low voltage FESEM examination is ideal for imaging nanomaterials, polymers, and thin films.

2.11 X-ray diffraction

X-ray diffraction (XRD) has acted as the cornerstone of twentieth-century science. It is defined as the nondestructive technique that provides detailed information about the crystallographic structure, chemical bonding, and physical properties of materials.

XRD is the elastic scattering of x-ray photons by atoms in a periodic lattice. When the beam of monochromatic incident on the target materials the interaction between them is happened and the scattering of those X-rays from atoms within the target material can be illustrated in Figure 2.29. Bragg's law was used to explain the interference pattern of X-rays scattered by crystals structure the diffraction of X-rays described by [120]:

$$n\lambda = 2d\sin\theta \tag{2.4}$$

where n is an integer called the order of reflection, λ is the wavelength of x-rays, d is the interplanar spacing generating the diffraction, and θ is the angle between the incident beam and the normal to the reflecting lattice plane.

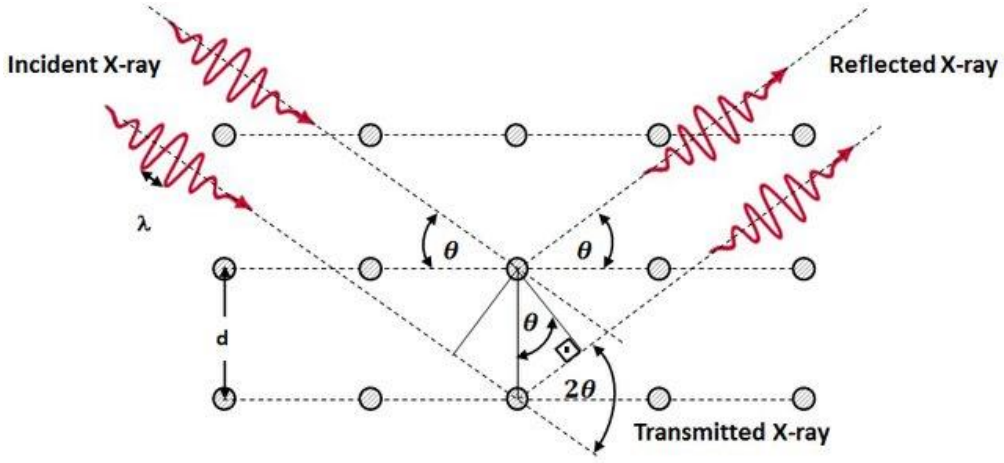

Figure 2.29 Schematic diagram of Bragg's law [122]

Equation 2.4 shows the essence of Bragg's law schematically shown in Figure 2.29. The diffracted X-rays are then detected, processed and counted. In the typical XRD spectrum the intensity of the diffraction signal is usually plotted against the diffraction angle 2θ (in degree). The observed features in a diffractogram are called Bragg or

diffraction peaks, lines or reflections. To determine what phases are present in the sample, experimental XRD data is compared to reference patterns. Each phase has a unique diffraction pattern. Crystalline materials produce a sharp diffraction peaks whereas for amorphous materials these peaks become more and more broadened.

2.12 Fourier transform infrared [119]

Fourier Transform-Infrared Spectroscopy (FTIR) is an analytical technique used to identify organic and inorganic materials. This technique measures the reflectance of infrared radiation by the sample material versus wavelength. The infrared absorption bands identify molecular components and structures. FTIR is often used to identify chemical bonds and functional groups in a molecule by producing an infrared absorption or reflectance spectrum (spectral range: 4000–400 cm^{-1} is commonly used for glass). When a material is irradiated with infrared radiation, absorbed IR radiation usually excites molecules into a higher vibrational state. The wavelength of light absorbed by a particular molecule is a function of the energy difference between the at-rest and excited vibrational states. The wavelengths that are absorbed by the sample are characteristic of its molecular structure.

The FTIR spectrometer uses an interferometer to modulate the wavelength from a broadband infrared source. A detector measures the intensity of transmitted or reflected light as a function of its wavelength. The signal obtained from the detector is an interferogram, which must be analyzed with a computer using Fourier transforms to obtain a single-beam infrared spectrum. The FTIR spectra are usually presented as plots of intensity versus wavenumber (cm^{-1}). Wavenumber is the reciprocal of the wavelength. The intensity can be plotted as the percentage of light transmittance or absorbance at each wavenumber. To identify the material being analyzed, the unknown IR absorption/transmission spectrum is compared with standard spectra in computer databases or with a spectrum obtained from a known material. The region from 1500–400 cm^{-1} is referred to as the fingerprint region. Absorption bands in this region are generally due to intramolecular phenomena and are highly specific to each material. The specificity of these bands allows computerized data searches within reference libraries to identify a material. Quantitative concentration of a compound can be determined from the area under the curve in characteristic regions of the IR spectrum.

2.13 Literature reviews

Bioactive glasses have recently been shown to promote regeneration of soft tissues by positively influencing tissue remodeling during wound healing. After the discovery of the first bioactive glass by Larry Hench, several other glass and glass-ceramic compositions have been developed to improve the properties and clinical abilities of traditional bioactive glass. Most work in this area has been directed at the development of candidates for the biomedical applications. In this work, the summarized literature involving bioactive glasses and their properties for bone tissue engineering scaffolds has been reviewed. The background of relevant studies and properties of various bioactive glasses used to fabricate scaffolds has also been summarized and elaborated in this section.

Recently, a variety of bioactive glasses with different chemical compositions have been developed, besides the original 45S5 Bioglass® (wt%: $45SiO_2$–$25CaO$–$25Na_2O$–$6P_2O_5$). There are three interesting types of bioactive glasses based on CaO-SiO_2, CaO-P_2O_5 and CaO-B_2O_3 combinations.

As a category of bioactive glasses, silica-based glasses have been afforded a considerable amount of importance as coating materials on the surface of biomedical implants, as well as bone replacements. There is an increasing evidence that silicon (Si) can promote the new bone formations and positive effects on bone mineral density by reducing bone resorption, as confirmed by both *in vitro* and *in vivo* studies. In 2008, Li et al. [123] investigated mesoporous CaO–SiO_2–P_2O_5–MO (M = Mg, Zn, Cu) bioactive glasses. The effects of the substitution of CaO by MgO, ZnO and CuO in the bioactive glasses on the structure and hydroxyapatite (HA)-forming ability were studied. The substitution of Ca with Mg, Zn or Cu inhibits the formation of HA deposition on the surface of the bioactive glasses, especially at high MgO, ZnO and CuO contents. The presence of MgO, ZnO and CuO slowed down the deposition rate of HA following a sequence of Cu < Mg < Zn. Therefore, the HA crystallite size and morphology can be easily tuned by the incorporation of Mg, Zn and Cu, which facilitates the wide application of the bioactive glasses. In 2010, $85SiO_2$–$10CaO$–$5P_2O_5$ bioactive glass was studied by Alcaide et al. [124]. They found that it is an excellent candidate as a graft for bone tissue regeneration, owing to its excellent textured properties, structural characteristics and crystalline apatite rate formation. It aimed to achieve the

performance of the biomaterial to match the replaced tissue with the least toxic reaction to the host. However, they are generally bioinert, and interact minimally with the surrounding tissues [47].

It is also known that most bioactive glasses and silica-based glasses possess mechanical and elastic properties similar to that of human bone, making them good candidates for orthopedic implants. There are bioactive glass compositions have been designed over the past two decades to overcome the limitations of 45S5 Bioglass®. Liu et al. [125] evaluated the mechanical properties of 13-93 bioactive glass ($53SiO_2$–$6Na_2O$–$12K_2O$–$5MgO$–$20CaO$–$4P_2O_5$ wt%). As fabricated, the scaffolds had a strength = 86 ± 9 MPa, elastic modulus = 13 ± 2 GPa, and a Weibull modulus = 12 when tested in compression. The compressive strength of the scaffolds decreased markedly during the first 2 weeks of immersion in SBF or implantation *in vivo*, but more slowly thereafter. The brittle mechanical response of the scaffolds *in vitro* changed to an elasto-plastic response after implantation for longer than 2–4 weeks *in vivo*. In 2014, Baino and Vitale-Brovarone [126] reported that the SCNA ($57SiO_2$–$34CaO$–$6Na_2O$–$3Al_2O_3$ mol.%) glass exhibited a compressive strength of 18 MPa, an elastic modulus around 380 MPa, and a Weibull modulus of 4, respectively. In another glass, the glass based on CEL2 ($43.8SiO_2$–$23.6CaO$–$15.0Na_2O$–$4.6MgO$–$6.1K_2O$–$6.9P_2O_5$ wt%) with total porosity of 65 and 85 vol.% was shown to achieve an elastic modulus of 16 and 1.1 GPa, respectively [127].

Calcium phosphate glasses and glass-ceramics have gained high interest as bone filling materials and for fabricating scaffolds for bone tissue engineering owing to their similarity with natural bone both in terms of chemical composition and mechanical properties [12]. However, the main problem of the phosphate glasses is that their solubilities are too fast, which makes decreasing of stabilization of the glass network and toxic effect on human fibroblast cells [128]. Therefore, several studies were conducted to improve its chemical resistance. Since the phosphate network former coupled with network modifying ions creates complex multicomponent oxides, consisting of varying strength covalent and ionic bonding. In order to tailor the solubility of phosphate glasses several oxides such as TiO_2, Al_2O_3, ZnO, MgO, SrO, Fe_2O_3 etc have been investigated as additives incorporated into the phosphate-based glass compositions in order to stabilize the glass network and to control the degradation rate.

Recently, starting with the Navarro et al. investigation in 2003 [129], the work has been focusing on the cellular response to P_2O_5–CaO–Na_2O–TiO_2 glass system with controlled solubility. The result indicates that the increase of TiO_2 has been shown to decrease the degradation rate and to affect the cellular response of this glass. The addition of 5 mol% TiO_2 resulted in a slower degradation of the glass. Additionally, the more soluble glass exhibited a higher toxic effect on human fibroblast cells than the undoped glass (when applied as glass extracts), but, surprisingly, an increased cell attachment was observed when cells were directly seeded on the glass samples. Brauer et al. [130] investigated the influence of TiO_2 and SiO_2 doping on the degradation behavior and the biological performance of P_2O_5–CaO–MgO–Na_2O glass. The authors reported that addition of TiO_2 decreased the solubility of the glass in water and SBF, while SiO_2 doping resulted in increased dissolution rates. Another study by Ahmed et al. [131] extensively reported on degradation kinetics of P_2O_5–CaO–Na_2O glass systems modified with MgO. It was observed that the addition of MgO to phosphate glasses resulted in a decrease of the degradation rate. The glass samples with 0 mol% MgO caused the lowest anabolic activity of osteoblast cells, while MgO contents of 10, 20 and 30 mol% resulted in osteoblast activity at similar levels as the positive control.

Apart from silicate and phosphate-based glass candidates, a new direction has begun by the extensive investigation of borate-based glasses. Borate glass structures can easily change its coordination number from three to four and hence, it can form the variable structural units. Recently, interest has increased in borate glasses, largely due to the very encouraging clinical results of healing of chronic wounds, such as diabetic ulcers, that would not heal using conventional treatments. Moreover, boron has been shown to play a significant role in potential stimulating new bone formation, which was observed by *in vitro* and *in vivo* studies [12].

Recently, silica free borate glasses have also been studied to biomedical applications [132]. It has been inferred that the corrosion mechanisms of borate glasses in aqueous environments, generally undergo hydration, hydrolysis, and ion exchange reactions. Only more recently, starting with the Deliormanl et al. investigation in 2012 [133], the research work has been focusing on the effects of the borate glass microstructure on its conversion to hydroxyapatite (HA) *in vitro*. When compared to silicate bioactive glass, borate bioactive glass has been shown to convert faster and more

completely to hydroxyapatite and enhance new bone formation *in vivo*. Anand et al. [134] evaluated the B_2O_3 and MgO effects on the bioactivity behavior of xB_2O_3–$(2x+2)MgO$–$(22.4-(2x+2))Na_2O$–$(46.1-x)SiO_2$–$26.9CaO$–$2.6P_2O_5$–$2ZnO$ glass. It was found that the prepared glasses have shown good bioactivity which confirmed by the presence of apatite peaks in XRD and presence of P–O bonds in FTIR spectra at 558 and 601 cm^{-1} during *in vitro* studies. Moreover, the increase of boron and magnesium contents leads to enhanced percentage of viable cells. All the prepared samples have been observed to be non-toxic in nature with more than 70.3% viable cells. Results indicate that samples prepared in this study can have potential clinical applications as osteoconductive carriers for treating bone infection. Two systems of glasses and glass ceramics derived from (Na_2O–CaO–B_2O_3) and (NaF–CaF_2–B_2O_3) were prepared and studied by ElBatal et al. in 2016 [10]. The results show that there is a difference in solubility in the sodium phosphate solution between fluoride and oxide glass systems due to the strong action of the leaching solution and ease of solubility of fluoride glasses than glass ceramics in this solution. SEM data indicate the formation of small rounded or nodular shape crystals which are characteristics for the formation of hydroxyapatite layer. In recent year, the borate bioactive glass invented by Bakry [135] was copyrighted in United States Patent Application Publication for using the dentin and enamel restoration. This glass comprised 40-60 wt % B_2O_3; 15-25 wt % CaO; 15-25 wt % Na_2O; and 2-15 wt % F_2O_5. This borate bioactive glass may be used for the restoration of dentin and enamel on a tooth surface by the precipitation of calcium phosphate, and also be used as a bone grafting material.

Nowadays, most of world society, however, have concerned about the use of pure chemicals. Glass prepared from natural materials is an interesting way to reduce chemical use. In 2017, Jaichueai et al. [136] prepared and studied the glass system derived from cassava rhizome on elastic and structural properties. In this study, cassava rhizome was successfully fabricated into a new glass system. The results showed that the elastic moduli depended on percentage of CaO in glass system, which is related to the formation of bridging oxygen (BO) and non-bridging oxygen (NBO). The results of FTIR spectra also support the result of the pulse echo technique. This research shows that CaO derived from cassava rhizomes can be substituted for the pure CaO and can be used as modifier in the glass system. In a similar way, glass series $[(TeO_2)_{0.7}$–

$(B_2O_3)0.3]_{1-x}$– $(SiO_2)_x$ were fabricated from the rice husk silicate (RHS) by Halimah et al. in 2019 [137]. The effects of rice husk silicate on the elastic, physical and structural properties were evaluated. The ultrasonic velocities, elastic moduli, and Debye temperature increased with the rice husk proportion increased. The XRD performed on the samples revealed no presence of sharp peaks, confirming the amorphous nature of the glasses. The FTIR spectra showed the presences of TeO_3, TeO_4, SiO_4, BO_3 and H_3BO_3 structural units in the glass system. In another study, Gunhakoon et al. [138] successfully fabricated barium-borate-bagasse-cassava rhizome-WO_3 glass using a popular melt-quenching method. Ultrasonic contact technique was used to measure the ultrasonic velocity as well as to evaluate elastic moduli and microhardness. Moreover, microhardness values were also studied using a microhardness testing machine. The results showed that the elastic moduli decreased with increase of dopant concentration in the glass system. Microhardness obtained from microhardness and ultrasonic testing showed the same decreasing trend as WO_3 concentration. The use of these waste materials, by replacing pure chemicals, can reduce the overall costs associated with glass material production, and consequently they can apply in many applications.

Taking into account the experimental evidence summarized in this review and the discussion above, an interesting challenge for developing scaffolds for bone regeneration is the preparation of bioactive glasses derivative from natural materials. Moreover, it is also controlled ion dissolution and bioactive behavior. In this regard, in future material-based approaches, novel bioactive glasses can serve as valid biomaterial platforms for the delivery of tailored concentrations.

CHAPTER 3
EXPERIMENTAL

3.1 Bagasse and cassava rhizome characterization

Ashes of bagasse and cassava rhizome were collected from electric power plant and agricultural plantation in Northeast region of Thailand, respectively. Each ash was crush in an agate mortar and it was graded to obtain particle size of 180 μm using a sieve shaker machine. After that, the fly ash of bagasse and cassava rhizome sample were calcined in an electric furnace under for 1 h at 800 and 1,000 ℃, respectively. The corresponding constituents of both ashes were analyzed by using WDXRF instrument (Panalytical, MagiX) with super sharp x-ray tube (rhodium anode) and two detectors (gas-filled proportional and scintillation). The constituents of bagasse and cassava rhizome were listed in Table 3.1.

3.2 Glass preparation

Two series of biomass-containing glasses based on composition of (68-*x*)B_2O_3–$3P_2O_5$–$17Na_2O$–12CaO–*x*BG and (68-*x*)B_2O_3–$3P_2O_5$–$17Na_2O$–12CaO–*x*CR where BG and CR are bagasse and cassava rhizome and x = 0, 5 and 10 wt% were prepared. These glasses were fabricated from reagent-grade powders of H_3BO_3, $(NH_4)_2HPO_4$, Na_2CO_3, and CaO as well as bagasse and cassava rhizome powders, mixed together in appropriate amounts until obtaining homogeneous in alumina crucibles. The homogeneous mixture was then calcined and melted in an electrically heated muffle furnace under normal laboratory condition without controlling the atmosphere. Temperature range of 1,100-1,200 ℃, depending on the composition, for 2 h-melting were employed to ensure the homogeneity before pouring onto a graphite block. Vitreous samples were then placed again into the furnace at appropriate temperature of 450 ℃ for an annealing process to reduce any residual stress in the glass. After 2 h, the furnace was switched off and such glass sample was allowed to cool slowly to room temperature. To generate good quality of ultrasonic velocity and Vickers hardness results, the glass samples were then obtained by cutting, grinding and polishing with parallel flat and smooth surface.

Table 3.1 Chemical compositions of treated bagasse and cassava rhizome by WDXRF method

Compounds	Bagasse (wt%)	Cassava rhizome (wt%)
MgO	1.430	16.300
Al_2O_3	5.990	1.230
SiO_2	77.100	16.700
P_2O_5	0.900	12.100
K_2O	3.530	14.600
CaO	5.180	37.079
TiO_2	0.395	0.227
Cr_2O_3	0.019	0.034
MnO	0.184	0.618
Fe_2O_3	5.182	0.787
CuO	0.013	–
ZnO	0.021	0.063
SrO	0.016	0.226
ZrO_2	0.040	0.036
Total	100.000	100.000

3.3 Density studies

A simple Archimedes' technique using n-hexane (C_6H_{14}) as the reference worked liquid was determined the density of the fragments of bulk glass. Knowing the apparent weight of the glass samples measured in air and reference fluid (W_a and W_r) allows us to calculate the density (ρ_m) by the expression in equation (1) where ρ_r is the density of C_6H_{14} solution equal to 0.6600 g/cm^3 [139-140].

$$\rho_m = \rho_r \left(\frac{W_a}{W_a - W_r} \right) \tag{3.1}$$

The calculated density for borate glasses with correlation factor 99.4% that proposed by Gaafar et al. [141] can calculated by following expressions:

$$\rho_{cal} = \gamma \sum_i \rho_i x_i \tag{3.2}$$

where ρ_{cal} is the theoretical glass density, whereas ρ_i and x_i are the density and its weight fraction of the i^{th} component, respectively. The slopes of the relation between measured and calculated densities are the modified coefficient (γ). For borate glasses, the modified coefficient values were found to be as 0.9, as show in Figure 3.1.

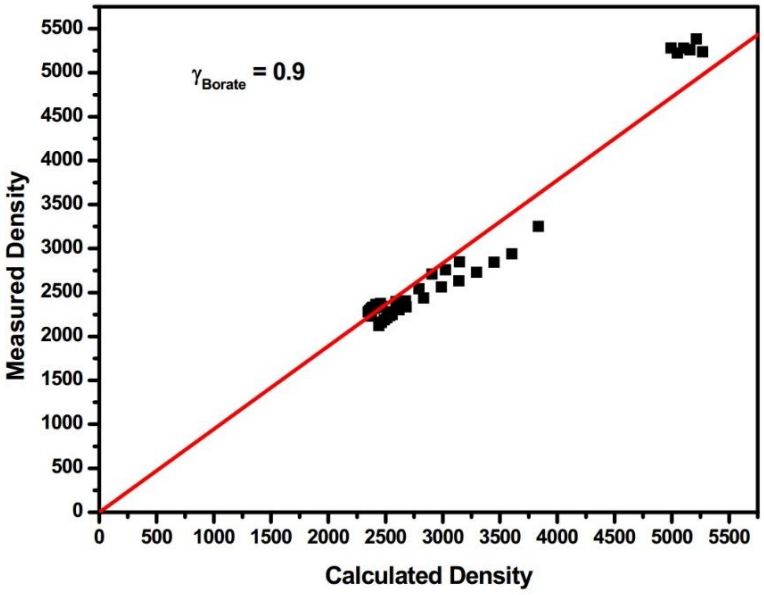

Figure 3.1 The relation between measured density and calculated density (in kg/m^3) of the compositions for borate glasses [141]

3.4 Elastic constants measurements

The suitable pressure-controlled ultrasonic method was applied to find the sound velocity values. The longitudinal (v_l) and shear (v_s) wave velocities were generated from SLG4-10 and SA04-45° transducer probes, respectively. Both velocities were operated at a fundamental frequency of 4 MHz along with ultrasonic flaw detector (GE Phasor XS) in mode A-scan, and a constant pressure of 0.98 N was also applied to control its pressure on the glass surface. The velocities of the proposed glasses are obtained by measurement of the time intervals between transmission of the pulse and reception of the reply appearing directly on the monitor.

After receiving the density and sound velocity of the glass samples, elastic moduli (*L*, *G*, *K* and *E*), Poisson's ratio (σ), and microhardness (*H*) were calculated in the following equations [137,142]:

Longitudinal modulus: $L = \rho v_l^2$ (3.3)

Shear modulus: $G = \rho v_s^2$ (3.4)

Bulk modulus: $K = L - \left(\frac{4}{3}\right)G$ (3.5)

Young's modulus: $E = 2(1+\sigma)G$ (3.6)

Poisson's ratio: $\sigma = \frac{L-2G}{2(L-G)}$ (3.7)

Microhardness: $H_{UT} = \frac{(1-2\sigma)E}{6(1+\sigma)}$ (3.8)

3.5 Vickers microhardness determination

The Vickers microhardness test is reliable for measuring the microhardness of metals, and also used on glass and ceramic materials. Figure 3.2 shows the geometry of Vickers indentation using a square pyramidal indenter with an angle of 136° between opposite faces. This microhardness tester and ASTM standard (Mitsubishi, Mitutoyo MVK-H1) was applied to determine the Vickers hardness number (H_V) of the glass samples at room temperature. An average of three values of each glass sample was taken and any crack is not observed on the indents of the glass surface. Then, the H_V value was generally calculated directly as [143]:

$$H_V = 1.8544\frac{F}{d^2} \quad (3.9)$$

where H_V is expressed in GPa, if the applied load (*F*) is in N unit and *d* is the arithmetic average of the diagonals of the indent (d_1 and d_2) in μm.

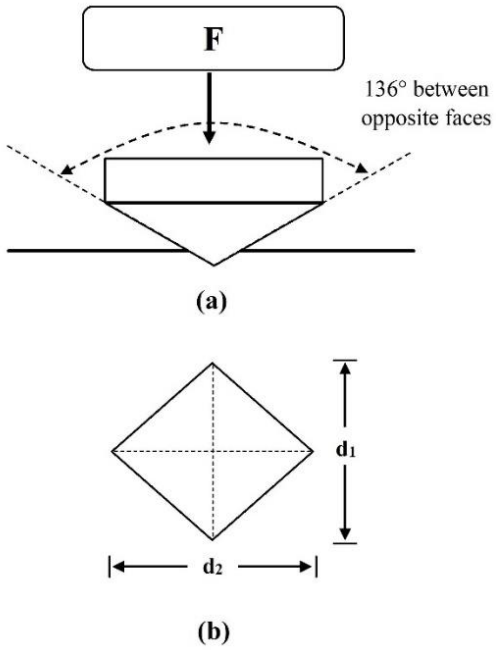

Figure 3.2 The geometry of Vickers pyramid diamond indenter indentation [144]

3.6 SBF solution preparation

To investigate the structural, morphological, bioactive and dissolved behaviors of the glass samples including pH after immersion in the *in vitro* environment, SBF solution was selected as its ion concentration is nearly equal to those of human blood plasma and the producibility of apatite formation on synthetic glasses. The details for preparing SBF solution were performed using the standard procedure described by Kokubo and Takadama [145]. Briefly, the SBF solution was prepared from the powder reagent grade chemicals with the amounts and ion concentrations as shown in Table 3.2. All the chemical reagents were dissolved in deionized water one by one by keeping it on a stirring bar into 1000 ml beaker with solution temperature between 35 and 38 ℃. In order to avoid increase in pH of solution, Tris ($(CH_2OH)_3{\cdot}CNH_2$) was added into the solution little by little taking careful note of the pH change. After adding a small amount of Tris, stop adding it and wait until the reagent already introduced is dissolved completely and the pH has become a constant. Final step, the solution was adjusted the pH of the solution to 7.40±0.5 at 37±0.5 ℃. The prepared SBF solution should be preserved in a plastic bottle with a lid put on tightly and kept at 5−10 ℃ in a refrigerator. After preparation, the SBF solution will be used within 30 days.

Table 3.2 Nominal ion concentrations (mM) of SBF in comparison with those in human blood plasma and amounts of chemical reagents for preparing 1000 ml of SBF solution [145]

Order	Ion	Ion concentrations (mM)		Reagent	Amount
		Blood plasma	SBF		
1	Na^+	142.0	142.0	NaCl	8.035 g
2	K^+	5.0	5.0	KCl	0.225 g
3	Mg^{2+}	1.5	1.5	$MgCl_2 \cdot 6H_2O$	0.311 g
4	Ca^{2+}	2.5	2.5	$CaCl_2$	0.292 g
5	Cl^-	103.0	147.8	1.0M−HCl	39 ml
6	HCO_3^-	27.0	4.2	$NaHCO_3$	0.355 g
7	HPO_4^{2-}	1.0	1.0	$K_2HPO_4 \cdot 3H_2O$	0.231 g
8	SO_4^{2-}	0.5	0.5	Na_2SO_4	0.072 g
9	–	–	–	Tris	6.118 g
10	–	–	–	1.0M−HCl	0−5 ml
–	pH	7.20−7.40	7.40	–	–

3.7 *In vitro* bioactivity

Assessments of vitro bioactivity was performed in 15 mL test tubes, containing 100 mm^2 of each glass sample (thin plate) and 10 mL of SBF solution. The volume of SBF (ml) that is used for testing using the expression of $V_s = S_a/10$, where S_a is the apparent surface area of specimen (mm^2) [145]. Sealed tubes are kept in a shaking incubator (ICP450, Memmert) at 37±0.5 °C for a total duration of 14 days. The glass samples were collected and characterized after immersion in SBF for 0, 1, 7 and 14 days. After each immersion period the glass samples are withdrawn from the SBF, dipped in deionized water and dried with cool air. All the samples were kept in a desiccator at room temperature for further SEM or XRD or FTIR analysis. Furthermore, the pH evolution of glasses in SBF during initial 14 days was measured using a pH meter (LAQUA-PH1300, Horiba Scientific). The solubility was determined by measuring the weight of each sample before immersion (W_b) and that after immersion (W_a). Then, percentage of weight loss was calculated using Eq. (10) [146]:

$$Weight\ loss[\%] = \frac{W_b - W_a}{W_b} \times 100\% \quad (3.10)$$

3.8 X-ray diffraction

The appearance of apatite phases after immersion of the glass samples was confirmed by using X-ray diffractometer (X' Pert Phillips). X'pert highscore plus software was applied to analyze the obtained data. In the XRD analysis, the diffractograms data were collected over the 2θ range from 10° to 80° using a step size of 0.02° with 0.5 second per step.

3.9 FTIR spectroscopy

The IR transmission spectra of the prepared glasses have been carried out in the spectral range of 400–4000 cm^{-1} using FTIR spectroscopy (Nicolet 6700, Thermo Scientific, USA). The measurements were made by the attenuated total reflectance (ATR) technique. The glass samples were cut and polished to a size of 10x10 mm^2 and made with an approximate thickness of 1 mm. Before the spectrum of all glass samples were recorded at ambient temperature, the blank air was measured for the background spectrum. FTIR spectra of all the glass samples after immersion in SBF solution were recorded using the same conditions as before immersion.

3.10 Scanning electron microscope analysis

SEM is one of the most widely used techniques in the characterization of materials because of its high resolution, high depth of field, that allows to have a tri-dimensional appearance of the images, and finally to the easiness of samples preparation.

A SEM analysis was performed to observe the morphology surfaces on the five glass samples before and after soaking in SBF solution. The spectroscopy analysis was characterized using a JEOL/JSM-7610F field emission scanning electron microscope. To generate good-quality SEM images, the glass samples with parallel flat and smooth surface were then obtained by cutting and polishing. All the studied glasses were coated with platinum in vacuum to be able to conduct electricity for morphological considerations of the textures.

3.11 Research method overview

The current research primarily focuses on developing bioactive glasses fabricated from agricultural wests for bone tissue engineering applications. The feasibility study of these glasses as bone replacement materials has to study in various properties such as physical, mechanical, structural and biological properties. A visual overview of research methods in this work is shown in Figure 3.3.

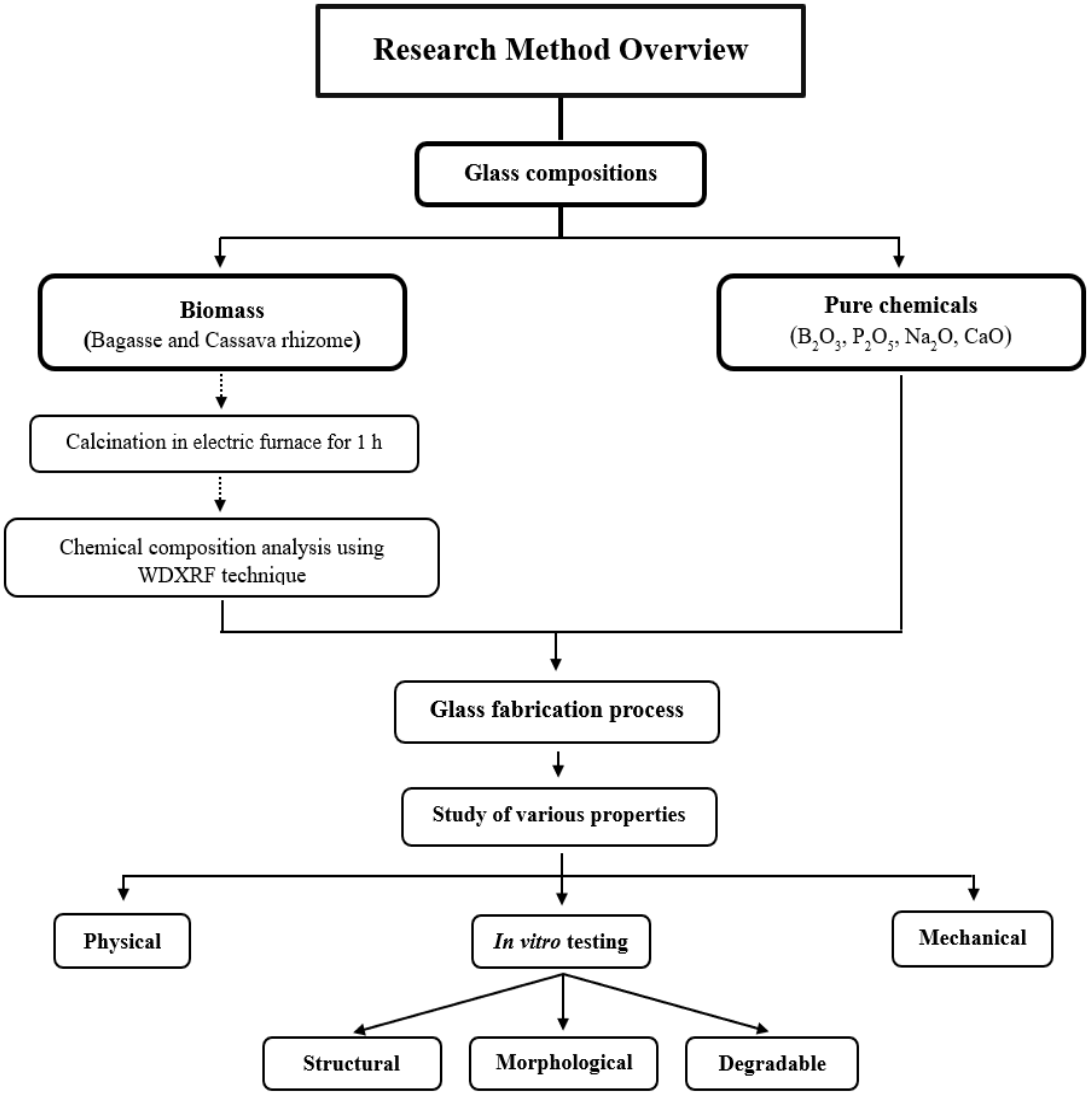

Figure 3.3 The overview of research methods

CHAPTER 4
RESULTS AND DISCUSSION

In general, glasses and glass-ceramics are popularly used as bone replacement materials, and their properties have been studied extensively. The mechanical properties of bioactive glass are extremely important for bone replacement. The suitable strength and flexibility of the glass also affect its performance. Preparation of the bioactive glass from natural materials is an interesting way. This bioactive glass may yield attractive features, besides the low cost and environmentally friendly.

This chapter was thus dedicated to study and characterize the bioactive glass with natural materials. Bagasse and cassava rhizome were chosen as the materials that obtained from nature for preparing the glass sample. The investigation in this chapter was focused on the feasibility study of using bagasse and cassava rhizome to fabricate a novel bioactive glass. The physical, mechanical and structural properties as well as *in vitro* bioactivity behaviors of the bioactive glasses were carried out. Hydroxyapatite formation on the surface of the prepared glass upon immersion in SBF solution, as a measure of the bioactivity, was investigated by using XRD, FTIR and SEM in this work.

4.1 Physical properties

4.1.1 Glass sample

The soda-lime borate glasses with different mix proportions of bagasse and cassava rhizome from 0 to 10 wt% were prepared. The chemical composition of the glass samples is presented in Table 4.1. The results of glasses preparation in the soda-lime borate system revealed that all the glass samples are stable and homogeneous without air bubble and crack. The homogeneity of the glasses indicates a satisfactory distribution of the element ions in the glass samples. The based glass and cassava rhizome-added glass samples exhibited clear transparency to visible light. However, the compositions with bagasse showed transparent light greenish-yellow in the glasses. The observed characteristics of the glass samples are shown in Figure 4.1.

Table 4.1 Glass composition and density of the glasses with different mix proportions of bagasse and cassava rhizome

Sample	Composition (wt%)						Density (g/cm^3)		%Error
	B_2O_3	P_2O_5	Na_2O	CaO	BG	CR	ρ_m	ρ_{cal}	
GS0	68	3	17	12	-	-	2.3403	2.3332	0.3053
BGS5	63	3	17	12	5		2.3550	2.3446	0.4424
BGS10	58	3	17	12	10		2.3857	2.3561	1.2563
CRS5	63	3	17	12	-	5	2.3692	2.3534	0.6711
CRS10	58	3	17	12	-	10	2.4051	2.3736	1.3304

*BG is the bagasse and CR is the cassava rhizome

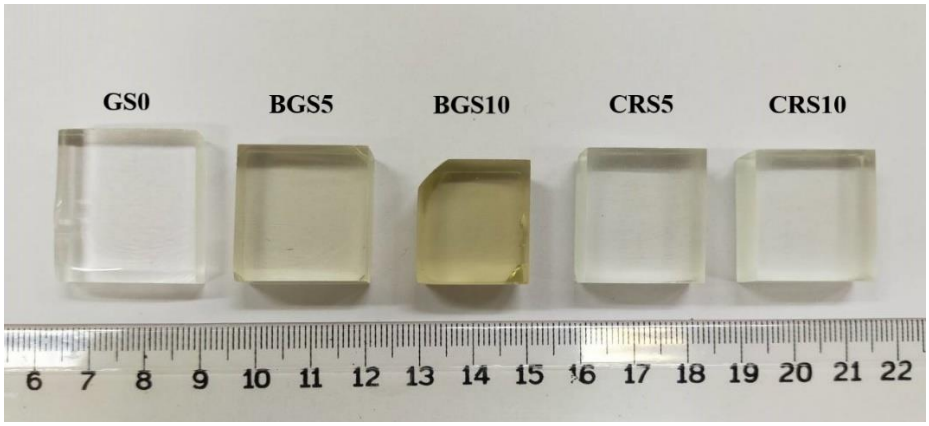

Figure 4.1 The observed appearances of the glass samples with different mix proportions of bagasse and cassava rhizome

4.1.2 Density of glass

Density is an important tool to understand the structural changes in the glass network with its composition. The structural changes related to the geometrical configuration, coordination number, cross-link density and interatomic spacing of constituent atoms [147]. The density of the prepared glasses has been measured by Archimedes' principle. The measured density of all the glass samples was calculated from Eq. (3.1). In addition, the theoretical density has been calculated based on the additive rule ($\rho = \sum \rho_i x_i$). To acquire the corrected value, the calculated density for borate

groups has been modified by the corrected factor (γ) according to Eq. (3.2) described in the research of Gaafar et al. [141]. Variations of the density of the whole glasses have been listed in Table 4.1. It was found that as the content of bagasse and cassava rhizome increased, both densities of the glass samples increased. The variation of density value in a glass system, generally, is associated with change in the standard molecular weight of its composition [142]. Thus, the increased behavior of density in the studied glasses indicates that the total molecular weight of bagasse and cassava rhizome is higher than the molecular weight of the borate agent in the glass system.

Comparison of the density between measured and calculated values of the glass samples with different mix proportions of bagasse and cassava rhizome is shown as a bar chart in Figure 4.2. It was clearly that the measured and calculated densities tend to be in the same direction. The measured density using Archimedes' technique is slightly greater than the calculated value. The minimum and maximum percentage errors between both values for all the prepared glasses were 0.3053% (GS0) and 1.3304% (CRS10), respectively (see in Table 4.1). Moreover, the substitution of B_2O_3 by the cassava rhizome yields the density values higher than that by the bagasse. This might be due to the change in the net molecular weight of its constituent component.

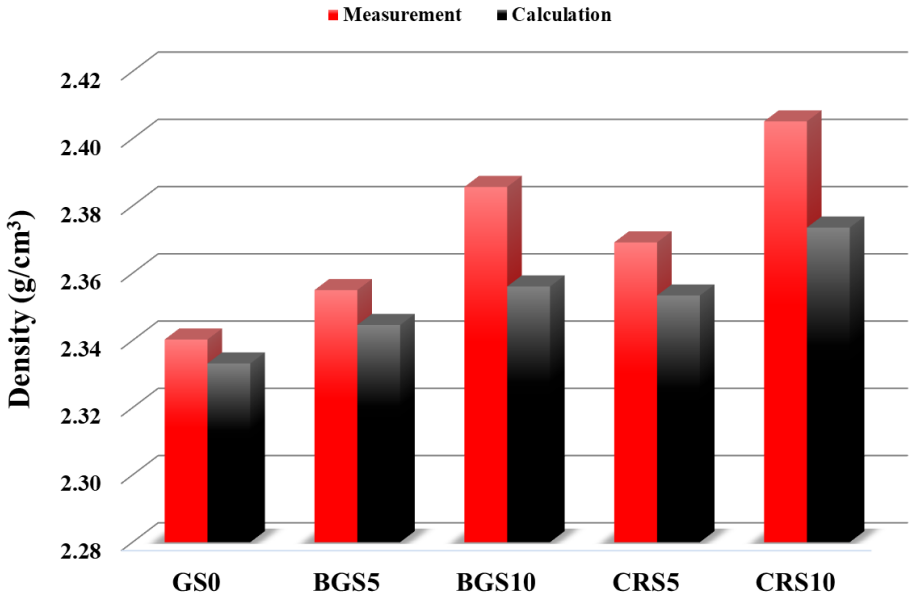

Figure 4.2 Comparison of density between measured and calculated values of the glasses added with bagasse and cassava rhizome

4.2 Mechanical properties

4.2.1 Ultrasonic velocity

The variant behavior of the acoustic velocity can be explained on the basis of the structural modification and rigidity of borate glass network. It is well known that an increase in ultrasonic wave velocity in borate glass system is associated with the change from the trigonal BO_3 to tetrahedral BO_4 units, resulting in the increase of glass rigidity [148-149]. Ultrasonic velocities (v_l, v_s) of the different glasses with respect to change in wt% of bagasse and cassava rhizome are shown in Table 4.2. It was found that the longitudinal and shear velocities increased with the amounts of bagasse and cassava rhizome. The increase in both longitudinal and shear acoustic velocities of the glass samples can be clarified by an increase of network-forming groups in the internal glass structure when these glasses were substituted by bagasse (representative of SiO_2) and cassava rhizome (representative of CaO). According to reports of Halimah et al. [138], Saddeek et al. [150] and Manupriya et al. [151], an increase of amounts of SiO_2 and CaO in borate glass led to the conversion of BO_3 to BO_4, supporting the increase in sound wave velocities in these glasses. As seen from Table 4.2, it is clearly that the bagasse-added glasses yield the higher values of ultrasonic velocities than the cassava rhizome-added glasses when comparing at the same concentration. These indicate that the glasses containing bagasse can form the BO_4 structure units more than that containing cassava rhizome.

Table 4.2 The ultrasonic velocities (v_l, v_s), elastic moduli (L, G, K, E) and Poisson's ratio (σ) of the prepared glasses

Sample	Ultrasonic velocities (m/s)		Elastic moduli (GPa)				σ
	v_l ±3	v_s ±5	L ±0.08	G ±0.08	K ±0.14	E ±0.13	
GS0	5786	3405	78.36	27.13	42.19	67.02	0.24
BGS5	5956	3524	83.54	29.25	44.54	71.99	0.23
BGS10	6112	3622	89.12	31.29	47.40	76.94	0.23
CRS5	5875	3482	81.78	28.72	43.49	70.61	0.23
CRS10	6005	3571	86.73	30.68	45.83	75.24	0.23

4.2.2 Elastic constants

Glass is considered as elastic substance and, consequently can be characterized via elastic constants such as longitudinal, shear, bulk and Young's modulus as well as Poisson's ratio [152]. These are key parameters for determining the mechanical effectiveness of an implant as a good stiffness match between bioactive glass and host tissue allows favorable stress transfer along the interfacial zone, therefore resulting in stable bonding and osteointegration [153]. The elastic modulus of glasses is highly dependent on their individual compositions and preparation methods. According to mechanical investigation with ultrasonic non-destructive technique, the ultrasonic velocity and density parameters were used to compute the elastic moduli, Poisson's ratio and microhardness of the studied glass. The variation of longitudinal modulus (L), shear modulus (G), bulk modulus (K), Young's modulus (E) and Poisson's ratio (σ) of the glasses with different mix proportions of bagasse and cassava rhizome has been depicted in Table 4.2. In the present glass system, Longitudinal modulus changes in range of 78.36 to 89.12 GPa, shear modulus changes in range of 27.13 to 31.29 GPa, bulk modulus changes in range of 42.19 to 47.40 GPa and Young's modulus changes in range of 67.02 to 76.94 GPa. From the results, the minimum and maximum values of all elastic moduli were found to be in the borate-based glass (GS0) and the glass added with 10% of bagasse (BGS10), respectively. The data of modulus of elasticity in Table 4.2 are plotted as a bar chart in Figure 4.3. The results presented that all the elastic moduli increased with the addition of bagasse and cassava rhizome and showed the same trend as the ultrasonic wave velocities. The enhanced elastic modulus in the borate glass points out the increase in bonding strength in the borate structure [149]. Almost all elements of the bagasse are SiO_2, while CaO is a most common representative in the cassava rhizome. Both substitutes can act as network-forming groups in borate glass. When oxide constitutes representing bagasse and cassava rhizome were added in the borate glasses, oxygen bonds in the glass structure are formed. This may have the effect of converting BO_3 triangles to BO_4 tetrahedra, and led to an increase of the elastic properties in the studied glasses. In addition, it may also be observed from Figure 4.3 that the rate of change of all the elastic moduli is more pronounced in longitudinal modulus and least in case of shear modulus. This indicates that the prepared glass is more resistance to deformation in longitudinal direction than shear direction.

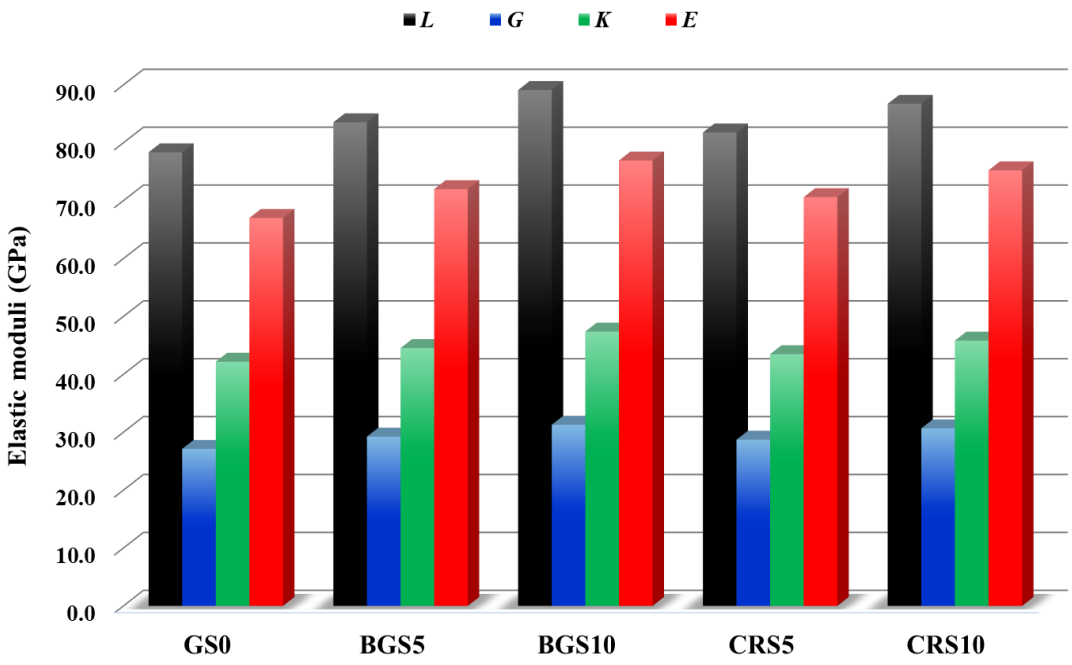

Figure 4.3 Comparison of elastic moduli (*L*, *G*, *K*, and *E*) of glass samples with different mix proportions of bagasse and cassava rhizome

Poisson's ratio (σ) is used to characterize mechanical behavior that related the ductility or brittleness of oxide glasses [105-106], has renewed attention to this quantity. As well known, Poisson's ratio value has sensitive on the variation in glass network which include both changes in its cross-link density and glass network dimensionality [29,147,152]. Poisson's ratio can be computed by using ultrasonic velocities according to Eqs. (3.7). Normally, Poisson's ratio is dimensionless and ranges between 0.1 and 0.45. Low Poisson's ratio (0.1–0.25), associated the distortion of the tetrahedral unit through bond bending, means glasses fracture easier whereas high Poisson's ratio (0.35–0.45) implies the glasses are harder to fracture [154-155]. As can be seen from Table 4.2, the value of Poisson's ratio of all the glass samples almost maintains a constant value and are less than 0.25 as the bagasse and cassava rhizome content increased. This indicates that a part of the energy results in the distortion of bond bending of the borate structure, and consequently the prepared glasses have been identified in the brittle fracture range.

4.2.3 Microhardness

Microhardness is an important parameter often used to specify the mechanical properties of a material on a microscopic scale. It suggested the disposed stress in its free volume and the dislocations deformation, or damage under an applied stress, and consequently its values depends on an applied load [32, 156]. In this study, microhardness value of all the glass samples has been evaluated using both pulse echo ultrasonic and Vickers indentation techniques. Results of the ultrasonic and Vickers microhardness values are listed in Table 4.3. It can be seen that the microhardness of the studied glasses in both measurements increased as bagasse and cassava rhizome content increased. This increment may point out an increase in its rigidity by addition of bagasse and cassava rhizome content due to the conversion of BO_3 into BO_4 glass network. The values of microhardness in the glasses added with the bagasse is higher than that added with cassava rhizome. Additionally, the microhardness values obtained from the ultrasonic and Vickers techniques tend to be in the same direction, and the ultrasonic method has a higher microhardness value than the Vickers method. This may be due to both techniques are based on different considerations. Ultrasonic microhardness is determined whole bulk of glass while Vickers microhardness is merely considered on glass surface. For percentage difference between both values, BGS10 was reported as low as 13.63% while the maximum of 25.41% in GS0 was identified.

Table 4.3 The microhardness obtained from ultrasonic (H_{UT}) and Vickers indentation (H_V) techniques of the glass samples

Sample	Microhardness (GPa)		%Difference
	H_{UT} ±0.04	H_V ±0.20	
GS0	4.79	3.71	25.41
BGS5	5.25	4.33	19.58
BGS10	5.64	4.99	13.63
CRS5	5.18	4.07	24.00
CRS10	5.60	4.84	14.56

4.3 *In vitro* bioactivity behaviors

The behavior that hydroxyapatite (HA) is formed on bioactive glass in a simulated body fluid (SBF) is known as the *in vitro* bioactivity, an important evaluation for the *in vivo* bioactivity of such bone-forming biomaterials [157]. A capable glass of stimulating bone regeneration requires a combination of behaviors such as biocompatibility, bioactive and degradation characteristics with adequate mechanical properties [94]. Proper composition of the selected materials is critical parameters in order to achieve the above requirements. The uniformity at which the HA layer is forming on the glass surface are very important and need to be coupled with the right release of ions in order to support bone formation.

A variety of glasses were tested for bioactive, in term of HA formation, after immersion in SBF. The formation of HA is a characteristic of bioactive materials. Literature has suggested that materials with suitable composition and high ionic solubility readily form HA precipitates on their surfaces. This takes place through a chain of reactions including dissolution, precipitation and ion exchange accompanied by absorption and incorporation of biological molecules. The degradation of the ions increases the degree of supersaturating of the surrounding fluid with respect to HA. The growth of the HA layer proceeds by reaction with the calcium, phosphate and hydroxide ions from the SBF; sometimes, ions such carbonate or fluoride are also incorporated in the structure.

4.3.1 Weight loss

Degradation behavior of bioactive glasses is a key parameter providing an idea about how fast glass will degrade in the human body. The method of measuring chemical durability of glasses has been formulated to estimate the weight loss change of glass plates or powders with the corroding solution. Weight loss change provides a convenient parameter and rapid method for monitoring the conversion kinetics of glasses. The corrosion process of glasses is commonly known to dissolve in aqueous solutions with variable degrees depending on several factors such as the kind of network former and its percentage including the time period and temperature of corrosion [10,66]. In addition, the nature of leaching solution whether it is acidic or alkaline solution or the constituent ionic species in the leaching solution is one of parameters that influential on its corrosion [158-159].

For the bioactive glasses, the *in vitro* degradation behavior was assessed by measuring plate weight loss after immersion in SBF solution for 1, 7 and 14 days, and graphical variation of weight loss data was showed in Figure 4.4. The obtained results clearly illustrate that all the glass specimens showed a similarly increasing trend upon SBF immersion. Additionally, GS0 has the highest degradation rate with reaching a mass loss of 3.38% whereas CRS10 has the lowest degradation rate with mass loss of 0.53% all over the considered interval. The addition of bagasse and cassava rhizome of 5 and 10 wt% results in an obvious decrease of degradation rate, especially, the glasses added with cassava rhizome. These observations confirmed that the borate-based glasses have a faster dissolution rate, however, the replacement of B_2O_3 by oxides of bagasse and cassava rhizome leads to conversion of $[BO]_3$ to $[BO]_4$ structural units, which are interlinked firmly in four equal directions and did not only noticeably increase the network connectivity but also increase the chemical durability and strength.

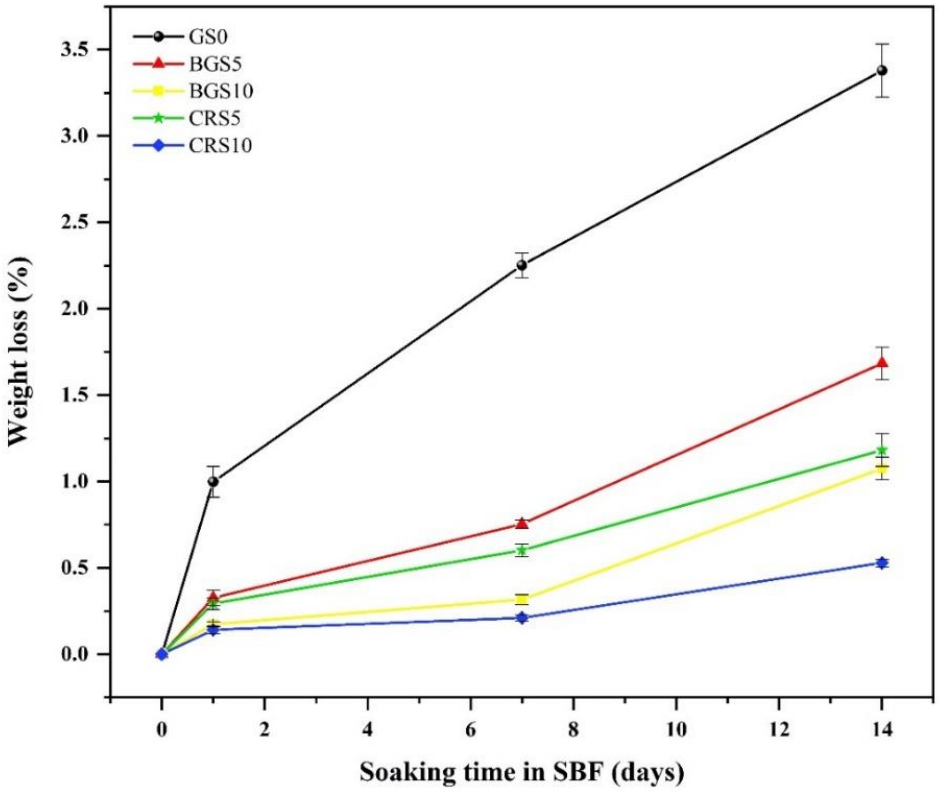

Figure 4.4 Weight loss (%) of the glasses in SBF solution as a function of time

4.3.2 pH evaluation

The degradation process of a bioactive glass takes place by ionic exchange of soluble ions, which depending on the glass composition, influence the pH of the surrounding media [160]. In order to evaluate the hydrolytic stability of the glass plates after immersion in SBF, the pH changes during exposure at 37 ℃ for 14 days of immersion were assessed. The pH changes during mixing of concentrated solutions were negligible and thus beneficial to avoid precipitation. After preparation, the initial pH of the SBF solution was 7.4±0.5.

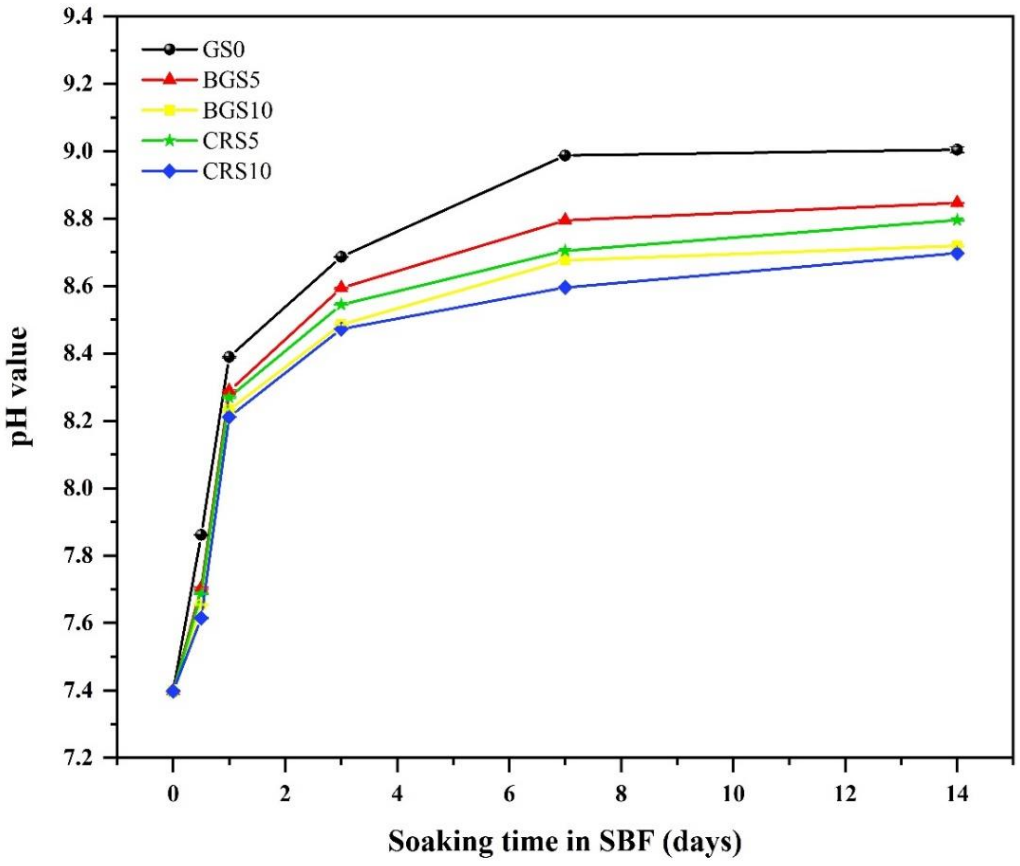

Figure 4.5 Variation of pH of the SBF solution measured on various time intervals for the B_2O_3–P_2O_5–Na_2O–CaO glasses during immersion

The variation in the pH value of the studied glasses that were incubated SBF at 37 ℃ as a function of time is represented in Figure 4.5. The observed changes in all the glasses are due to ion exchange that takes place between the glasses and SBF

solution. The results suggested that there is a rapid change of pH value during first day of immersion, after that the pH value of all the glass samples gradually increases up to the seventh day, and then it is almost constant. The increase of the pH value may be due to the release of alkaline ions from the glasses to the solution and more absorption of supplementary ions and sufficient use of OH^- ions from the SBF [161-163]. In addition, migration of Ca and P ions from the solution also contributed in increasing trend of pH which led to the precipitation of hydroxyapatite (HA) layer formation on the glass surface [157]. On the other hand, the deposition of saturated PO_4^{3-} and Ca^{2+} ions on the glass particles influences the pH value to remain constant after 7^{th} day. After incubation in SBF, the glass plates are collected and again characterized using XRD, FTIR, and SEM to ensure the HA layer formation on the glass surface.

4.3.3 X-ray diffraction (XRD)

Both before and after immersion, XRD analysis was performed on each sample to check apatite phases formed on surface of all the prepared glasses. The whole series of reference patterns for brushite (ICDD No. 00-011-0293) and hydroxyapatite (JCPDC No. 00-009-0432) can be found in the appendix. As well known, apatite-forming on glass surface originates in two steps, in the first step one amorphous calcium phosphate layer (non-crystalline apatite) is formed, while it is eventually converted into crystalline calcium phosphate (crystalline apatite) in the second step [146]. If the crystalline phase of apatite forms on the surface, some sharp peaks will appear in the XRD patterns. However, in some cases, the hydroxyapatite can also be formed by the transformation of the brushite phase.

The obtained results of XRD patterns of each glass sample are presented Figure 4.6–4.10. Before immersion, the obtained results show that the five samples exhibit similar XRD patterns and two broad bands in the ranges between $15^o \leq 2\theta \leq 35^o$ and $40^o \leq 2\theta \leq 50^o$ were observed. An absence of any sharp diffraction peaks in the typical XRD patterns confirms that the glass sample takes amorphous state indicative of the short-range order arrangement of atoms and glassy nature of these materials [164]. This is worth mentioning that all the prepared glasses do not show any crystalline states. After immersion at various times in SBF solution, the presence of some unique peaks as well as the decrease of the board hump intensity indicates the formation of brushite and hydroxyapatite phases on their surfaces. The diffraction peaks in all patterns

corresponded to the peaks of a reference ICDD No. 00-011-0293 and JCPDC No. 00-009-0432. Although the brushite and hydroxyapatite phases in GS0 (based glass) were observed, as could be seen in XRD results (Figure 4.6 to 4.10), the addition of bagasse and cassava rhizome into the glasses does show only diffraction peak of brushite phase located at 11° after 1 day immersion, however, their brushite and hydroxyapatite phases were observed when immersed in SBF for 7 and 14 days. After 1 day of immersion in the SBF for GS0 sample, the recorded pattern revealed the presence of amorphous and crystalline phases, the weak peaks appeared at 11° and 28° indicated the crystalline phase of brushite and hydroxyapatite phases while the one hump about 20°–25° attributed the amorphous calcium phosphate. After 7 days of reaction, the major peaks of the brushite and hydroxyapatite phases at 11° 23° and 28° appeared in all the glasses excluding the glasses doped with cassava rhizome which revealed just peaks of 11° and 26°. These diffraction peaks confirm the formation of calcium phosphate phases on the glass surface. Both amorphous and crystalline phases of calcium phosphate revealed after immersion in SBF, and all the peaks that appear in the XRD patterns became more apparent as more immersion time.

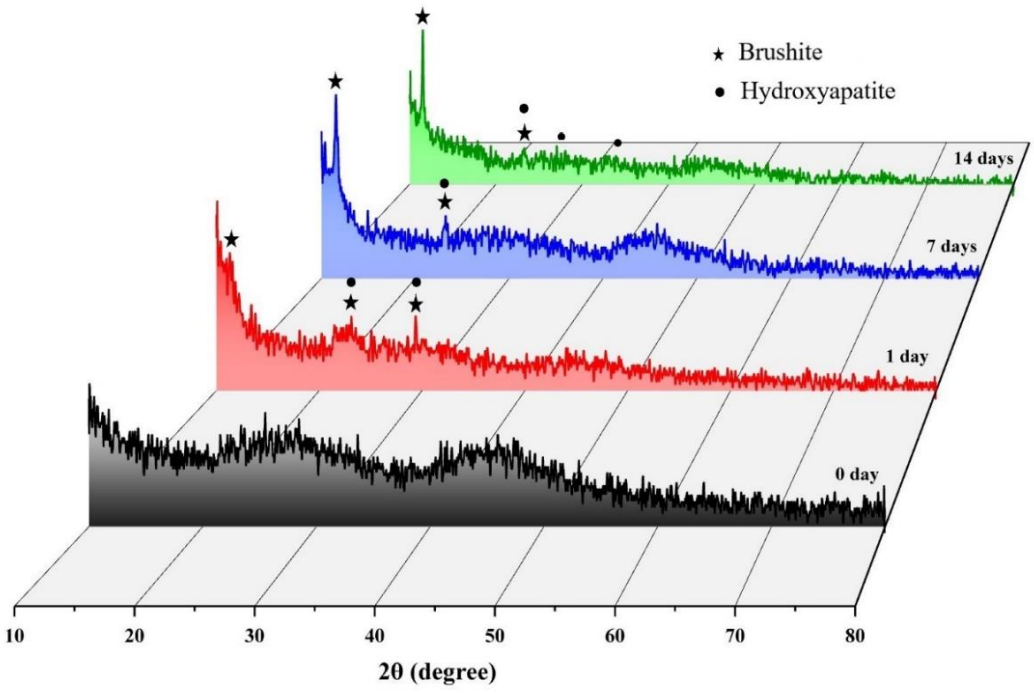

Figure 4.6 XRD patterns of GS0 before and after immersion in SBF solution

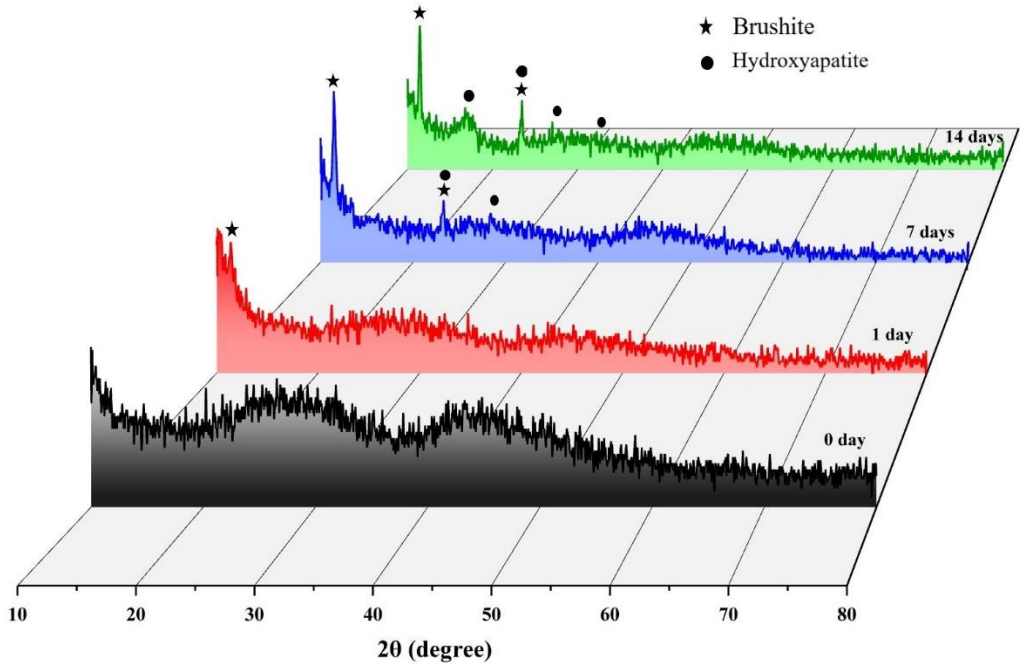

Figure 4.7 XRD patterns of BGS5 before and after immersion in SBF solution

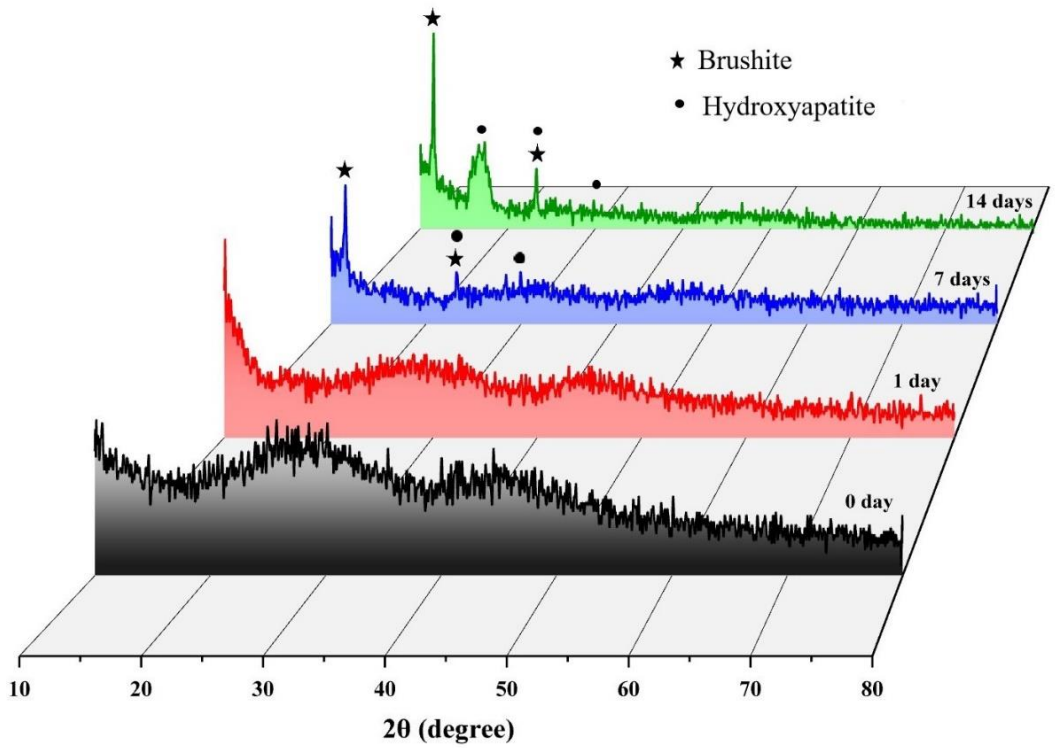

Figure 4.8 XRD patterns of BGS10 before and after immersion in SBF solution

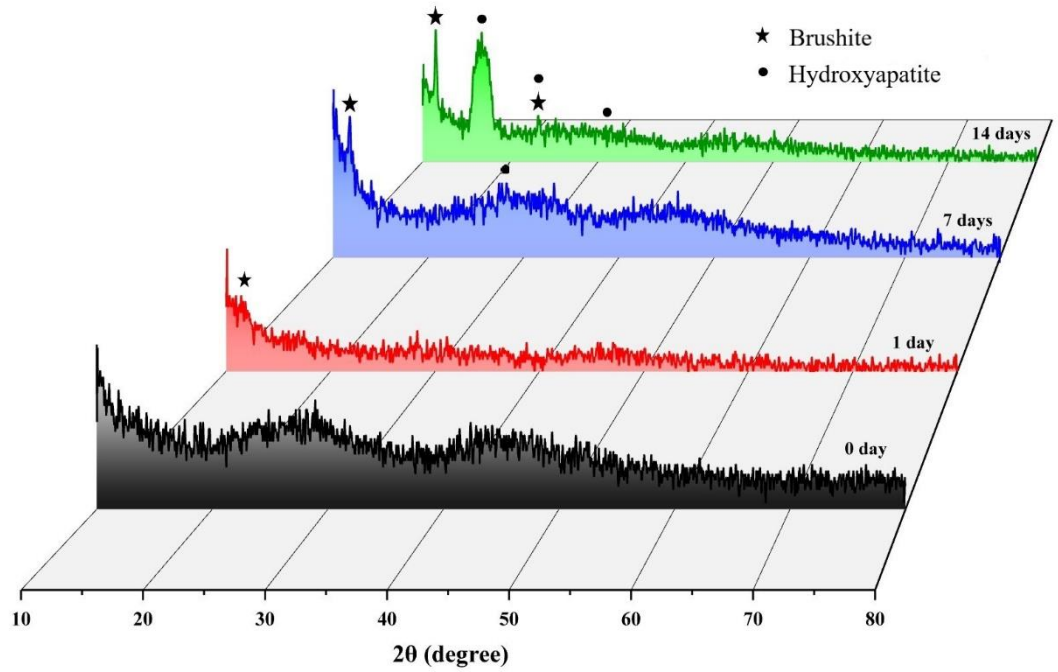

Figure 4.9 XRD patterns of CRS5 before and after immersion in SBF solution

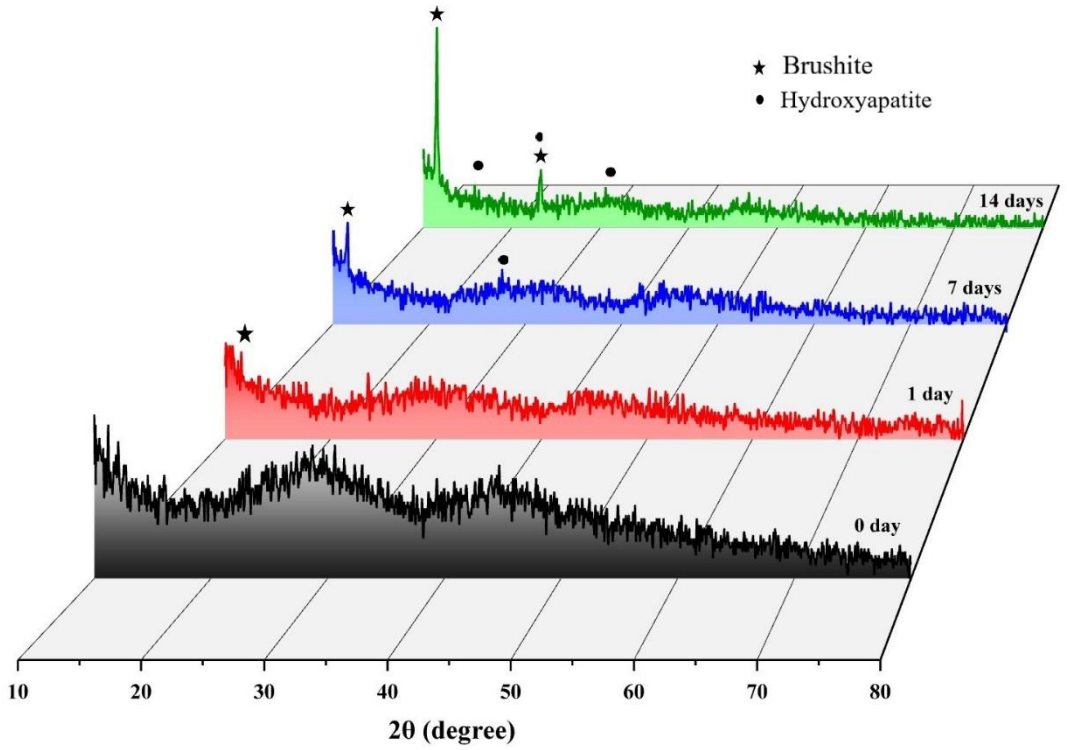

Figure 4.10 XRD patterns of CRS10 before and after immersion in SBF solution

4.3.4 Fourier transform infrared spectroscopy (FTIR)

Infrared spectroscopy is a beneficial analytical technique for understanding the internal structural units in the glass science, and it can be identified the bone bonding or bioactivity behavior in various bioactive glasses [10,165]. Attention was next turned to the spectral characterization of apatite via FTIR, using attenuated total reflectance (ATR) to indicate chemical bonding of the apatite on surface that is formed during immersion in SBF solution. The B_2O_3 percent in our glass is 58−68 % which is more than the percent of SiO_2 (0~10%) and P_2O_5 (3~5%). Therefore, vibrational signals are expected to arise mainly from the borate network, with a contribution from the vibrations of the silicate and phosphate networks. IR spectra in the region range of 400–4000 cm^{-1} of each glass before and after interaction with SBF solution at various times are illustrated in Figure 4.11−4.15. Depended on the compositions of the starting material, it was observed that the main spectra of borate, silicate and phosphate groups appeared clearly. In addition, the observed IR spectra with their assigned structural units are also provided in Table 4.4.

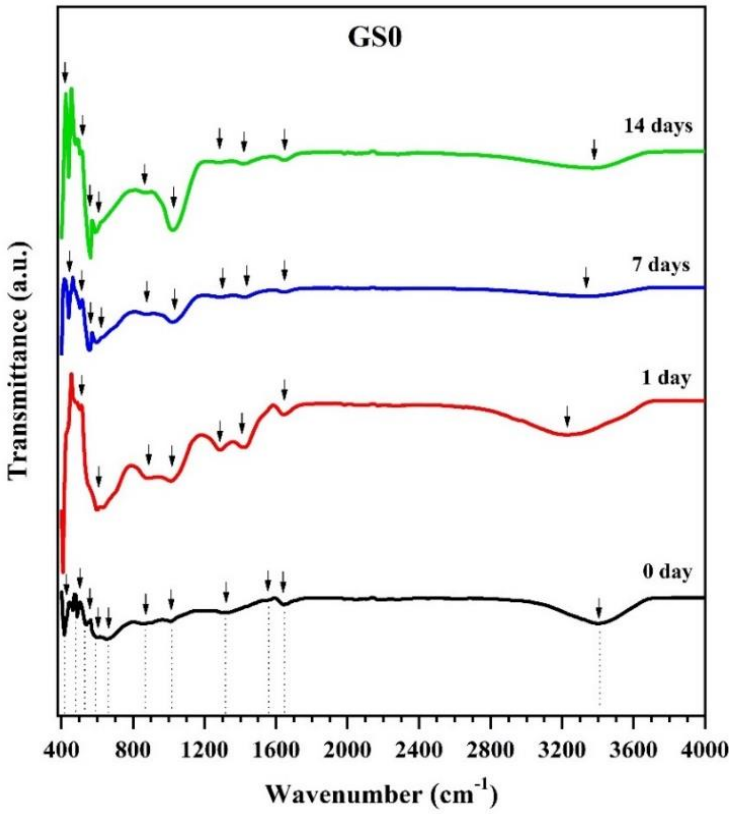

Figure 4.11 FTIR spectra of GS0 before and after immersion in SBF solution

Figure 4.11 shows the FTIR spectra of GS0 sample before and after immersion in SBF solution for different time periods. Before immersion in SBF, the FTIR spectra of the GS0 exhibited infrared bands positioned at: ~416, ~462, ~486, ~539, ~594, ~675, ~856, ~1018, ~1326, ~1548, ~1642 and ~3412 cm^{-1}. The bands located at 416 and 462 cm^{-1} are related to the bending vibration modes of borate groups overlapped by the vibration attributed to the presence of modifier cations (Ca^{2+}, Na^{2+}) [10,159,166]. Briefly, the vibrational peaks within the wave number of 400−700 cm^{-1} are related to the frequencies of bending vibration modes of borate and phosphate groups [166-167]. For borate groups, the main absorption bands at, 550–750 cm^{-1} and 1250–1400 cm^{-1} are attributed to the B–O bending and stretching modes of BO_3 groups, respectively, while the resonances at 400−500 cm^{-1} and 800–1200 cm^{-1} are assigned to the B–O bending and stretching vibrational modes of tetrahedral borate units (BO_4 groups), respectively [168-171]. The major functional phosphate groups for bending mode is attributed to the following peaks at 500−650 cm^{-1} while the bands in area range of 800–1100 cm^{-1} are due to the stretching P–O bonds [172]. The other resonances in the region extending from 1400 to 1600 cm^{-1} are attributed to the carbonate groups while 1600 to 3600 cm^{-1} are observed due to the presence of hydrogen bonding and OH groups [173-174]. After immersion, the distinct vibrational spectra of GS0 were positioned at ~439, ~478, ~501, ~563, 594, ~879, ~1026, ~1289, ~1420, ~1640, ~3324 and ~3412 cm^{-1}. After interaction with SBF reveals some strong peaks located at 563, 594 and 1026 cm^{-1}. These new vibrational bands after immersion related to the phosphate network associated with the formation of calcium phosphate or hydroxyapatite [175-177]. Moreover, the peak located at 1420 cm^{-1} was found, which is related to the carbonate groups [178]. This is expected to be caused by the formation of hydroxycarbonate apatite on the glass surface.

When introduced bagasse and cassava rhizome into the glass composition, the infrared spectra of the glasses reveal other structural units (i.e. Si–O–P and B–O–Si units), as shown in Figure 4.12−4.15 and Table 4.4. Before reaction with SBF (0 day), the strongly infrared bands observed in the glasses adding bagasse and cassava rhizome. The spectra positioned at: ~408, ~439, ~482, ~556, ~601, ~663, ~856, ~1195, ~1326, ~1642 and ~3412 cm^{-1} were observed before immersion in BGS5, BGS10, CRS5 and CRS10. Resonances in the spectra around 480 and 882 cm^{-1} is associated with bending

and stretching modes in the Si–O bonds in the silicate groups [179], respectively, moreover, at 882 cm^{-1} overlapped by the vibrational mode attributed to the tetrahedral borate units [170-171]. The increased intensity of the vibrational peaks at 882, 1018 and 1195 cm^{-1} also indicate the additional formation of boron–oxygen network in BO_4 units when added bagasse and cassava rhizome, however, their distinctiveness decreases after immersion. After interaction with SBF, the spectra represented internal structural units of the glasses added with bagasse and cassava rhizome were observed at 416, 439, 455, 470, 493, 524, 539, 563, 578, 594, 609, 694, 1026, 1420, 1432, 1643, 3324 and 3412 cm^{-1}. The major resonances presented at about 524–609 cm^{-1} after immersion can be attributed to bending modes of P–O bonds characteristic for amorphous HA phase while the band around 1026 cm^{-1} assigned to PO_4^{3-} vibrational modes for crystalline HA phase [180-181]. Moreover, the peaks located at 1420 and 1432 cm^{-1} are related to the carbonate groups with the formation of hydroxycarbonate apatite [178]. Formation of the phosphate group within the synthesized HA is therefore confirmed via FTIR studies.

Table 4.4 Assignment of vibrational modes in the IR spectra of the glass system

Assignment	Wave number (cm^{-1})	
	Before	After
Modifier cation vibrations	416, 439	408, 416, 439
Bending vibrations of BO_4 unit	462, 478, 486	455, 482, 493, 501
Bending vibrations of PO_4 unit	524, 590	524, 539, 563, 578, 594, 609
Bending vibrations of BO_3 unit	678	-
Stretching vibrations of BO_4 unit	879	694
Vibrations of B–O, Si–O, P–O units	1195	-
P–O vibrations associated with HA	-	524, 539, 563, 578, 594, 609, 1026
Stretching vibrations of BO_3 unit	1326	1295
Carbonate groups	-	1420, 1432
Water, O–H vibrations	1528, 1642, 3412	1642, 3324, 3412

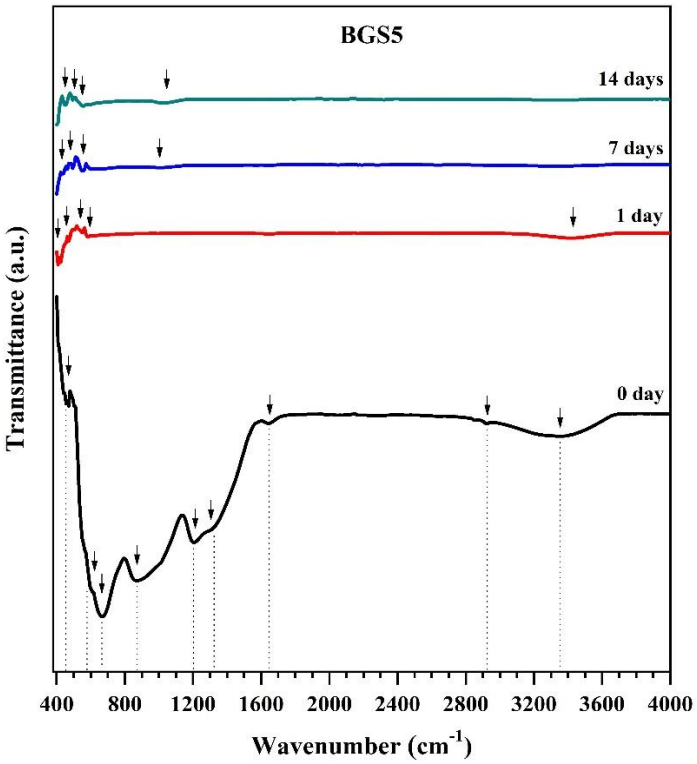

Figure 4.12 FTIR spectra of BGS5 before and after immersion in SBF solution

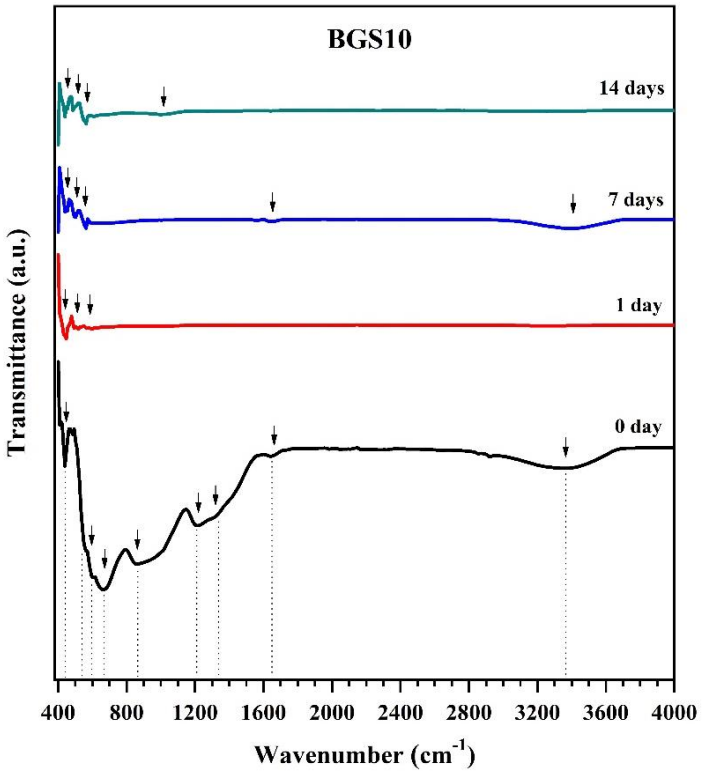

Figure 4.13 FTIR spectra of BGS10 before and after immersion in SBF solution

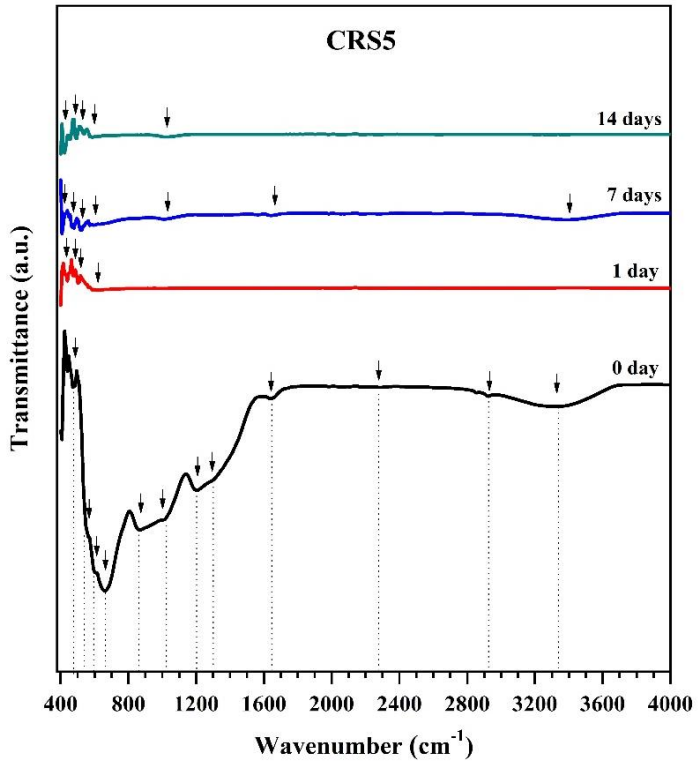

Figure 4.14 FTIR spectra of CRS5 before and after immersion in SBF solution

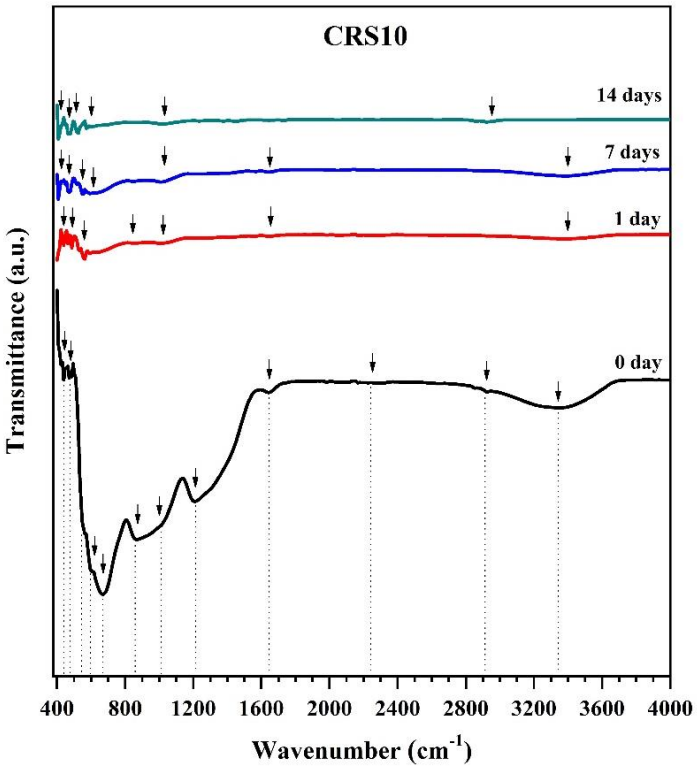

Figure 4.15 FTIR spectra of CRS10 before and after immersion in SBF solution

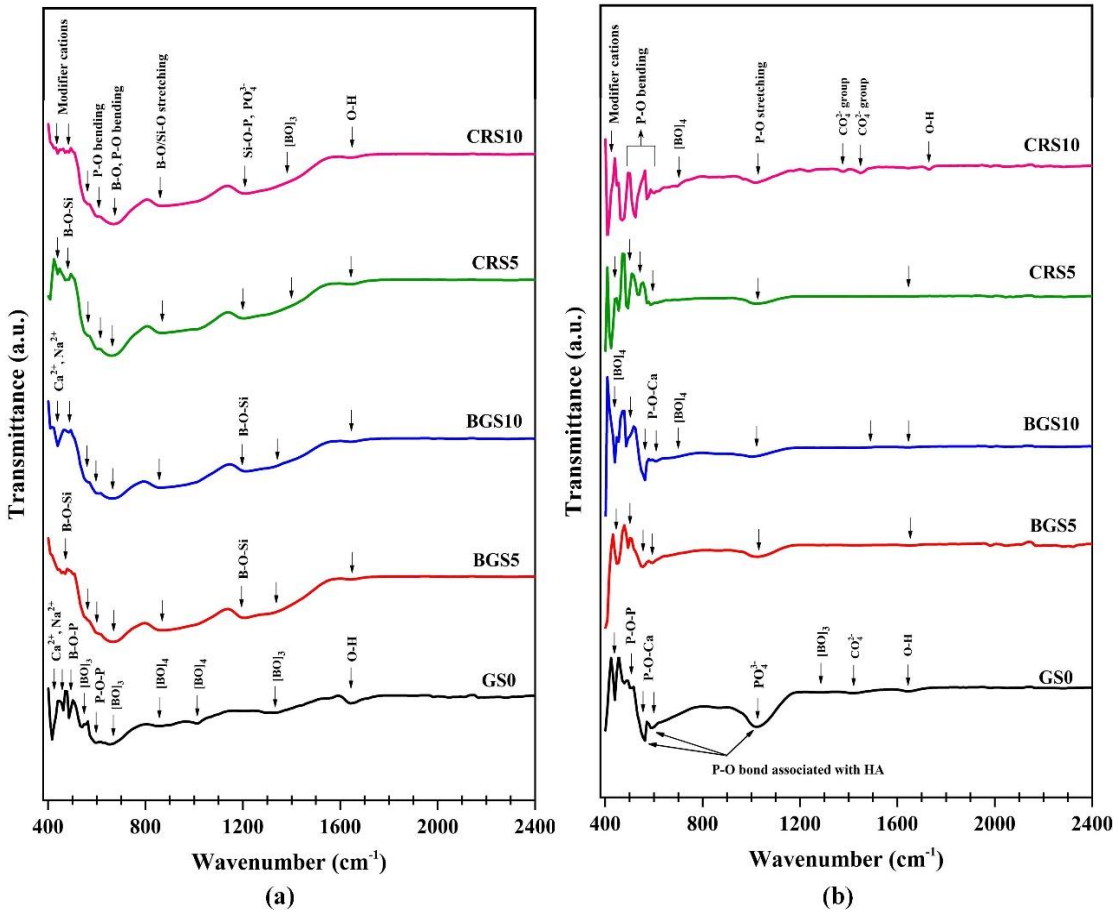

Figure 4.16 Comparison of FTIR spectra of all the glasses; (a) before and (b) after immersion in SBF solution for 14 days

Comparison of IR spectra of all the glasses before and after 14th day of immersion in SBF is presented in Figure 4.16. The results showed that the main spectra of borate along with a contribution from silicate and phosphate groups appeared clearly before immersion in SBF solution. After 14 days of interaction with SBF, the sharpness and broadness of some peaks are takes place. This confirms the formation of new groups related to exchanges of ions between the glass composition and SBF solution. It can be seen from Figure 4.16(a) before immersion that the FTIR spectra of GS0 reveal the vibrational modes of the major borate and phosphate groups, however, the addition of bagasse and cassava rhizome leads to the expression of the additional structural units related to silicate groups. After 14 days of immersion, the intensity of some bands represented borate groups in region around 600−1400 cm^{-1} decreased while some new

sharp peaks in the range of 400−600 cm^{-1} appeared clearly. The fading of IR bands of borate groups indicates that the glass surface is covered by the formation of some particles caused by ion exchange mechanisms after immersion in the SBF solution. The penetration depth of FTIR-ATR into the sample is typically between 0.5 and 5 microns depending on the material [182], so this leads to the fading of the spectrum representing the structural units in the glass due to the deposition of new particle groups on the glass surface. The IR spectra obtained for the studied glasses, as shown in Figure 4.16(b), exhibit strong bands corresponding to P–O bonds that are associated with the amorphous and crystalline calcium phosphate layers, confirming the formation of hydroxyapatite layer. The bands represented P–O vibrations around 500–650 cm^{-1} and 980–1060 cm^{-1} as well as the carbonate groups located at 1420 and 1432 cm^{-1} were observed in all the glasses [178-179]. These bands indicate the HA formation on the glass surface.

4.3.5 Scanning electron microscope (SEM)

SEM technique has been popularly applied for the morphological characterization on material surface. It produces images of a sample surface by scanning with a beam of electrons. The electrons interact with the different atoms presented at the sample surface, producing various signals that reveal information on the sample surface morphology. In the present study, the morphological analysis using SEM was used to characterize and confirm the HA formation on the glass surface of soda-lime borate glasses with different mix proportions of bagasse and cassava rhizome before and after immersion in SBF solution for 0, 1, 7, and 14 days. Simultaneously, the HA formation on glass surface is compared and discussed. Before and after immersion in SBF, the SEM images of glass sample; GS0, BGS5, BGS10, CRS5, and CRS10 are presented Figures 4.17, 4.18, 4.19, 4.20, and 4.21, respectively. It was observed that the morphological characteristic of all the studied glasses before immersion shows flat surface with deep grooves, which were caused by polishing with silicon carbide paper. After immersion, different surfaces with micro fracture along with particle agglomeration (HA formation) which depended on the soaked time were observed. The glass surfaces showed many micro cracks, which are expected to result from the cumulative stress and the drying process in the glass forming process as well as the rapid release of ion in the glass composition after a day of immersion [183-185]. In the case of borate containing bioactive glasses, the degradation of some ions and simultaneous

formation of a borate-rich layer at the glass interface is the proposed mechanism for HA formation, similar to the silicate-rich layer in silicate-based bioactive glass [186]. This borate-rich layer, which is the foundation for the formation of HA, is represented by smooth surfaces and micro cracks in the studied bioactive glasses. After interaction with SBF solution for 7 and 14 days, respectively, calcium phosphate (CaP) or HA formation was observed on the surface of plate glass. An increasing number of small round agglomerated particles can be seen on the surface when soaked in the solution for longer. Therefore, the longer time period leads to an increase of chemical reaction that formed the HA or CaP layer. This reaction involves ion exchanges between the glass composition and the surrounding environment (SBF). Of course, some ions from the glasses were released to the solution while Ca and P ions from the SBF solution were immigrated onto the glass surface. These led to the precipitation of hydroxyapatite layer formation on the glass surface.

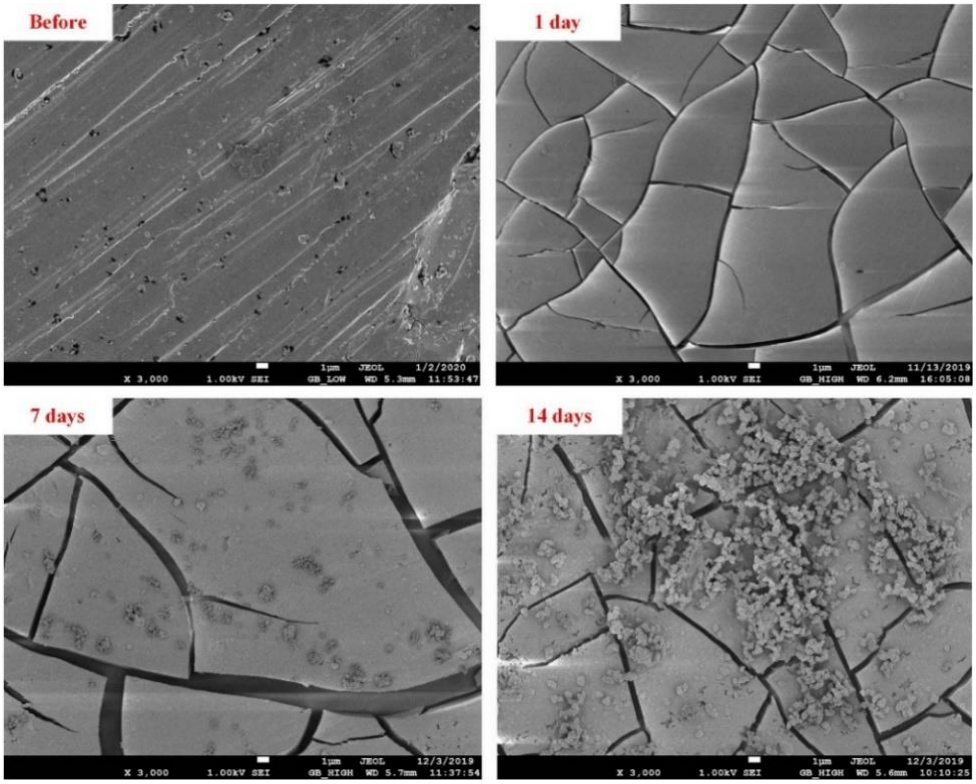

Figure 4.17 SEM images of GS0 before and after soaking in SBF solution

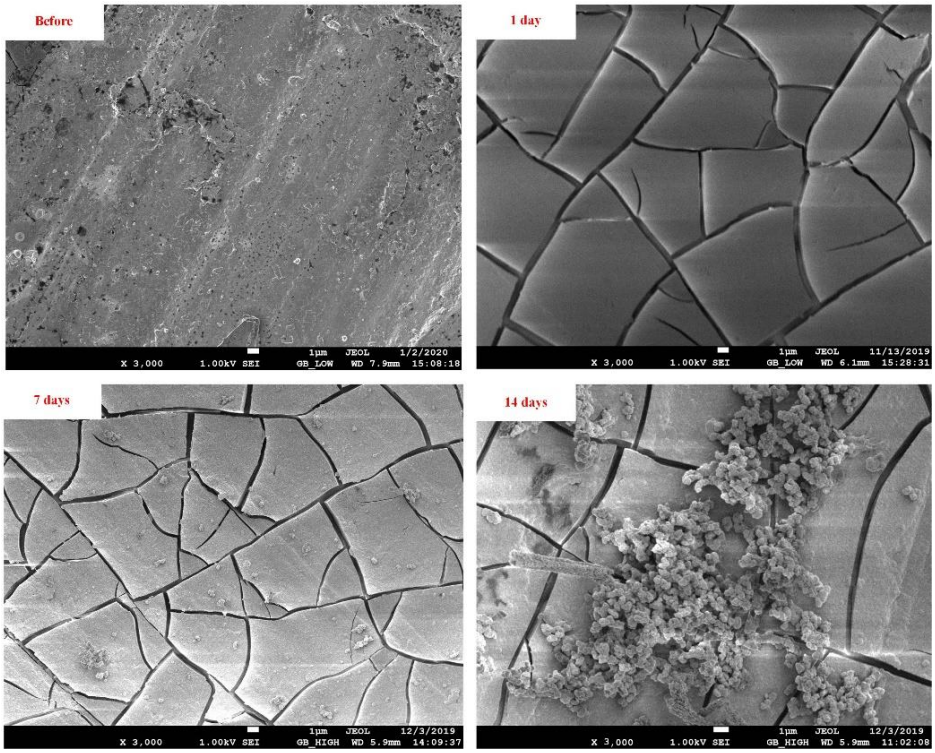

Figure 4.18 SEM images of BGS5 before and after soaking in SBF solution

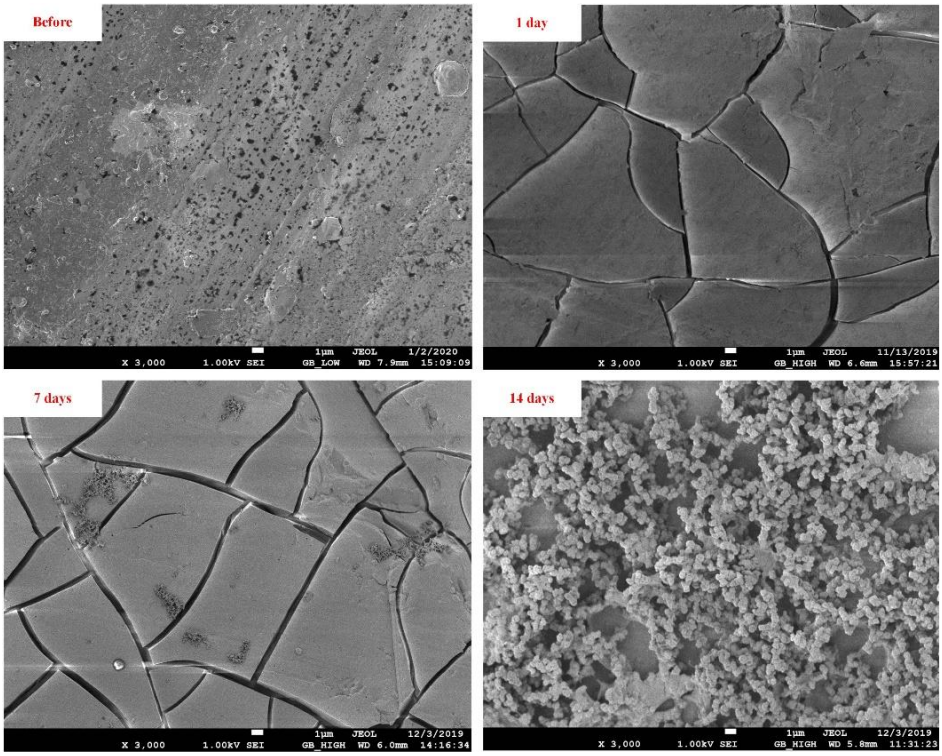

Figure 4.19 SEM images of BGS10 before and after soaking in SBF solution

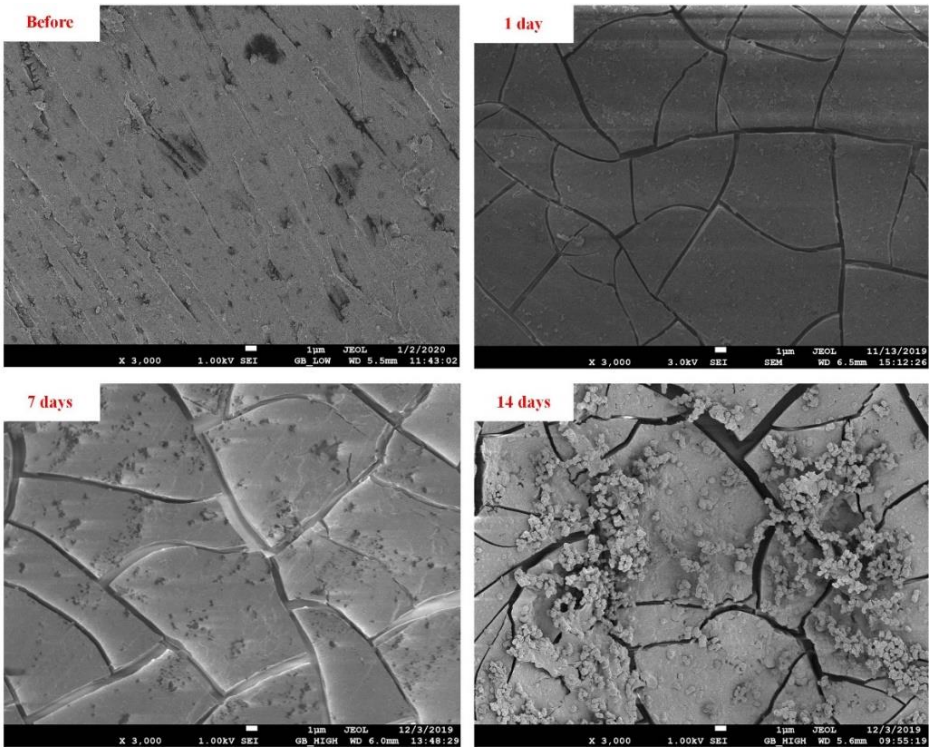

Figure 4.20 SEM images of CRS5 before and after soaking in SBF solution

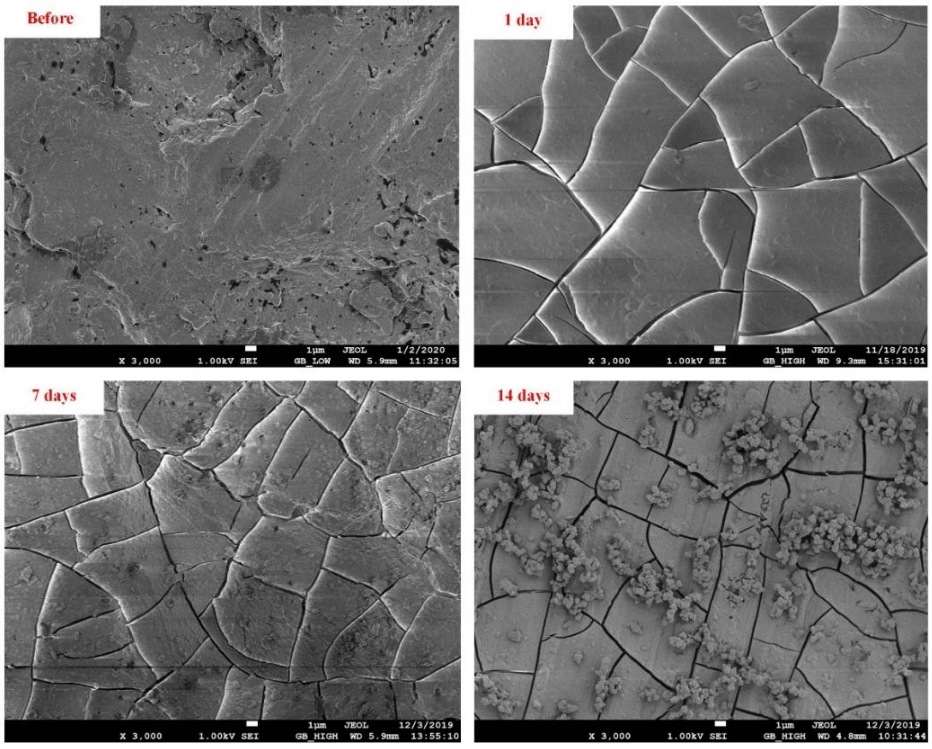

Figure 4.21 SEM images of CRS10 before and after soaking in SBF solution

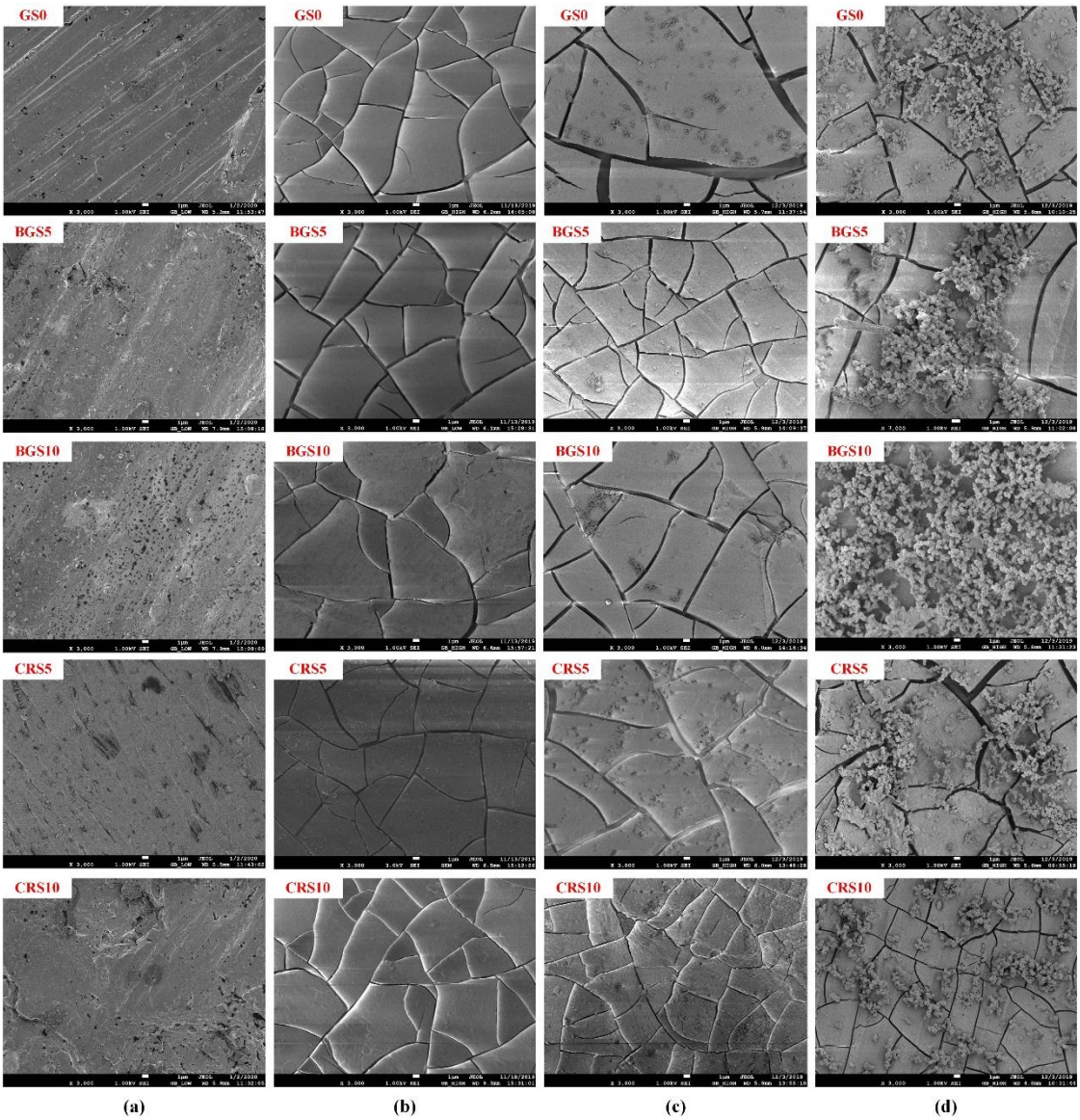

Figure 4.22 Comparison of SEM images on surface of all the prepared glasses with different time (a, b, c, and d represent soaking time of 0, 1, 7, 14 days, respectively)

Figure 4.22 shows the comparison of morphological characteristic of all the glasses with different immersion time; (a) before (0 day), (b) after 1 day, (c) after 7 days, and (d) after 14 days. Before immersion, it was clearly that the flat surface along with traces of polishing was observed in all the prepared glasses. After immersion in SBF solution for 1 day, all the bioactive glasses showed many micro-cracking traces on their surfaces. These micro cracks have formed similar characteristics independently. The

adhesion of small round particles on the sample surface after ion exchanges between the glass composition and SBF solution for 7 days was observed, and it was clearly noticed more and more when soaked for 14 days. This observation is expected to be the formation of the HA layer. The results after 7 days of reaction indicate from Figure 4.22c that the GS0 sample can form more HA layer on the glass surface than other samples, while the HA formation was less noticeable when the bagasse and cassava rhizome increased. After 14 days of immersion in the SBF solution, however, these glass samples (BGS5, BGS10, CRS5, CRS10) clearly exhibited the agglomeration of calcium phosphate particles meanwhile there is lower weight loss than GS0 (see in Figure 4.22d). This behavior suggests that the addition of bagasse and cassava rhizome into glass composition promotes the growth of the HA layer on the glass surfaces, implying a better ability of bone-bonding when implanted in the body for more longer time. Also, the glass samples added with bagasse (BGS5 and BGS10) revealed more the HA formation than that of cassava rhizome (CRS5 and CRS10), however, the resistant to corrosion of the glass samples added with bagasse are poorer when compared at same percentage. This may be related to its composition and dissolution rate. Moreover, the XRD patterns and FTIR spectra support the results of SEM.

CHAPTER 5
CONCLUSIONS

Two series of a novel bioactive glass were successfully fabricated by adding treated bagasse and cassava rhizome. The influence of oxides in bagasse and cassava rhizome on the physical, mechanical, structural, morphological, and chemical dissolution behaviors based on soda-lime borate bioactive glass was investigated to consider the feasibility and efficacy of bone tissue engineering applications. The key points of obtained result of the results can be summarized as follows.

5.1 Physical properties

The glasses prepared by melt quenching method yielded satisfactory homogeneity and stability without air bubble and crack. The based glass and the glasses added with cassava rhizome exhibited clear transparency to visible light while the compositions with bagasse showed transparent light greenish-yellow in the glasses.

The density of the prepared glasses was evaluated through measurement and calculation based on Archimedes' principle and additive rule, respectively. Both densities tend to increase with the higher molecular weight of the additives. Moreover, the glasses added with cassava rhizome yield more density value than that of bagasse. Furthermore, the obtain result of density of the glasses measured values was in good agreement with the calculated values.

5.2 Mechanical properties

The results from ultrasonic technique revealed that the partial replacement of B_2O_3 by oxides of bagasse and cassava rhizome leads to the increase of acoustic velocities, elastic moduli and microhardness in the glass samples while Poisson's ratio almost maintains a constant value. This behavior indicates that the oxides of bagasse and cassava rhizome act as modifier oxide in soda-lime borate glass. The addition of bagasse and cassava rhizome leads to the conversion of triangle to tetrahedron in borate

structural units, and results in an increase of the network rigidity as well as the modulus in the studied glasses. Beside elastic moduli, microhardness is also a parameter used to specify the dislocations deformation, or damage under an applied stress in microscopic scale. The increment of microhardness when added bagasse and cassava rhizome into the glasses pointed out an increase in glass rigidity like sound velocities and elastic moduli, moreover, this also indicated increased resistance to bending, scratching, abrasion, or cutting of the prepared glass. Although the microhardness obtained from ultrasonic and Vickers methods was observed a same trend, their values are slightly different due to different considerations.

5.3 *In vitro* bioactivity behaviors

Determination of bioactive behavior of the prepared glass has been considered in terms of degradation behavior, pH change, structure and morphological characteristic on formation of calcium phosphate layer before and after in SBF solution for 1, 7 and 14 days. The obtained results suggested that the introduction of bagasse and cassava rhizome into soda-lime borate leads to a decrease of dissolution rate (%weight loss). The corrosion process by SBF solution is explained on the basis of different leaching of triangular borate phases faster than tetrahedral borate phases due to the strong bonding of BO_4 units in four equal dimensions in difference the BO_3 units. Moreover, the percentage of weight loss in all the prepared glass tend to increase with time periods because of the release of ions from the glass into the environment (SBF). This behavior corresponded with an increase of pH in the solution. The XRD patterns showed two broad humps in all the glass before immersion while the diffraction peaks were observed after immersion. An absence of any sharp diffraction peaks in the typical XRD patterns confirms the glass nature in all the glasses before immersion. The presence of specific peaks after immersion indicates the formation of the calcium phosphate layer in the form of brushite and hydroxyapatite. IR spectral studies of undoped glass appear characteristic bands due to vibrational modes of combined phosphate and borate networks including vibration of modifier cations. The partial replacement of B_2O_3 by oxides of bagasse and cassava rhizome led to variations of the IR curves which observed additional bands of silicate and phosphate groups. The vibrational intensity of BO_3

trigonal units in the band regions about 1326 cm^{-1} decreased while the additional peak of BO_4 unit at 1195 cm^{-1} revealed when the bagasse and cassava rhizome were added. These suggest the conversion of BO_3 into BO_4 by addition of bagasse and cassava rhizome into soda-lime borate glass, supporting the results of ultrasonic velocities. The appearance of characteristic peaks in the range of 500–650 cm^{-1}, 980–1060 cm^{-1} and 1420–1432 cm^{-1} after immersion indicates the bone bonding ability as represented by the hydroxyapatite formation. The results of SEM images that agglomerated particles are formed on the glass surface indicate that the surface morphology change linked to the ionic exchanges between the glasses and SBF solution. These exchanges result in modifications of the vitreous matrix into the crystal which caused the formation of hydroxyapatite layer on the glass surface. Moreover, the progressive addition of bagasse and cassava rhizome also significantly reduced the rate of dissolution of the prepared glass in SBF solution. The formation of hydroxyapatite layer on the prepared glass surface was confirmed by the corresponding results of XRD patterns, FTIR spectra and SEM images.

Based on these results, the glasses fabricated from bagasse and cassava rhizome provide interesting properties, besides the low cost and environmentally friendly. Moreover, the physical and mechanical properties as well as the bioactive behaviors in terms of chemical degradation, pH change, structure, and morphology observed in this study indicate that the prepared glasses are a potential candidate for bone tissue engineering applications.

REFERENCES

REFERENCES

[1] Rahaman M.N. and et al. "Bioactive glass in tissue engineering", **Acta Biomaterialia**. 7(6): 2355–2373; March, 2011.

[2] Yin H. and et al. "Fabrication and characterization of strontium-doped borate-based bioactive glass scaffolds for bone tissue engineering", **Journal of Alloys and Compounds**. 743: 564–569; January, 2018.

[3] Sadeghzade S. and et al. "Hardystonite-diopside nanocomposite scaffolds for bone tissue engineering applications", **Materials Chemistry and Physics**. 202: 95–103; September, 2017.

[4] Department of Health and Human Services. **Bone Health and Osteoporosis: A Report of the Surgeon General**. Washington D.C.: United States Public Health Service, 2004.

[5] Baino F., Hamzehlou S. and Kargozar, S. "Bioactive Glasses: Where Are We and Where Are We Going", **Journal of Functional Biomaterials**. 9(1): 25–33; March, 2018.

[6] Hench L.L. "The story of Bioglass®", **Journal of Materials Science: Materials in Medicine**. 17: 967–978; February, 2006.

[7] Kaya S., Cresswell M. and Aldo R.B. "Mesoporous silica-based bioactive glasses for antibiotic-free antibacterial applications", **Materials Science & Engineering C**. 83: 99–107; February, 2018.

[8] Placek L.M. and et al. "Investigating the effect of TiO_2 on the structure and biocompatibility of bioactive glass", **Journal of Biomedical Materials Research Part B Applied Biomaterials**. 104(8): 1703–1712; November, 2016.

[9] Hench L.L. "Bioceramics", **Journal of the American Ceramic Society**. 81(7): 1705–28; May, 1998.

[10] ElBatal F.H., Ouis M.A. and ElBatal H.A. "Comparative studies on the bioactivity of some borate glasses and glass–ceramics from the two systems: Na_2O–CaO–B_2O_3 and NaF–CaF_2–B_2O_3", **Ceramics International**. 42(7): 8247–8256; May, 2016.

REFERENCES (CONTINUED)

[11] Rabiee S.M. and et al. "Effect of ion substitution on properties of bioactive glasses: A review", **Ceramics International**. 41(6): 7241–7251; July, 2015.

[12] Hoppe A., Güldal N.S. and Boccaccini A.R. "A review of the biological response to ionic dissolution products from bioactive glasses and glass-ceramics", **Biomaterials**. 32(11): 2757–2774; April, 2011.

[13] Shahrayar Y. and et al. "Structure-solubility relationships in fluoride-containing phosphate based bioactive glasses", **Journal of Materials Chemistry B**. 3(48): 9360–9373; November, 2015.

[14] Fernandes H.R. and et al. "Bioactive glasses and glass-ceramics for healthcare applications in bone regeneration and tissue engineering", **Materials**. 11(12): 2530; December, 2018.

[15] Hench L.L. and Polak J.M. "Third-generation biomedical materials", **Science**. 295(5557): 1014–1017; February, 2002.

[16] Tripathi H. and et al. "Structural characterization and in vitro bioactivity assessment of SiO_2–CaO–P_2O_5–K_2O–Al_2O_3 glass as bioactive ceramic material", **Ceramics International**. 41(9): 11756–11769; November, 2015.

[17] Brauer D.S. and et al. "Fluoride-containing bioactive glasses: Effect of glass design and structure on degradation, pH and apatite formation in simulated body fluid", **Acta Biomaterialia**. 6(8): 3275–3282; August, 2010.

[18] Tang Y., Pang L. and Wang D. "Preparation and characterization of borate bioactive glass cross-linked PVA hydrogel", **Journal of Non-Crystalline Solids**. 476: 25–29; November, 2017.

[19] Krishnamacharyulu N. and et al. "Effect of ZrO_2 on the bioactive properties of B_2O_3–SiO_2–P_2O_5–Na_2O–CaO glass system", **Journal of Non-Crystalline Solids**. 452: 23–29; November, 2016.

[20] Bengisu M. "Borate glasses for scientific and industrial applications: a review", **Journal of Materials Science**. 51(1): 2199–2242; November, 2015.

REFERENCES (CONTINUED)

[21] Lucacel R.C. and et al. "Synthesis, structure, bioactivity and biocompatibility of melt-derived P_2O_5–CaO–B_2O_3–K_2O–MoO_3 glasses", **Journal of Non-Crystalline Solids**. 439: 67–73; May, 2016.

[22] Ding H. and et al. "A novel injectable borate bioactive glass cement as an antibiotic delivery vehicle for treating osteomyelitis", **PLOS ONE**. 9(1): 85472; January, 2014.

[23] Growney Kalaf E.A. and et al. "Electrospun biomaterials for dermal regeneration", In **Electrospun Materials for Tissue Engineering and Biomedical Applications**. Tamer Uyar and Erich Kny Editors. p.179–231. Cambridge: Woodhead Publishing, 2017.

[24] Henao J. and et al. "Bio-active glass coatings manufactured by thermal spray: a status report", **Journal of Materials Research and Technology**. 8(5): 4965–4984; August, 2019.

[25] Koudelka L. and et al. "Structural investigation of BaO–B_2O_3–P_2O_5 glasses by NMR and Raman spectroscopy", **Journal of Molecular Structure**. 1119: 212–219; April, 2016.

[26] Rahaman M.N. and et al. "On the connectivity of borate tetrahedra in borate and borosilicate glasses", **Physics and Chemistry of Glasses: European Journal of Glass Science and Technology Part B**. 56(5): 203–211; October, 2015.

[27] Kaur N. and Khanna A. "Structural characterization of borotellurite and alumina-borotellurite glasses", **Journal of Non-Crystalline Solids**. 404: 116–123; November, 2014.

[28] Saddeek Y.B. and Gaafar, MS. "Physical and structural properties of some bismuth borate glasses", **Materials Chemistry and Physics**. 115(1): 280–286; May, 2009.

[29] Palani R. and Selvarasi J. "Elastic and structural properties of potassium and calcium–doped borate lithium glasses", **International Journal of Current Research and Review**. 9(10): 71–79; May, 2017.

REFERENCES (CONTINUED)

[30] Saddeek, Y.B. and et al. "Ultrasonic investigations of some bismuth borate glasses doped with Al_2O_3", **Bulletin of Materials Science**. 38(1): 241–246; February, 2015.

[31] Hasnimulyati L. and et al. "A comparative study of the experimental and the theoretical elastic data of Tm^{3+} doped zinc borotellurite glass", **Materials Chemistry and Physics**. 192: 228–234; January, 2017.

[32] Patil A.L. "Measurements of Vickers hardness and refractive index properties of Na-borophosphate glasses", **International Journal of ChemTech Research**. 10(12): 138–142; December, 2017.

[33] Elkhoshkhany N. and et al. "Mechanical and thermal properties of TeO_2–Bi_2O_3–V_2O_5–Na_2O–TiO_2 glass system", **Ceramics International**. 42(16): 19218–19224; December, 2016.

[34] Chindaprasirt P., Sujumnongtokul P. and Posi, P. "Durability and mechanical properties of pavement concrete containing bagasse ash", **Materials Today: Proceedings**. 17: 1612–1626; September, 2019.

[35] Kuprianov V.I., Se C. and Ninduangdee P. "The influence of fluidized bed co-combustion of cassava rhizome and eucalyptus bark on the combustor performance and time-related physiochemical changes of the bed material", **Biomass and Bioenergy**. 127: 105250; August, 2019.

[36] Sahiron N., Rahmat N. and Hamzah F. "Characterization of sodium silicate derived from sugarcane bagasse ash", **Malaysian Journal of Analytical Sciences**. 21(2): 512–517; June, 2016.

[37] Silva F.S. and et al. "$PM_{2.5}$ and PM_{10}: The influence of sugarcane burning on potential cancer risk", **Atmospheric Environment**. 44(39): 5133–5138; December, 2010.

[38] Lee H.H., Iraqui O. and Wang C. "The impact of future fuel consumption on regional air quality in southeast asia", **Scientific Reports**. 9(2648): 1–20; February, 2019.

REFERENCES (CONTINUED)

[39] Bahurudeen A. and et al. "Performance evaluation of sugarcane bagasse ash blended cement in concrete", **Cement & Concrete Composites**. 59: 77–88; May, 2015.

[40] Baharuddin N.H. and et al. "Potential of cassava root as a raw material for bio composite development", **ARPN Journal of Engineering and Applied Sciences**. 11(9): 6138–6147; January, 2016.

[41] Santos D.T. and et al. "Use of sugarcane bagasse as biomaterial for cell immobilization for xylitol production", **Journal of Food Engineering**. 86(4): 542–548; June, 2008.

[42] Dzobo K. and et al. "Advances in Regenerative Medicine and Tissue Engineering: Innovation and Transformation of Medicine", **Stem Cells International**. 2018(2495848): 1–24; July, 2018.

[43] Li W. **45S5 Bioactive Glass-Based Composite Scaffolds with Polymer Coatings for Bone Tissue Engineering Therapeutics**. Doctor's Thesis: University of Erlangen–Nuremberg, 2015.

[44] Courtenay J.C. and et al. "Recent Advances in Modified Cellulose for Tissue Culture Applications", **Molecules**. 23(3): 1–20; March, 2018.

[45] Wu S. and et al. **Materials Science and Engineering R**. 80: 1–36; June, 2014.

[46] Furth M.E. and et al. "Smart biomaterials design for tissue engineering and regenerative medicine", **Biomaterials**. 28(34): 5068–5073; December, 2007.

[47] Qu H. and et al. "Biomaterials for bone tissue engineering scaffolds: a review", **RSC Advances**. 9(45): 26252–26262; January, 2019.

[48] Zorzi A.R. and Miranda J.B. **Bone Grafting**. London: IntechOpen, 2017.

[49] Wang W. and Yeung K.W.K. "Bone grafts and biomaterials substitutes for bone defect repair: A review", **Bioactive Materials**. 2(4): 224–247; December, 2017.

REFERENCES (CONTINUED)

[50] Kiernan C., Knuth C. and Farrell E. "Endochondral Ossification: Recapitulating Bone Development for Bone Defect Repair", In **Developmental Biology and Musculoskeletal Tissue Engineering**. Martin J. Stoddart Editor. p.125–148. Cambridge: Academic Press, 2018.

[51] Blue Cross and Blue Shield of Alabama. **Bone Morphogenetic Protein**. Birmingham: BCBSAL, 2019.

[52] Zang J., Lu L. and Yaszemski M.J. "Bone Disorders", In **Materials and Devices for Bone Disorders**. Susmita Bose and Amit Bandyopadhyay Editors. p.83–113. Cambridge: Academic Press, 2017.

[53] Roberts T.T. and Rosenbaum A.J. "Bone grafts, bone substitutes and orthobiologics: the bridge between basic science and clinical advancements in fracture healing", **Organogenesis**. 8(4): 114–124; December, 2012.

[54] Biga L.M. and et al. **Anatomy & Physiology**. Corvallis: Oregon State University, 2013.

[55] Ott S.M. "Bone Biology and Effects of Pharmaceutical Intervention on Bone Quality", In **Materials and Devices for Bone Disorders**. Susmita Bose and Amit Bandyopadhyay Editors. p.29–70. Cambridge: Academic Press, 2017.

[56] Currey J.D. "The design of mineralised hard tissues for their mechanical functions", **Journal of Experimental Biology**. 202(23): 3285-3294; December, 1999.

[57] Rho J.Y. and et al. "Mechanical properties and the hierarchical structure of bone", **Medical Engineering & Physics**. 20(2): 92–102; March, 1998.

[58] G. Donald Whedon and Robert Proulx Heaney. **Bone**. Chicago: Encyclopaedia Britannica, Inc., 2019.

[59] Hejazi F. and Mirzadeh H. "Roll-designed 3D nanofibrous scaffold suitable for the regeneration of load bearing bone defects", **Progress in Biomaterials**. 5(3-4): 199–211; December, 2016.

[60] Gao C. and et al. "Bone biomaterials and interactions with stem cells", **Bone Research**. 5: 1–33; December, 2017.

REFERENCES (CONTINUED)

[61] Brett E. and et al. "Biomimetics of Bone Implants: The Regenerative Road", **BioResearch open access**. 6(1): 1–6; January, 2017.

[62] Silva R.F. and et al.. "Biology of Bone Tissue: Structure, Function, and Factors That Influence Bone Cells", **BioMed Research International**. 2015(421746): 1–17; July, 2015.

[63] Ansari M. "Bone tissue regeneration: biology, strategies and interface studies", **Progress in Biomaterials**. 8(4): 223–237; November, 2019.

[64] Hasan A. and et al. "Advances in osteobiologic materials for bone substitutes", **Journal of Tissue Engineering and Regenerative Medicine**. 12(6): 1448–1468; June 2018.

[65] Paul H. King, Richard C. Fries and Arthur T. Johnson. **Design of Biomedical Devices and Systems**. Florida: CRC Press, 2015.

[66] Eliaz N. "Corrosion of Metallic Biomaterials: A Review", **Materials**. 12(3): 1–92; January, 2019.

[67] Bose S., Banerjee D. and Bandyopadhyay A. "Introduction to Biomaterials and Devices for Bone Disorders", In **Materials and Devices for Bone Disorders**. Susmita Bose and Amit Bandyopadhyay Editors. p.1–28. Boston: Elsevier/Academic Press, 2017.

[68] ASM International. **Handbook of Materials for Medical Devices**. Ohio: ASM International, 2003.

[69] Ratner B.D., Hoffman A.S., Schoen F.J., and Lemons J.E. "Biomaterials Science: A Multidisciplinary Endeavor.", In **Biomaterials Science**. Buddy Ratner Editor. p.1–20. Cambridge: Academic Press, 2004.

[70] Burny F., Donkerwolcke M. and Muster D. "Biomaterials education: a challenge for medicine and industry in the late 1990s", **Materials Science and Engineering: A**. 199(1): 53–59; August, 1995.

[71] Ning C., Zhou L. and Tan G. "Fourth-generation biomedical materials", **Materials Today**. 19(1): 2–3; February, 2016.

REFERENCES (CONTINUED)

[72] Zhang L.C. and Chen L.Y. "A Review on Biomedical Titanium Alloys: Recent Progress and Prospect", **Advanced Engineering Materials**. 21(4): 1–29; April 2019.

[73] Bovo N. **Structure-properties relationships in bioactive glasses for PAA-based polyalkenoate cements**. Master's Thesis: Polytechnic University of Catalonia, 2007.

[74] Nandi S.K. and et al. "Doped Bioactive Glass Materials in Bone Regeneration", In **Advanced Techniques in Bone Regeneration**. Alessandro Rozim Zorzi Editor. p.275–328. London: IntechOpen, 2016.

[75] Navarro M. and Serra T. "Biomimetic mineralization of ceramics and glasses", In **Biomineralization and Biomaterials**. Conrado Aparicio and Maria-Pau Ginebra Editors. p.316–338. Cambridge: Woodhead Publishing, 2016.

[76] Ibrahim M.S., El-Wassefy N.A. and Farahat D.S. "Biocompatibility of dental biomaterials", In **Biomaterials for Oral and Dental Tissue Engineering**. Lobat Tayebi and Keyvan Moharamzadeh Editors. p.117–140. Cambridge: Woodhead Publishing, 2017.

[77] Carvalho S.M. and et al. "Bioactive glass nanoparticles for periodontal regeneration and applications in dentistry", In **Nanobiomaterials in Clinical Dentistry**. Karthikeyan Subramani and Waqar Ahmed Editors. p.351–383. New York: Elsevier, 2013.

[78] Hench L.L. **Bioglass and Similar Materials**. New York: Elsevier, 2001.

[79] Khalid M.D. and et al. "Bioactive Glasses and their Applications in Dentistry", **Journal of the Pakistan Dental Association**. 26(1): 32–38; March 2017.

[80] Sirirat T. **Bioactive Glass Scaffolds through the Sol-gel Route for Bone Tissue Engineering**. Nakhon Ratchasima: Suranaree University of Technology, 2014.

[81] Tayebi L. and Moharamzadeh K. **Biomaterials for Oral and Dental Tissue Engineering**. Cambridge: Woodhead Publishing, 2017.

[82] Knowles J.C. "Phosphate based glasses for biomedical applications", **Journal of Materials Chemistry**. 13(10): 2395–2401; August, 2003.

REFERENCES (CONTINUED)

[83] Ferrell S.K. **Effect of metal and semiconducting nanoparticles on the fluorescence and optical band gap of Dy^{3+} ions doped lead borate and bismuth borate glasses**. Master's Thesis: Western Illinois University, 2015.

[84] Marchi J. **Biocompatible Glasses: From Bone Regeneration to Cancer Treatment**. Cham: Springer International Publishing, 2016.

[85] Karasu B. and et al. "Bioactive glasses" **El-Cezerî Journal of Science and Engineering**. 4(3): 436–471; August, 2017.

[86] Kaushal A.M., Gupta P. and Bansal A.K. "Amorphous Drug Delivery Systems: Molecular Aspects, Design, and Performance", **Critical Reviews™ in Therapeutic Drug Carrier Systems**. 21(3): 133–193; March, 2004.

[87] Kumar A. **Effect of Ti & Al addition on the mechanical properties of Cu-Zr based metallic glasses: A molecular dynamic simulation study**. Master's Thesis: National Institute of Technology Rourkela, 2013.

[88] Zarzycki J. **Glasses and the vitreous state**. New York: Cambridge University Press, 1991.

[89] Pujol M.C. **Synthesis and characterization of optical nanocrystals and nanostructures: An approach to transparent laser nanoceramics**. Doctor's Thesis: Rovira I Virgili University, 2010.

[90] Dahiya M., Tomer V.K. and Duhan S. "Bioactive glass/glass ceramics for dental applications", In **Applications of Nanocomposite Materials in Dentistry**. Abdullah Asiri, Inamuddin and Ali Mohammad Editors. p.1–26. Cambridge: Woodhead Publishing, 2018.

[91] Velez J. **Ceramic Biomaterials**. Cambridge: OpenWetWare, 2016.

[92] The Quartz Corporation. (2019). "The Mechanism of Bioactive Glass", **The Quartz Corp**. https://www.thequartzcorp.com/2019/09/23/the-mechanism-of-bioactive-glass/. 10 March, 2020.

[93] Soundrapandian C. and et al. "Studies on novel bioactive glasses and bioactive glass–nano-Hap composites suitable for coating on metallic implants", **Ceramics International**. 37: 759–769; November, 2010.

REFERENCES (CONTINUED)

[94] Gerhardt L.C. and Boccaccini A.R. "Bioactive Glass and Glass-Ceramic Scaffolds for Bone Tissue Engineering", **Materials (Basel, Switzerland)**. 3(7): 3867–3910; July, 2010.

[95] Mohazzabi P. "Archimedes' Principle Revisited", **Journal of Applied Mathematics and Physics**. 5: 836–843; April, 2017.

[96] Encyclopaedia Britannica, Inc. (2020). "Archimedes' principle", **Encyclopaedia Britannica**. https://www.britannica.com/science/Archimedes-principle. 29 March, 2020.

[97] Dowling N.E. **Mechanical Behavior of Materials**. London: Pearson, 2012.

[98] Beer F.P. and et al. **Mechanics of Materials**. New York: McGraw-Hill, 2012.

[99] Gere J.M. **Mechanics of Materials**. Belmont: Bill Stenquist, 2004.

[100] Yu P. and Bai H.Y. "Poisson's ratio and plasticity in CuZrAl bulk metallic glasses", **Materials Science and Engineering A**. 485(1): 1–4; July, 2007.

[101] Wang W.H. "The elastic properties, elastic models and elastic perspectives of metallic glasses", **Progress in Materials Science**. 57(3): 487–656; April, 2012.

[102] Suryanarayana C. "Mechanical behavior of emerging materials", **Materialstoday**. 15(11): 486–498; November, 2012.

[103] Wang K. and Pierscionek B.K. "Biomechanics of the human lens and accommodative system: Functional relevance to physiological states", **Progress in Retinal and Eye Research**. 71: 114–131; July, 2019.

[104] Roylance D. **Mechanical Properties of Materials**. Cambridge: MIT OpenCourseWare, 2008.

[105] Greaves G.N. and et al. "Poisson's ratio and modern materials", **Nature Mater**. 10: 823–837; November, 2011.

[106] Rouxel T. and et al. "Poisson's Ratio and the Glass Network Topology - Relevance to High Pressure Densification and Indentation Behavior", **Advanced Materials Research**. 39–40: 137–146; April, 2008.

REFERENCES (CONTINUED)

[107] Sagadevan S. and Anandan S.S. "A Study of Mechanical Behaviour of Anilinium D-Tartrate Single Crystal", **International Journal of Materials Engineering**. 4(2): 70–74; April, 2014.

[108] Schwalm R. **UV Coatings: Basics, Recent Developments and New Applications**. New York: Elsevier, 2006.

[109] Knezovic, N. and Dolsak, B. "In-process non-destructive ultrasonic testing application during wire plus arc additive manufacturing", **Advances in Production Engineering & Management**. 13(2): 158–168; June, 2018.

[110] Hijazi A. (2019). "Introduction to Non-Destructive Testing Techniques", **Non-Destructive Testing (NDT)**. https://sites.google.com/view/alahijazi/classes/non-destructive-testing-ndt. 23 March, 2020.

[111] Mishra M. **A Bayesian approach to NDT Data Fusion for St. Torcato Church**. Master's Thesis: University of Minho, 2013.

[112] Singh J.P. "Review of Ultrasonic Testing Technique", **International Journal in IT and Engineering**. 2(3): 1–14; March, 2014.

[113] Sigrist R.M.S. "Ultrasound Elastography: Review of Techniques and Clinical Applications", **Theranostics**. 7(5): 1303–1329; March, 2017.

[114] Roeder R.K. "Mechanical Characterization of Biomaterials", In **Characterization of Biomaterials**. Amit Bandyopadhyay and Susmita Bose Editors. p.49–104. New York: Elsevier, 2013.

[115] Alex A.V. **Ultrasonic measurement of the elastic constants of selected Nonlinear Optical/Semiorganic Crystals with Orthorhombic System**. Doctor's Thesis: Cochin University of Science and Technology, 2001.

[116] Marzouk S.Y. "Ultrasonic and infrared measurements of copper-doped sodium phosphate glasses", **Materials Chemistry and Physics**. 114(1): 188–193; March, 2009.

[117] Al-Dafaee T.A. **Effect of gamma ray irradiation on strontium oxides immobilized by glass materials**. Master's Thesis: University of Baghdad, 2007.

REFERENCES (CONTINUED)

[118] Voort G.F.V. and Buehler Ltd. "Micro indentation Hardness Testing", In **Mechanical testing and evaluation, ASM Handbook**. H. Kuhn and D. Medlin Editors. p.221–231. Ohio: ASM International, 2000.

[119] Materials Evaluation and Engineering, Inc. **Handbook of Analytical Methods for Materials**. Minneapolis: Materials Evaluation and Engineering, Inc., 2001.

[120] Ali A.S. "Application of Nanomaterials in Environmental Improvement", In **Nanotechnology and the Environment**. Mousumi Sen Editor. p.1–20. London: IntechOpen, 2020.

[121] Chauhan A. **Deformation and damage mechanisms of ODS steels under high-temperature cyclic loading**. Doctor's Thesis: Karlsruhe Institute of Technology, 2018.

[122] Sowińska M. **In-operando hard X-ray photoelectron spectroscopy study on the resistive switching physics of HfO_2-based RRAM**. Master's Thesis: Brandenburg University of Technology, 2014.

[123] Li X. and et al. "Synthesis and characterization of mesoporous CaO–MO–SiO_2–P_2O_5 (M =Mg, Zn, Cu) bioactive glasses/composites", **Journal of Materials Chemistry**. 18(34): 4103–9; August, 2008.

[124] Alcaide M. and et al. "Interaction of an ordered mesoporous bioactive glass with osteoblasts, fibroblasts and lymphocytes, demonstrating its biocompatibility as a potential bone graft material", **Acta Biomaterialia**. 6(3): 892–899; March 2010.

[125] Liu X. and et al. "Mechanical properties of bioactive glass (13-93) scaffolds fabricated by robotic deposition for structural bone repair", **Acta Biomaterialia**. 9(6): 7025–34; June, 2013.

[126] Baino F. and Brovarone C.V. "Mechanical properties and reliability of glass-ceramic foam scaffolds for bone repair", **Materials Letters**. 118: 27–30; March, 2014.

REFERENCES (CONTINUED)

[127] Tagliabue S. and et al. "Micro-CT based finite element models for elastic properties of glass-ceramic scaffolds", **Journal of the Mechanical Behavior of Biomedical Materials**. 65: 248–255; August, 2016.

[128] Lapa A. and et al. "Phosphate glass fibres with therapeutic ions release capability–a review", **Advances in Applied Ceramics**. 119(1): 1–14; January, 2019.

[129] Navarro M., Ginebra M.P. and Planell J.A. "Cellular response to calcium phosphate glasses with controlled solubility", **Journal of Biomedical Materials Research Part A**. 67(3): 1009–15; December, 2003.

[130] Brauer D.S. and et al. "Effect of degradation rates of resorbable phosphate invert glasses on in vitro osteoblast proliferation", **Journal of Biomedical Materials Research Part A**. 77(2): 213–219; May, 2006.

[131] Ahmed I. and et al. "Cytocompatibility and effect of increasing MgO content in a range of quaternary invert phosphate-based glasses", **Journal of Biomaterials Applications**. 24(6): 555–575; February, 2010.

[132] Abdelghany A.M. and Kamal H. "Spectroscopic investigation of synergetic bioactivity behavior of some ternary borate glasses containing fluoride anions", **Ceramics International**. 40(6): 8003–8011; July, 2014.

[133] Deliormanl A.M., Liu X. and Rahaman M.N. "Evaluation of borate bioactive glass scaffolds with different pore sizes in a rat subcutaneous implantation model", **Journal of Biomaterials Applications**. 28(5): 643–653; December, 2012.

[134] Anand V. and et al. "B_2O_3–MgO–SiO_2–Na_2O–CaO–P_2O_5–ZnO bioactive system for bone regeneration applications", **Ceramics International**. 42(2): 3638–3651; November, 2015.

[135] Bakry A.S.I. **Borate bioactive glass and methods of use for dentin and enamel restoration**. United States Patent Application 15,609,581, 2019.

REFERENCES (CONTINUED)

[136] Jaichueai Y. and et al. "The investigation of xCaO–(50-x)SrO–50B_2O_3 glass systems added with CaO from cassava rhizome on elastic and structural properties", **Journal of science and technology Ubon Ratchathani University**. 19(1): 152–162; January, 2017.

[137] Halimah M.K. and et al. "Study of rice husk silicate effects on the elastic, physical and structural properties of borotellurite glasses", **Materials Chemistry and Physics**. 238: 121891; July, 2019.

[138] Gunhakoon P. and et al. "Influence of WO_3 on elastic and structural properties of barium-borate-bagasse-cassava rhizome glass system", **Materials Chemistry and Physics**. 243: 122587; December, 2019.

[139] Laopaiboon R. and et al. "Elastic properties investigation of gamma-radiated barium lead borosilicate glass using ultrasonic technique", **Annals of Nuclear Energy**. 38(11): 2333–2337; November, 2011.

[140] Suebsing N. and et al. "Luminescent properties of calcium-alumino-silicate glasses (CaAlSi) doped with Sm_2O_3 and co-doped with Sm_2O_3 + Eu_2O_3 for LED glass applications", **Journal of Non-Crystalline Solids**. 523: 119598; August, 2019.

[141] Gaafar M.S. and et al. "Simulation of Acoustic Properties of Borate and Tellurite Glasses", **International Scholarly and Scientific Research & Innovation**. 9(10): 1858–1867; 2011.

[142] Sopapan P. and et al. "Feasibility study of recycled CRT glass on elastic and radiation shielding properties used as x-ray and gamma-ray shielding materials", **Progress in Nuclear Energy**. 119: 103149; January, 2020.

[143] Januchta K. and et al. "Mechanical property optimization of a zinc borate glass by lanthanum doping", **Journal of Non-Crystalline Solids**. 520: 119461; May, 2019.

[144] Mahmoud G.M. and Hegazy R.S. "Comparison of GUM and Monte Carlo methods for the uncertainty estimation in hardness measurements", **International Journal of Metrology and Quality Engineering**. 8(14): 1–8; May, 2017.

REFERENCES (CONTINUED)

[145] Kokubo T. and Takadama H. "How useful is SBF in predicting in vivo bone bioactivity", **Journal of Materials Research and Technology**. 27(15): 2907–2915; May, 2006.

[146] Magyari K. and et al. "Bioactivity evolution of calcium-free borophosphate glass with addition of titanium dioxide", **Journal of Non-Crystalline Solids**. 410: 112–117; February, 2015.

[147] Gaafar M.S. and et al. "Structural studies and mechanical properties of some borate glasses doped with different alkali and cobalt oxides", **Current Applied Physics**. 13(1): 152–158; January, 2013.

[148] Yousef E.S. and et al. "Effect of rare earth (Pr_2O_3, Nd_2O_3, Sm_2O_3, Eu_2O_3, Gd_2O_3 and Er_2O_3) on the acoustic properties of glass belonging to bismuth–borate system", **Solid State Communications**. 139(3): 108–113; June, 2006.

[149] Vasantharani P. and Rajeswari S. "Ultrasonic Studies of Physical and Elastic Properties of Sodium Borate Glasses", **International Journal for Research in Applied Science & Engineering Technology**. 5(8): 519–524; August, 2017.

[150] Saddeek Y.B. and et al. "Constants of elasticity of Li_2O–B_2O_3–fly ash: Structural study by ultrasonic technique", **Materials Chemistry and Physics**. 94(2–3): 213–220; December, 2005.

[151] Manupriya and et al. "Structural and acoustic investigations of calcium borate glasses", **Physica Status Solidi (A) Applications and Materials**. 203(10): 2356–2364; August, 2006.

[152] Sidek H.A.A. and et al. "Synthesis and Elastic Behaviour of Borate Glass Doped with High Tellurite Content", **Journal of Applied Sciences**. 6(2): 274–279; March, 2006.

[153] Baino F, Fiume E. "Elastic Mechanical Properties of 45S5-Based Bioactive Glass-Ceramic Scaffolds", **Materials (Basel)**. 12(19): 3244; October, 2019.

REFERENCES (CONTINUED)

[154] Chen C.C. and et al. "Temperature dependence of elastic properties of ZBLAN glasses", **Materials Chemistry and Physics**. 65(3): 306–309; August, 2000.

[155] Belyadi H. Fathi E. and Belyadi F. **Hydraulic Fracturing in Unconventional Reservoirs**. West Virginia: Gulf Professional Publishing, 2017.

[156] Bar A.K. and et al. "Vickers Micro hardness Measurement of Glass-Nanocomposites", **Journal of Material Science and Mechanical Engineering**. 1(1): 18–22; October, 2014.

[157] Islam M.T. and et al. "Bioactive calcium phosphate–based glasses and ceramics and their biomedical applications: A review", **Journal of Tissue Engineering**. 8: 1–16; June, 2017.

[158] Frankel G.S. and et al. "A comparative review of the aqueous corrosion of glasses, crystalline ceramics, and metals", **NPJ Materials Degradation**. 2(15): 1–17; May, 2018.

[159] Abdelghany A.M. and et al. "Role of SrO on the bioactivity behavior of some ternary borate glasses and their glass ceramic derivatives", **Spectrochimica Acta Part A: Molecular and Biomolecular Spectroscopy**. 152: 126–133; January, 2016.

[160] Mancuso E. and et al. "Sensitivity of novel silicate and borate-based glass structures on in vitro bioactivity and degradation behaviour", **Ceramics International**. 43(15): 12651–12657; October, 2017.

[161] Motealleh A. and et al. "Robocast 45S5 bioglass scaffolds: in vitro behavior", **Journal of Materials Science**. 52: 9179–9191; August, 2017.

[162] Aguilar-Reyes E.A. and et al. "Processing and in vitro bioactivity of high-strength 45S5 glass-ceramic scaffolds for bone regeneration", **Ceramics International**. 43(9): 6868–6875; June, 2017.

[163] Bunker B.C. "Molecular mechanisms for corrosion of silica and silicate glasses", **Journal of Non-Crystalline Solids**. 179: 300–308; November, 1994.

REFERENCES (CONTINUED)

[164] Shelby J.E. **Introduction to Glass Science and Technology**. London: Royal Society of Chemistry, 2005.

[165] Rezaei Y. and et al. "Synthesis, Characterization, and In Vitro Bioactivity of Sol-Gel-Derived SiO_2–CaO–P_2O_5–MgO-SrO Bioactive Glass", **Synthesis and Reactivity in Inorganic, Metal-Organic, and Nano-Metal Chemistry**. 44(5): 692–701; December, 2013.

[166] Egorysheva A.V. and et al. "Vibrational Spectra of Crystals of Bismuth Borates", **Crystallography Reports**. 50: 127–136; January, 2005.

[167] Ullah I. and et al. "Simultaneous co-substitution of Sr^{2+}/Fe^{3+} in hydroxyapatite nanoparticles for potential biomedical applications", **Ceramics International**. 44(17): 21338–21348; December, 2018.

[168] Kartha S.A. **A Preparation of B_2O_3-Li_2O-MO (M=Pb, Zn) glass thin films and study of thin properties**. Doctor's Thesis: Mahatma Gandhi University, 2001.

[169] Balachander L. and et al. "IR analysis of borate glasses containing three alkali oxides", **ScienceAsia**. 39(2): 278–283; August, 2013.

[170] Gaafar M.S., Shaarany I. and Alharbi T. "Structural investigations on some cadmium-borotellurate glasses using ultrasonic, FT-IR and X-ray techniques", **Journal of Alloys and Compounds**. 616: 625–632; December, 2014.

[171] Ichoja A. and et al. "Physical, structural and optical studies on magnesium borate glasses doped with dysprosium ion", **Journal of Rare Earths**. 36(12): 1264–1271; December, 2018.

[172] Stefanic M. and et al. "The influence of strontium release rate from bioactive phosphate glasses on osteogenic differentiation of human mesenchymal stem cells", **Journal of the European Ceramic Society**. 38(3): 887–897; March, 2018.

[173] Khalil E.M.A. and et al. "Infrared absorption spectra of transition metals-doped soda lime silica glasses", **Physica B: Condensed Matter**. 405(5): 1294–1300; March, 2010.

REFERENCES (CONTINUED)

[174] Singh G.P. and et al. "Structural and optical properties of WO_3–ZnO–PbO–B_2O_3 glasses", **Physica B: Condensed Matter**. 406(10): 1890–1893; May, 2011.

[175] Kaur K. and et al. "Magnesium and silver doped CaO–Na_2O–SiO_2–P_2O_5 bioceramic nanoparticles as implant materials", **Ceramics International**. 42(11): 12651–12662; August, 2016.

[176] Rocton N. and et al. "Fine analysis of interaction mechanism of bioactive glass surface after soaking in SBF solution: AFM and ICP-OES investigations", **Applied Surface Science**. 505: 144076; March, 2020.

[177] Mozafari M. and et al. "Investigation of the physico-chemical reactivity of a mesoporous bioactive SiO_2–CaO–P_2O_5 glass in simulated body fluid", **Journal of Non-Crystalline Solids**. 356(28-30): 1470–1478; June, 2010.

[178] Boujaady H.E. and et al. "Adsorption of a textile dye on synthesized calcium deficient hydroxyapatite (CDHAp): Kinetic and thermodynamic studies", **Journal of Materials and Environmental Science**. 7(11): 4049–4063; September, 2016.

[179] Vyas V.K. and et al. "Effect of Cr_2O_3 Addition on the Bioactivity and Physico-Mechanical Properties of 45S5 Bioactive Glass and Glass-Ceramic", **International Journal of Engineering Research & Technology**. 3(2): 1479–1493; February, 2014.

[180] Guo W. and et al. "Characterization of the mechanical behaviors and bioactivity of tetrapod ZnO whiskers reinforced bioactive glass/gelatin composite scaffolds", **Journal of the Mechanical Behavior of Biomedical Materials**. 68: 8–15; April, 2017.

[181] Tripathi H. and et al. "Structural characterization and in vitro bioactivity assessment of SiO_2–CaO–P_2O_5–K_2O–Al_2O_3 glass as bioactive ceramic material", **Ceramics International**. 41(9): 11756–11769; November, 2015.

[182] PerkinElmer Life and Analytical Sciences. **FT-IR Spectroscopy Attenuated Total Reflectance (ATR)**. Shelton: PerkinElmer Inc., 2005.

REFERENCES (CONTINUED)

[183] Chen J. and et al. "Preparation and characterization of bioactive glass tablets and evaluation of bioactivity and cytotoxicity in vitro", **Bioactive materials**. 3(3): 315–321; December, 2017.

[184] Kumar A. and et al. "Mesoporous 45S5 bioactive glass: synthesis, in vitro dissolution and biomineralization behavior", **Journal of Materials Chemistry B**. 5(44): 8786–8798; October, 2017.

[185] Bonadio T.G.M. and et al. "Bioactivity and structural properties of nanostructured bulk composites containing Nb_2O_5 and natural hydroxyapatite", **Journal of Applied Physics**. 113: 223505; June, 2013.

[186] Chen Q. and et al. "Progress and challenges in biomaterials used for bone tissue engineering: bioactive glasses and elastomeric composites", **Progress in Biomaterials**. 1(2): 1–22; September, 2012.

APPENDICES

APPENDIX A
TOOLS

The instruments used in data collection in this work

1. Sieve shaker machine

Figure A.1 Sieve shaker machine: Retsch AS200 digit

2. Mortar for grinding material

Figure A.2 Mortar for grinding materials

3. Alumina crucible

Figure A.3 Alumina crucible for melting the glass in an electric furnace

4. Electric furnace

Figure A.4 Electric furnace fabricated by Glass Technology Excellent Center (GTEC) at Department of Physics, Faculty of Science, Ubon Ratchathani University

5. Graphite mold

Figure A.5 Graphite mold for forming the glass samples

6. Electric furnace for annealing glass sample

Figure A.6 Electric furnace for annealing the glass samples fabricated by Glass Technology Excellent Center (GTEC) at Department of Physics, Faculty of Science, Ubon Ratchathani University

7. Device for cutting the glass sample

Figure A.7 Device for cutting the glass samples model: Herbert Arnold

8. Device for polishing the glass sample

Figure A.8 Device for polishing the glass samples fabricated by Glass Technology Excellent Center (GTEC) at Department of Physics, Faculty of Science, Ubon Ratchathani University

9. Ultrasonic flaw detector

Figure A.9 Ultrasonic flaw detector model: GE Phasor XS in mode A-scan

10. Vickers microhardness testing

Figure A.10 Vickers microhardness tester model: Mitsubishi, MVK-H1

11. SBF solution preparation

Figure A.11 Preparation of SBF solution at Department of Chemistry, Faculty of Science, Ubon Ratchathani University

12. pH measurement

Figure A.12 pH meter model: HORIBA, PH1300

APPENDIX B
XRD PATTERNS AND FTIR SPECTRA OF HYDROXYAPATITE

1. X-ray diffractograms of brushite and hydroxyapatite

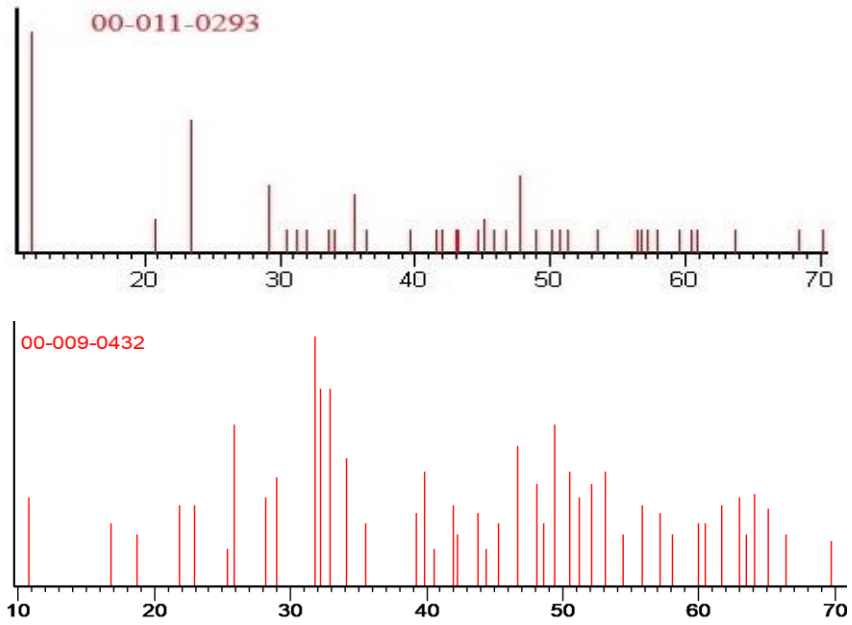

Figure B.1 XRD patterns of brushite (standard ICDD card No. 00-011-0293) and hydroxyapatite (standard JCPDC card No. 09-0432)

2. FTIR spectra of hydroxyapatite

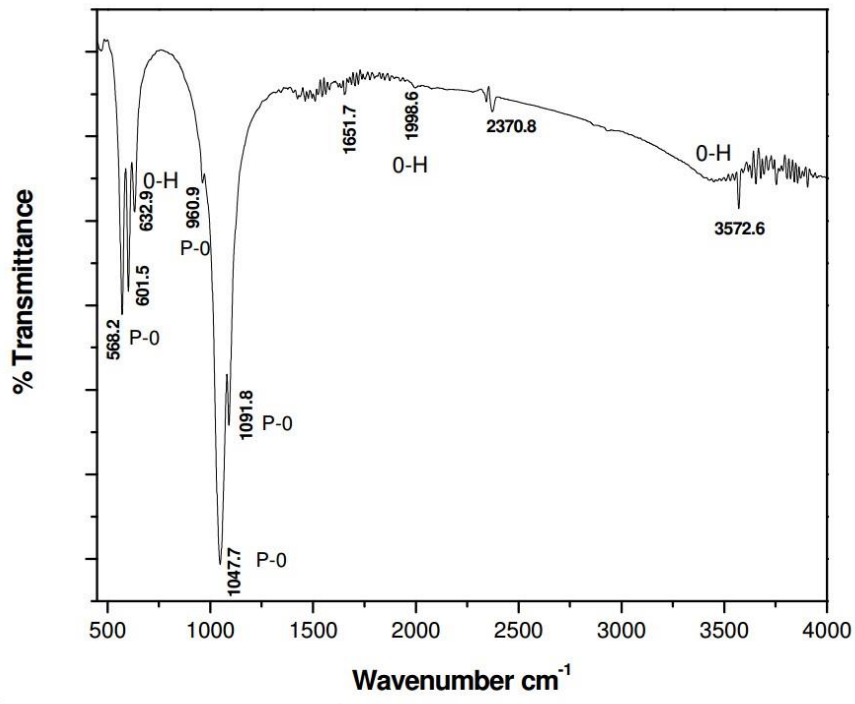

Figure B.2 FTIR spectra associated with the formation of HA

APPENDIX C
PUBLICATIONS AND CONFERENCES

Publications:

[1] ***P. Sopapan***, R. Laopaiboon, J. Laopaiboon, P. Gunhakoon, T. Thongklom, O. Jaiboon, Study of bagasse and cassava rhizome effects on the physical, mechanical and structural properties of soda-lime borate glasses. SN Appl. Sci. 2, 929 (2020).

[2] ***P. Sopapan***, J. Laopaiboon, O. Jaiboon, C. Yenchai, R. Laopaiboon, Feasibility study of recycled CRT glass on elastic and radiation shielding properties used as x-ray and gamma-ray shielding materials. Progress in Nuclear Energy 119, 103149 (2020).

[3] P. Gunhakoon, T. Thongklom, ***P. Sopapan***, J. Laopaiboon, R. Laopaiboon, O. Jaiboon, Influence of WO_3 on elastic and structural properties of barium-borate-bagasse-cassava rhizome glass system. Materials Chemistry and Physics 243, 122587 (2020).

[4] ***P. Sopapan***, J. Laopaiboon, O. Jaiboon, P. Gunhakoon, R. Laopaiboon, Effect of zinc oxide on elastic and structural properties of recycled window glass: a comparative study between before and after gamma irradiation. J. Phys.: Conf. Ser. **1285** 012032 (2019).

[5] P. Gunhakoon, ***P. Sopapan***, J. Laopaiboon, O. Jaiboon, R. Laopaiboon, Influence of gamma ray on elastic and structural properties of recycled window glass doped with chromium oxide using ultrasonic contact technique and FTIR spectroscopy. J. Phys.: Conf. Ser. **1285** 012033 (2019).

[6] ***P. Sopapan***, J. Laopaiboon, O. Jaiboon, C. Bootjomchai, U. Patakham, R. Laopaiboon, A Study of the Effect of Lead Oxide on Structural and Elastic Properties of Recycled Silica Gel Glass by Ultrasonic and FTIR Technique. Journal of Science and Technology, Ubon Ratchathani University, 19(3), (2018).

Conferences:

[1] **International Nuclear Science and Technology Conference (INST) 2019**; *Effect of ZnO on elastic and structural properties of recycled window glass: a comparative study between before and after gamma irradiation.* Bangkok, Thailand

[2] **Siam Physics Congress (SPC) 2017**; *Effect of doping by different transition metal oxides on the elastic and structural properties of recycled borosilicate glasses*. Rayong, Thailand

[3] **International Scientific Conference on Engineering and Applied Sciences (ISCEAS) 2016**; *Investigation of the elastic properties of CRT–K_2O–BaO glass for gamma-ray shielding application*. Beijing, China

[4] **Siam Physics Congress (SPC) 2016**; *Gamma-ray shielding and elastic properties of recycled silica gel glasses*. Ubon Ratchathani, Thailand

[5] **North Eastern Science and Technology Conference (NESTC) 2015**; *Investigation of structural and elastic properties of calcium–lead–silicate glass systems for gamma-ray shielding application*. Ubon Ratchathani University, Thailand

[6] **Siam Physics Congress (SPC) 2014**; *Elastic properties investigation of alkaline borosilicate glasses with Nd_2O_3 content by ultrasonic technique*. Nakhon Ratchasima, Thailand

APPENDIX D
EXPERIENCES AND QUALIFICATIONS

Experiences:

December 2017 ***Laboratory workshops (~1 month)*** *at Department of Nuclear Engineering, Chulalongkorn University*

- Establishing and designing a system for measuring the radiation shielding properties of materials.
- Studying the use of the Genie-2000 program for spectral analysis of x-ray and gamma-ray.
- Evaluating the radiation shielding properties of glass and concrete.

April 2014 ***Apprenticeship (~2 months)*** *at National Metal and Materials Technology Center (MTEC)*

- Studying the preparation of mechanical alloying using a ball mill.
- Studying the preparation of single crystal metal for structural analysis using EBSD and SEM techniques.
- Practicing the use of SEM and analysing the results

March 2012 ***Conducting short-term research (~2 months)****, Faculty of Science, Mahidol University*

- Studying the efficiency of thin film thickness by rotating linearly polarized light produced by polarizing Mach-Zehnder interferometer.

2016 - Present ***Mathematics and Physics Tutor at "The First One School"***

Qualifications:

August, 2020 *Co-Resource person for training in the application of x-ray, gamma ray and neutron for utilization in research and industrial*

April, 2019 *Training course on protect from harmful radiation level 1*

December, 2018 *Workshop on non-destructive testing (NDT) by Siwa Testing Inspection & Consulting Co., Ltd.*

July, 2018 *KidBright Workshop for Trainer*

September, 2017 *Workshop on Research Publishing*

2014-2020 *Co-Trainer for Little Scientist House of Thailand*

VITAE

NAME	Mr. Poonnapbob Sopapan
DATE OF BIRTH	February 21, 1993
NATIONALITY	Thai
ADDRESS	30 Village No.15, Huana Sub-district, Khemarat District, Ubon Ratchathani, 34170 Thailand
MOBILE	(+66) 82 320 0659
E-MAIL ADDRESS	p.sopapan1993@hotmail.com
EDUCATION	2015−2017: Master of Science (Physics) Ubon Ratchathani University, Thailand (Excellent thesis) 2011−2015: Bachelor of Science (Physics) Ubon Ratchathani University, Thailand (GPAX=3.51)
SCHORLARSHIP	2011−2020: Research Professional Development Project Under the Science Achievement Scholarship of Thailand (SAST)
PUBLICATIONS	6 papers 1 proceeding of international conferences